Universität Rostock

Traditio et Innovatio

Synthesis and Reactivity of Pacman Phosphanes

Cumulative Dissertation

to acquire the academic degree

Doctor rerum naturalium (Dr. rer. nat.)

of the Faculty of Mathematics and Natural Sciences

at the University of Rostock

submitted by Liesa Henrike Eickhoff, born on 14 February 1995 in Hamburg

Rostock, 17.04.2023

https://doi.org/10.18453/rosdok_id00004406

The present work was accomplished at the Department of Chemistry of the University of Rostock, at the chair of Inorganic Chemistry in the working group of Professor Dr Axel Schulz during the period from October 2019 to April 2023.

Reviewer:

Professor Dr Axel Schulz, Universität Rostock

Professor Dr Carsten von Hänisch, Philipps-Universität Marburg

Dr habil Wolfgang Baumann, Leibniz-Institut für Katalyse e. V. (Rostock)

Date of thesis defence: 11 July 2023

Statement of Authorship

I hereby affirm that I have written this thesis independently and without outside assistance. Except as indicated, no other resources were used. All references as well as verbatim extracts were quoted and all sources of information were specifically acknowledged.

Ich versichere hiermit an Eides statt, dass ich die vorliegende Arbeit selbstständig angefertigt und ohne fremde Hilfe verfasst habe. Dazu habe ich keine außer den von mir angegebenen Hilfsmitteln und Quellen verwendet und die den benutzten Werken inhaltlich und wörtlich entnommenen Stellen habe ich als solche kenntlich gemacht.

Rostock, 17.04.2023

Liesa Eickhoff

Danksagung (Acknowledgements)

Die in dieser Arbeit vorgestellten Ergebnisse wären ohne die Unterstützung durch zahlreiche Personen über die gesamte Zeit des Studiums und der Promotion nicht möglich gewesen.

Daher möchte ich zunächst meiner **Familie** danken. Zum einen dafür, dass ihr mir dieses Studium ermöglicht und mich all die Jahre dabei unterstützt habt (auch wenn es vielleicht nicht immer einfach ist, zu verstehen, was ich den ganzen Tag so mache). Zum anderen dafür, dass wir immer mit offenen Armen empfangen werden, so viel entspannende und erholsame Zeit bei und mit euch verbringen und einfach die Seele baumeln lassen dürfen.

Liebe **Brokkolis**, ihr habt vom ersten Tag an die Zeit in Rostock zu etwas ganz Besonderem gemacht und über all die Jahre für so viele schöne Erinnerungen gesorgt. Ich bin gespannt, wo unsere Wege uns im nächsten Jahr und darüber hinaus hinführen! Ebenso danke ich **Lilli** für die lustige WG-Zeit, ihre Verlässlichkeit und Zielstrebigkeit und **Jonas** S. für die Gesellschaft und Bereicherung an langen Labortagen und die herausragende Bewirtung bei unseren Spieleabenden.

Mein spezieller Dank gilt **Axel Schulz** für sein Vertrauen in meine Arbeit an diesem anspruchsvollen, explorative aber auch aufregenden Thema, den unkomplizierten Austausch und die zahlreichen Denkanstöße.

In gleichem Maße möchte ich **Jonas Bresien** danken. Ohne deine hervorragende Betreuung, die zahlreichen, aufschlussreichen Gespräche und die jahrelange Einführung in das wissenschaftliche Arbeiten und insbesondere in die quantenchemischen Berechnungen würde ich heute nicht dort stehen, wo ich bin.

In Zusammenhang mit Letzterem gilt mein Dank außerdem dem **HPC-Team des ITMZ** für die Bereitstellung und Wartung der Hochleistungsrechner.

Leon Ohms und **Pascal Kramer** möchte ich für ihre engagierte und ergiebige Arbeit und das Durchhaltevermögen in ihren Abschlussarbeiten danken. Diese Chemie war und ist nicht immer einfach!

Dem gesamten **Arbeitskreis** und der **anorganischen Abteilung** gilt mein Dank für die angenehme und entspannte Arbeitsatmosphäre und den regen Austausch. Insbesondere möchte

ich den „Ehemaligen“ **Max**, **Kevin**, **Lilli**, **Tim**, **Henrik** und **Julia** für die hervorragende Einführung in die Laborarbeit und all ihre Ratschläge und Hinweise danken, sowie den „Aktuellen“ **Jonas** S., **Basti**, **Yannic**, **Leon** und **Pascal** für die harmonische und produktive Zusammenarbeit in diversen Laborgemeinschaften in den letzten Jahren.

Synthesearbeit baut immer auf analytischen Daten auf. Daher möchte ich insbesondere **Heike Borgwaldt** und **Dirk Michalik** für die Durchführung und Berücksichtigung zahlreicher Sondermessungen und –Wünsche in der NMR-Spektroskopie danken sowie für die sehr angenehme Zusammenarbeit. Man kommt immer gerne auf Sie zu! Gleiches gilt für **Isabel Schicht**, die zuverlässig für einen sehr unkomplizierten Ablauf der X-Ray-Messungen sorgt. **Alexander Villinger** danke ich für das Lösen der Kristallstrukturen und die Zeit und den Aufwand, den er in fehlgeordnetes Lösemittel und Anionen in meinen Strukturen gesteckt hat. Ich danke außerdem der gesamten weiteren analytischen Abteilung, insbesondere **Angela Weihs** und **Jana Pittner** für ihr Engagement hinsichtlich der Elementaranalyse luftempfindlicher Proben. **Paula Thiem** und **Nils Pardemann** gilt mein besonderer Dank für die Instandhaltung des MS-Geräts – ich hoffe ihr wisst, was für eine Erleichterung das für uns alle ist!

Des Weiteren gilt mein Dank **Nadja Kohlmann**, der **elektronischen** und **feinmechanischen Werkstatt**, **Jörg Harloff** und **Ronald Wustrack** sowie **Kerstin Bohn**, **Paul Goschnick** und **Jana Unger** dafür, dass sie mir auf unterschiedlichste Weise mit Hilfe und Rat zur Seite standen.

Der **August-Wilhelm-von-Hofmann-Stiftung** und dem **Promotionsstipendienprogramm der Universität Rostock** danke ich für die finanzielle Unterstützung meines Bachelor- und Promotionsstudiums.

Lieber **Edgar**, ich danke dir für deine nicht endenden Ideen, Tipps und Tricks im Labor. Ich bin froh, dass wir so viel Zeit zusammen verbringen können, ohne uns in die Quere zu kommen und dass wir es trotzdem schaffen (wenn auch vielleicht etwas zu selten) gemeinsam von der Arbeit abzuschalten. Ich bin dir unendlich dankbar, dass du mich in schwierigen Momenten immer wieder aufbaust und auf mich aufpasst und weiß, dass wir noch viele weitere schöne, gemeinsame Momente genießen werden, sei es im oder außerhalb des Labors.

Vielen Dank!

Summary

This work describes investigations about a new access to metal-free activation chemistry. Therefore, concepts enabling the cooperative reaction behaviour of Pacman complexes are transferred to phosphorus chemistry. The introduction of two phosphorus(III) units in a calix[4]pyrrole Schiff base ligand allowed the first syntheses of Pacman phosphanes. Connection to the ligand is achieved via two pyrrole nitrogen atoms binding each phosphorus atom. Additionally, either a chlorine atom or an organic substituent is bound to the phosphorus atoms, depending on the phosphorus precursor. The steric bulk of the substituents leads to the formation of different isomers of the Pacman phosphanes. The chlorinated Pacman phosphane behaves highly dynamic in solution, inverting the orientation of its P-Cl units. In halogen exchange reactions, the chlorine substituents act as leaving groups, allowing the isolation of the fluorinated, brominated and iodinated Pacman phosphanes. By halide abstraction, a dicationic species is formed. This reaction is accompanied by a cooperative intramolecular redox-isomerism process leading to the oxidation of the phosphorus atoms to oxidation state +V.

The organically substituted Pacman phosphanes can act as multidentate ligands. As shown upon the coordination of coinage metal salts, not only linear diphosphane coordination is possible. Additionally, further coordination modes are realized under participation of the imine nitrogen atoms of the Pacman scaffold, among them distorted tetrahedral as well as “see-saw”-like or square planar coordination.

Overall, this work confirms the cooperative potential of the newly introduced Pacman phosphanes. Together with first results of follow-up chemistry, this provides the basis for manifold perspectives of this compound class in cooperative non-metal activation chemistry as well as in coordination chemistry and catalysis.

Zusammenfassung

Diese Arbeit beschreibt Untersuchungen über einen neuen Zugang zu Metall-freier Aktivierungschemie. Dafür werden Konzepte, die kooperative Reaktionen von Pacman Komplexen ermöglichen, auf die Phosphorchemie übertragen. Das Einführen von zwei Phopshor(III)-Einheiten in einen Calix[4]pyrrol-Imin-Liganden führte zu ersten Synthesen von Pacman-Phosphanen. Darin ist jedes Phosphoratom über zwei pyrrolische Stickstoffatome mit dem Liganden verbunden. Zusätzlich trägt jedes Phosphoratom ein Chloratom oder einen organischen Substituenten, abhängig von der verwendeten Phosphor-haltigen Ausgangsverbindung. Der sterische Anspruch der Substituenten führt zur Bildung verschiedener Isomere der Pacman-Phosphane. Das chlorierte Pacman-Phosphan zeigt in Lösung stark dynamisches Verhalten in Form von Inversion der P-Cl-Orientierungen. In Halogenaustauschreaktionen können die Chlor-Substituenten als Abgangsgruppen dienen und so die Synthese der fluorierten, bromierten und iodierten Pacman-Phosphane ermöglichen. Halogenid-Abstraktion führt zur Bildung eines Dikations. Die Reaktion geht mit kooperativer, intramolekularer Redox-Isomerie einher, die die Oxidation der Phosphoratome zu Phosphor(V) zur Folge hat.

Die organisch substituierten Pacman-Phosphane fungieren als multidentate Liganden. Die Koordination von Münzmetallen zeigt, dass nicht nur eine rein Phosphan-basierte, lineare Koordination möglich ist. Weitere Koordinationsmoden können durch die Beteiligung der iminischen Stickstoffatome des Pacman-Gerüsts realisiert werden, darunter verzerrt tetraedrisch, wippenartig und quadratisch planar.

Insgesamt bestätigt diese Arbeit das kooperative Potential der neu eingeführten Pacman-Phosphane. Zusammen mit ersten Ergebnissen zur Folgechemie bildet dies die Grundlage für vielfältige Perspektiven dieser Verbindungsklasse in der kooperativen Metall-freien Aktivierungschemie sowie in der Koordinationschemie und Katalyse.

to Edgar

Table of Contents

List of Abbreviations

18c6	18-crown-6
CCDC	Cambridge Crystallographic Data Centre
COD	cyclooctadiene
DA	donor-acceptor
DBU	1,8-diazabicyclo[5.4.0]undec-7-ene
DFT	density-functional theory
DMAP	4-dimethylaminopyridine
ELF	electron localization function
EPR	electron paramagnetic resonance
equiv.	equivalent(s)
ESP	electrostatic potential
exptl.	experimental
FLP	frustrated Lewis pair
^{i}Pr	*iso*-propyl
LB	Lewis base
LP	lone pair
LUMO	lowest unoccupied MO
MO	molecular orbital
NBO	natural bond orbital
NLMO	natural localized MO
NMR	nuclear magnetic resonance
ref.	reference
SCXRD	single crystal X-ray diffraction
SI	International System of Units
sim.	simulated
^{t}Bu	*tert*-butyl
OTf	triflate (CF_3SO_3)
THF	tetrahydrofuran
TMS	trimethylsilyl
xs	excess

Units of Measurement

The International System of Units (SI) is applied throughout this work. All derived units and their expression in terms of the SI base units are listed below:

Quantity	**Unit**	**Name**	**Conversion to SI base units**
Energy	kJ	Kilojoule	1 kJ = 1 × 10^3 m^2 kg s^{-2}
Frequency	MHz	Megahertz	1 MHz = 1 × 10^6 s^{-1}
	Hz	Hertz	1 Hz = 1 s^{-1}
Length	Å	Ångström	1 Å = 1 × 10^{-10} m
Pressure	mbar	Millibar	1 mbar =1 × 10^2 kg·m^{-1}·s^{-2}
Temperature	°C	Degree Celsius	ϑ/°C = T/K − 273.15
Time	d	Day	1 d = 8.64 × 10^4 s
	h	Hour	1 h = 3.6 × 10^3 s
	min	Minute	1 min = 60 s
Volume	mL	Millilitre	1 mL = 1 cm^3 = 1 × 10^{-6} m^3

List of Synthesized Compounds

Abbr.	Structural formula
1	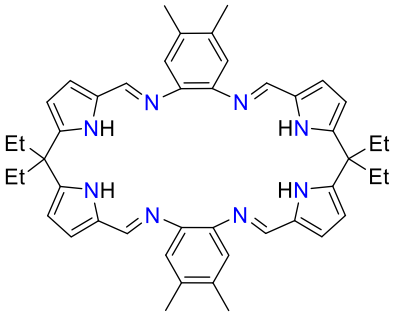
2R	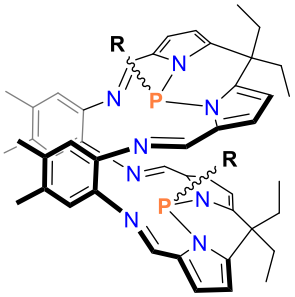 *endo-endo*: **R** = **F** *endo-exo*: **R** = **F**, **Cl**, **Br**, **I**, **N^{i}Pr$_2$**, **Ph** *exo-exo*: **R** = **NiPr$_2$**, **Ph**, **DMAP$^+$**
[3]X$_2$	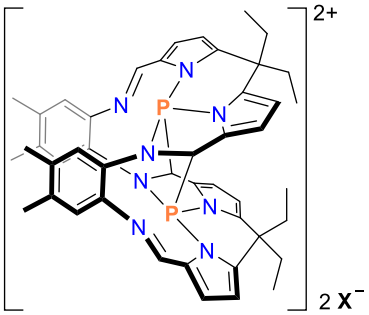 **X** = **Br**, **I**, **OTf**
[4][OTf]$_2$	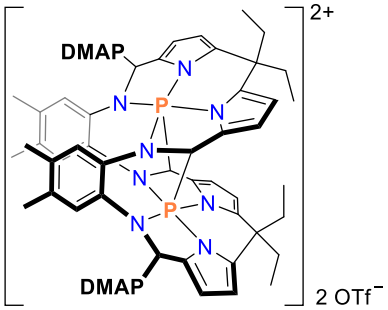

Abbr.	Structural formula
[5M]X	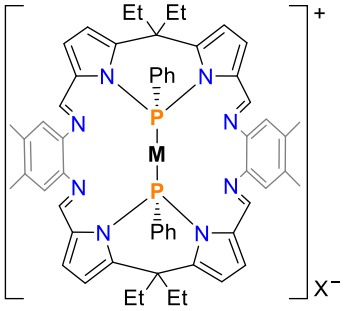 **M** = **Au**, X = Cl **M** = **Ag**, X = OTf **M** = **Cu**, X = OTf
[6M]X	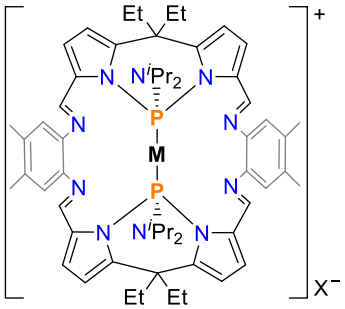 **M** = **Au**, X = [AuCl$_2$] **M** = **Ag**, X = OTf **M** = **Cu**, X = OTf
7	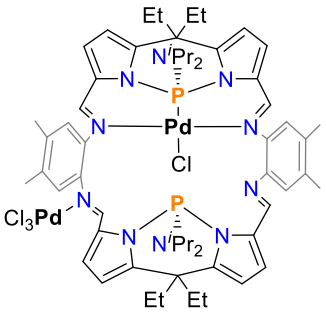

1 Motivation

The aim of this thesis is the development of a new, metal-free system, prospectively capable of small-molecule activation, including its synthesis and characterisation. Thereby, the target molecule (Figure 1) is inspired by coordination chemistry, in particular by Pacman complexes.[1–3] Composed of two linked chelators, Pacman ligands force two metal centres in close proximity to enable cooperative reactivity. To transfer these properties to non-metal chemistry, we want to replace the metal centres of Pacman complexes by phosphorus. Therefore, in a first step, different Pacman phosphanes should be synthesized, which can act as precursors for reactive species. To enable follow-up chemistry at the phosphorus centres, a leaving group on each phosphorus atom is necessary.

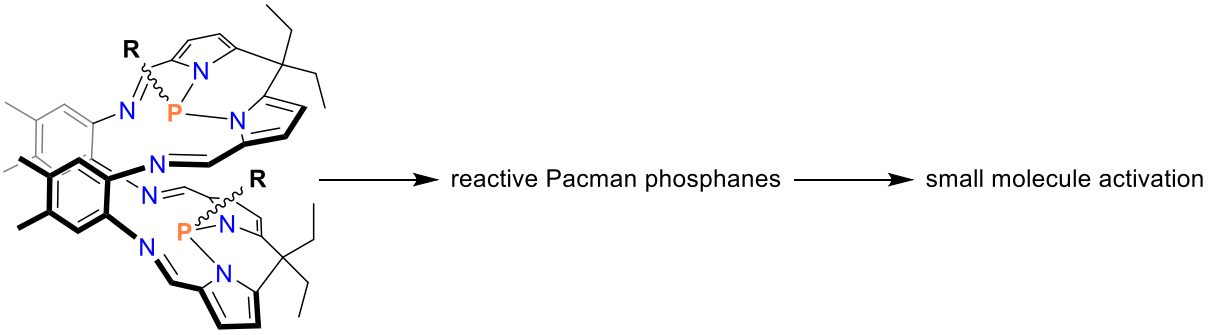

Figure 1. General depiction of target compound and concept of this and future work.

Besides the synthesis of Pacman phosphanes, the investigation of their properties is of interest to understand e.g. the influence of the substituents at the phosphorus atoms or the interaction between the imine nitrogen atoms and phosphorus atoms in the target molecule (Figure 1). The latter could play a significant role in the stabilization of reactive intermediates e.g. during reduction of the phosphorus centres, leading to a biradical, as well as upon formation of a (di-)cation or in future activation reactions of Pacman phosphanes.

2 Introduction

In nature, numerous complex reactions can be achieved by enzymes, which is often enabled by the cooperation of multiple reactive centres arranged close to each other at the active site of the enzyme.[4–6] To transfer this often highly selective and efficient reactivity to the lab, chemists try to mimic the conditions in the enzyme pockets, having multiple reactive centres in close proximity, with the aim of enabling cooperative reaction behaviour.[7] Most approaches are either based on interaction between a metal centre and its ligand or in-between two or more metal centres.[8–11] For the latter, two metals have to be brought in close proximity. To accomplish this, in the late 70s cofacial ligands were developed, in which two chelators are held in a parallel position by multiple linkers.[12–15] This concept has been extended to so-called Pacman ligands, of which the first examples are shown in Figure 2.[12,16] In contrast to cofacial ligands, the linkers connecting the two chelators are only located on one side of the molecule.[12] If a rigid spacer is used, even a single connection is sufficient (Figure 2, right).[16] This structural feature enables a flexibility regarding the distance of the two chelators, so that upon coordination of two metal centres by a Pacman ligand, its bite angle and hence the metal-metal distance can be adapted, for example, to allow additional coordination of substrates. Because the resulting movement is reminiscent of the figure in the video game "Pac-Man™",[17] it is referred to as "Pacman flexibility" which consequently led to the establishment of the term "Pacman ligand" for this ligand class.[18]

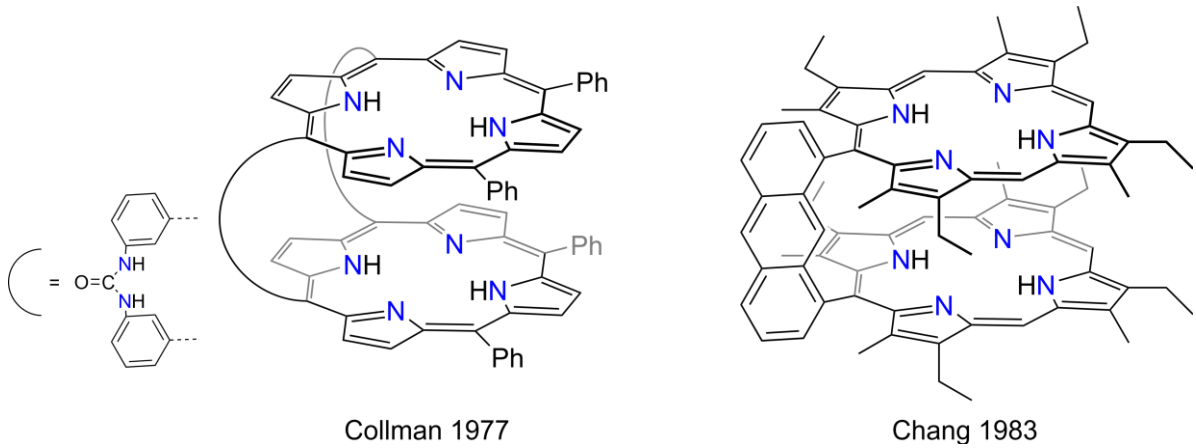

Figure 2. First examples of Pacman ligands (left: with two linkers; right: with one linker).[12,16]

The possibilities regarding coordination of metal centres by Pacman ligands are very diverse and include a high number of different metals. In most examples, both chelators coordinate the same type of metal but also mixed species are possible.[19,20] By coordination of additional ligands or variation of the chelating units in different Pacman ligands, multiple coordination environments can be realized, although the majority of Pacman ligands is build up by porphyrins.[3,21–23] Cooperative reactions investigated for Pacman complexes mainly cover the fields of energy and electron transfer between the two molecule halves as well as dioxygen reduction under contribution of both metal centres and (subsequent) oxygen transfer to organic molecules.[1,3,19,24]

While the porphyrin based Pacman ligands entail elaborate syntheses, in 2003, the groups of Love and Sessler independently introduced calix[4]pyrrole Schiff base ligands, which are easily synthesized in three steps in multi-gram scale.[25,26] The ligands themselves are very flexible in solution but adopt the typical Pacman conformation upon coordination of two metal centres (Figure 3, left). Numerous (earth-)alkali, transition metal, lanthanide and actinide complexes of this ligand type have been reported.[2]

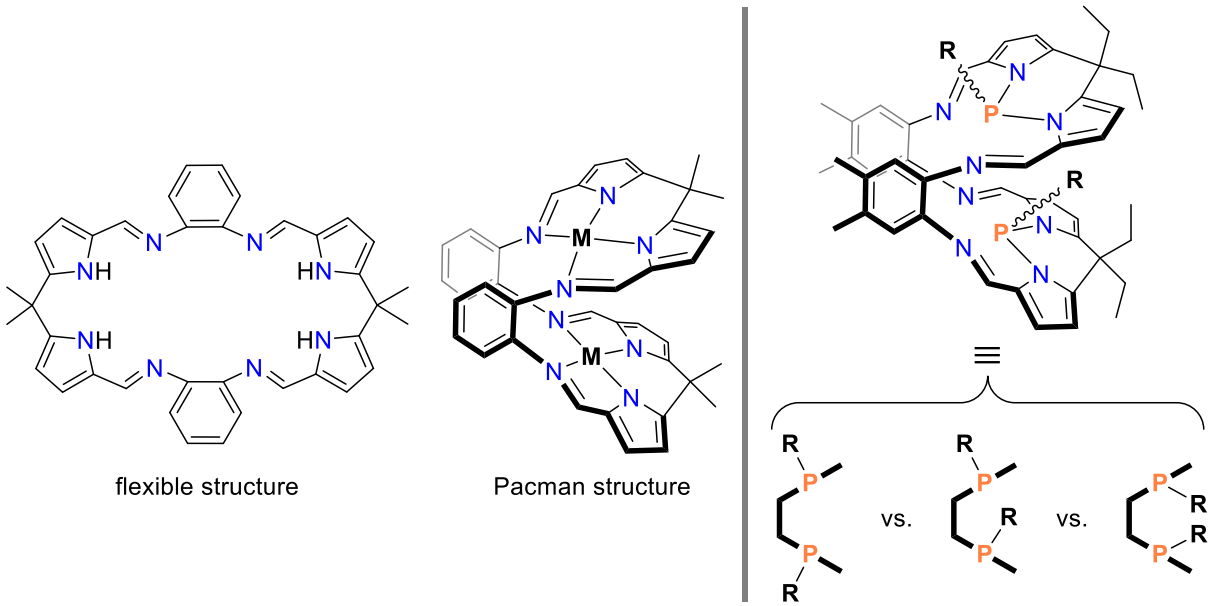

Figure 3. Calix[4]pyrrole Schiff base ligand and its metal complex (left, M = metal, e.g. Pd)[25,26] and target phosphane compound including simplified depiction of the *exo-exo*, *endo-exo* and *endo-endo* isomer (right).

Besides ongoing interest in metal containing cooperative systems, the role of cooperative non-metal chemistry increased significantly during the last decade. Three strategies cover the main achievements in metal-free small-molecule activation: frustrated Lewis pairs (FLP),[27] multi-

radical systems[28] and element ligand cooperativity.[29,30] As discussed above for metal based compounds, also in non-metal systems spatial proximity of two reactive centres is essential for cooperative behaviour. Although a transfer of the benefits of Pacman complexes to non-metal chemistry promises further progress in this field, non-metal complexes of Pacman ligands are not yet know (except for the uncoordinated, protonated ligands, cf. Figure 2 and Figure 3, left). Even examples of p-block complexes are rare and include only metals of the 13th (Al, Ga, In)[20,31,32] or 14th group (Ge, Sn and Pb).[33,34] For the first introduction of a non-metal into a Pacman ligand, we decided to use phosphorus. Calix[4]pyrrole Schiff base ligands seemed most suitable for first investigations, due to their comparably easy synthesis and the two neighboured pyrrole functions in each molecule half to which a phosphorus atom can be attached. In total, the ligand can therefore bind two phosphorus atoms (Figure 3, right). Moreover, an additional substituent and a lone pair are located on phosphorus(III) atoms. Due to the two P-R units in each Pacman molecule, different isomers defined by the orientation of the P-R bonds are possible: 1) an *exo-exo* isomer with both substituents located outside the molecules pocket, 2) an *endo-exo* isomer, in which one substituent is positioned inside the cavity and one outside and 3) a sterically crowded *endo-endo* isomer with both substituents in the cavity (Figure 3, right).

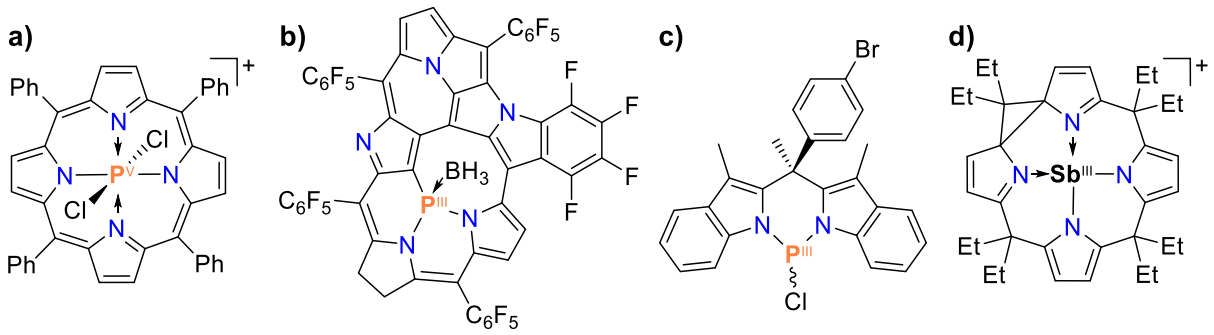

Figure 4. Pnictogen-containing molecules related to the target compound.[35–38]

Compared to our target molecule, only loosely related molecules have been reported so far. In all of them, the second phosphorus atom in spatial proximity is missing, so that they only represent one half of our targeted Pacman phosphanes. Porphyrins, which are often used to build up Pacman ligands, are known to bind phosphorus(V) but not phosphorus(III) (Figure 4a).[36] Nevertheless, three examples of phosphorus(III) porphyrinoids have been reported, of which the first is depicted in Figure 4b.[37,39,40] In those structures the phosphorus atoms do not bear a leaving group and are therefore not suitable for follow-up chemistry. A P-Cl unit bound

to a calix[2]pyrrole was presented in 2012 by the group of Richeson (Figure 4c).[35] Recently, the group of Greb published a heavier group 15 calix[4]pyrrole, the Sb^{III}-cation shown in Figure 4d.[38]

3 Results and Discussion

3.1 Synthesis of Pacman Phosphanes

3.1.1 Pacman Chlorophosphane (**2Cl**)

As starting material for the introduction of phosphorus to a calix[4]pyrrole Schiff base ligand, PCl_3 was chosen. Due to the chlorine substituents, the formation of P-N bonds to the pyrrole nitrogen atoms in the ligand should be possible by base assisted HCl elimination. Additionally, one chlorine atom remains on each phosphorus centre in the target molecule and thereby opens many possibilities for follow-up reactions.

Best results for the synthesis of the chlorinated Pacman phosphane (**2Cl**) were obtained from the reaction of Pacman ligand **1** with NEt_3 and addition of PCl_3 at −80 °C (Scheme 1). The reaction was also performed using DBU (diazabicycloundecene) as base but lower yields were achieved this way.[41]

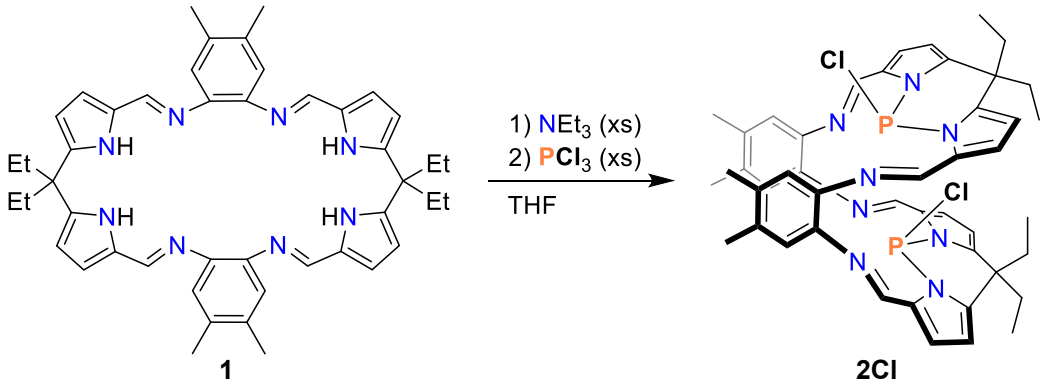

Scheme 1. Synthesis of Pacman chlorophosphane **2Cl**.[41]

In addition to **1**, other calix[4]pyrrole Schiff base ligands were tested for the synthesis of the respective chlorophosphane. They varied in the substitution of the phenylene linkers (hydrogen or methyl groups) and *meso*-carbon atoms in-between the two pyrrole units (phenyl or ethyl groups; Figure 5). In all cases, phosphorus could be introduced using NEt_3 as base, but with

ligands deviating from **1**, separation of the product from NEt_3·HCl was not possible due to solubility issues. For the ligand with hydrogen on the phenylene linkers and ethyl groups in *meso*-position, these problems were overcome by the usage of KH as base but the following reaction with PCl_3 was less selective, leading to very low yields.[41]

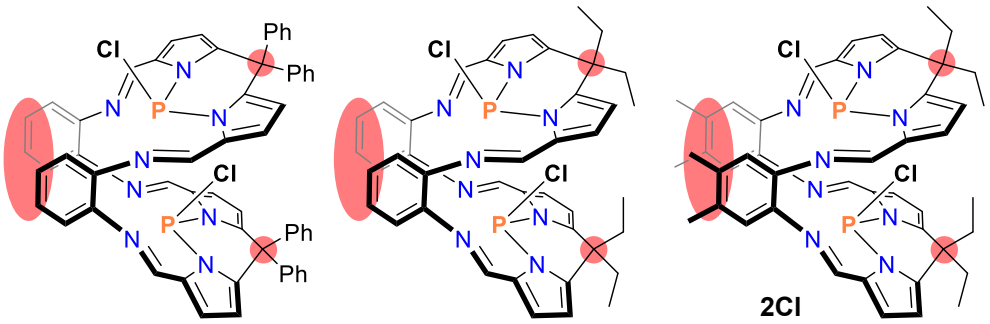

Figure 5. Pacman chlorophosphanes of different calix[4]pyrrole Schiff base ligands. Substitution areas marked in red.[41]

2Cl was crystallized from THF or benzene. According to SCXRD (single crystal X-ray diffraction) both molecular structures are very similar, therefore only the one received from benzene is discussed here (Figure 6).[41]

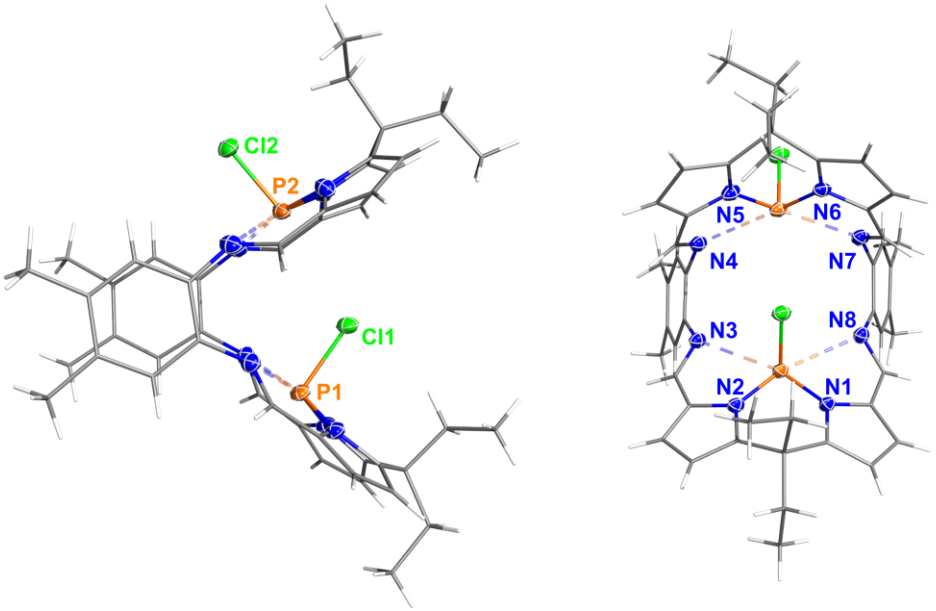

Figure 6. Molecular structure of **2Cl** in the crystal (left: side view, right: front view). Ellipsoids set at 50% probability at 123(2) K. Solvent omitted for clarity.[41]

Upon introduction of two phosphorus atoms, the molecule adopts the typical Pacman conformation, analogous to metal complexes of this ligand type. As expected, each phosphorus

atom is bound to two pyrrole nitrogen atoms in one molecule half and additionally one P-Cl bond remains intact during the reaction. The chlorine substituents in **2Cl** exclusively form the *endo-exo* isomer, in which chlorine atom Cl1 is located in the pocket of the Pacman molecule, while Cl2 is located outside (Figure 6). All bond lengths in **2Cl** lie in the expected range. Taking a closer look at the pocket of the Pacman phosphane, the two phosphorus atoms have an interatomic distance of 4.6383(9) Å, while the distance between the *endo*-chlorine atom Cl1 and the *exo*-substituted P2 is 3.3552(8) Å. The latter value is slightly shorter than the sum of the van der Waals radii (3.55 Å)[42] but no significant interaction was found in the NBO (natural bond orbital) analysis of **2Cl** (cf. Figure 7, left).[41] However, the electrostatic potential (ESP) of **2Cl** reveals the possibility of attractive dipole-dipole interactions between the negatively charged *endo*-chlorine and the positively charged *exo*-phosphorus atom (PBE-D3/*m*TZVP).[43]

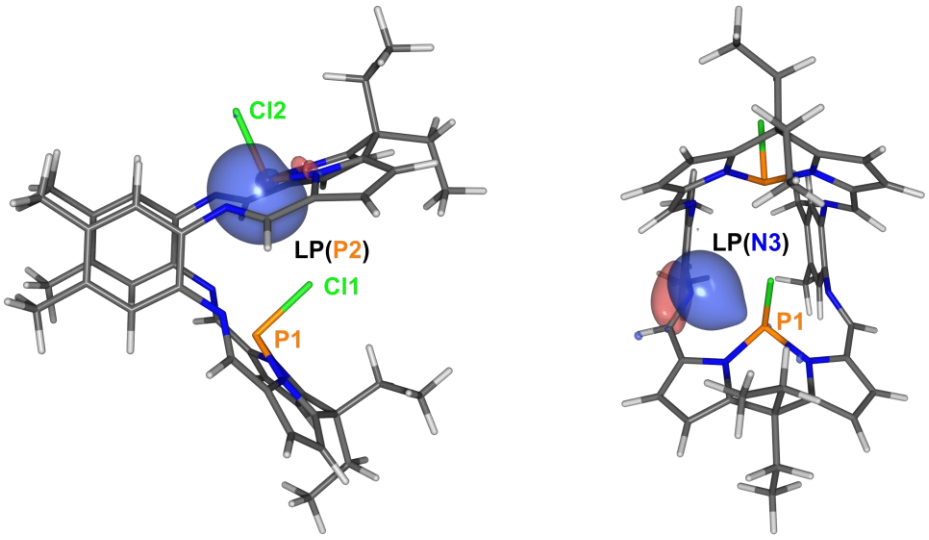

Figure 7. Natural localized molecular orbitals (NLMOs) of the lone pairs (LP) localized at the *exo*-substituted P2 atom of **2Cl** (left) and at the imine N3 atom (right). While the lone pair of P2 does not show any deformation towards Cl1, a slight deformation of the lone pair of N3 towards P1 is observed, in accordance with the respective donor-acceptor energies.[41]

In addition to the covalent bonds of the phosphorus atoms in **2Cl** with two pyrrole nitrogen atoms and a chlorine atom, the distances to the imine nitrogen atoms in the respective molecule half of 2.86(3) Å (averaged) are significantly shortened compared to the sum of the van der Waals radii of 3.35 Å.[42] The NBO analysis shows that this is not just due to limited space in the Pacman cavity but an effect of a small donor-acceptor interaction between the lone pairs of the imine nitrogen atoms and the antibonding orbital of the opposite P-N bonds with the pyrrole nitrogen atoms (Figure 7, right; PBE-D3/*m*TZVP). They amount to 31.3 kJ·mol^{-1} in the *endo*-half (including P1) and 59.1 kJ·mol^{-1} in the *exo*-half (including P2, also see Table 2, p. 36).[41]

Regarding follow-up chemistry towards more reactive phosphorus species, this interaction could be advantageous for the stabilization of reactive intermediates due to compensation of electron deficiency on the phosphorus atoms.

Not only in solid state, also in solution exclusively the *endo-exo* isomer of **2Cl** was observed. Two singlets are present in the $^{31}P\{^{1}H\}$ NMR spectrum with chemical shifts of 80.8 and 82.6 ppm. They belong to the two chemically inequivalent phosphorus atoms in the molecule but an exact assignment is impossible. Additionally, the NMR spectra show significant signal broadening at ambient temperature, indicating a dynamic behaviour of **2Cl**.[41] Detailed investigations of this process are presented in the following chapter.

3.1.2 Dynamic Behaviour of **2Cl**

The investigations regarding the dynamic behaviour of **2Cl** focused on NMR studies and quantum chemical calculations. Although ^{31}P is a very important NMR nucleus, mainly ^{1}H NMR spectra were used because they could deliver more information due to multiple signals, better resolution and higher signal-to-noise ratio.

In general, Pacman chlorophosphane **2Cl** can be divided in two chemically inequivalent halves of which one contains the *endo*-substituted and the other the *exo*-substituted phosphorus atom. This also affects the chemical shifts of the protons, so that for each type of protons in **2Cl** (e.g. the imine C-H functions or the methyl groups on the phenylene linkers) two signals are present in the ^{1}H NMR spectra (Figure 8, bottom), which we refer to as “double set of signals”. Of the two ethyl groups on each *meso*-carbon atom, one is directed in *endo*- and one in *exo*-direction. In combination with the orientation of the P-Cl function in the respective molecule half, four chemically inequivalent ethyl groups result, leading to four signals for CH_2- and CH_3-groups.[41]

As reported above for the $^{31}P\{^{1}H\}$ NMR spectra, also the signals in the ^{1}H NMR spectrum of **2Cl** are significantly broadened. Coupling patterns are neither resolved for the ethyl groups nor for the two pyrrole C-H functions. To find out, whether this is caused by a dynamic effect, an NMR sample of **2Cl** in toluene was heated to 100 °C. Although still broadened, the NMR spectra at this elevated temperature only show a single set of signals (Figure 8, middle).[41,43] This means that each pair of two signals for the same type of protons, which is caused at 25 °C due to the P-Cl-orientations, coalesces at high temperatures to form one single signal. Consequentially, the information about the *endo* or *exo* orientation of the P-Cl functions in **2Cl** is lost at elevated temperature. The signals in the NMR spectra at 100 °C are located at the

averaged chemical shift of the signals at 25 °C, meaning that no new isomer is formed upon heating. The observed effect is therefore only explained by a fast interconversion of the orientations of the P-Cl bonds (from *endo* to *exo* and at the same time from *exo* to *endo*, as depicted in the centre of Figure 9).[41]

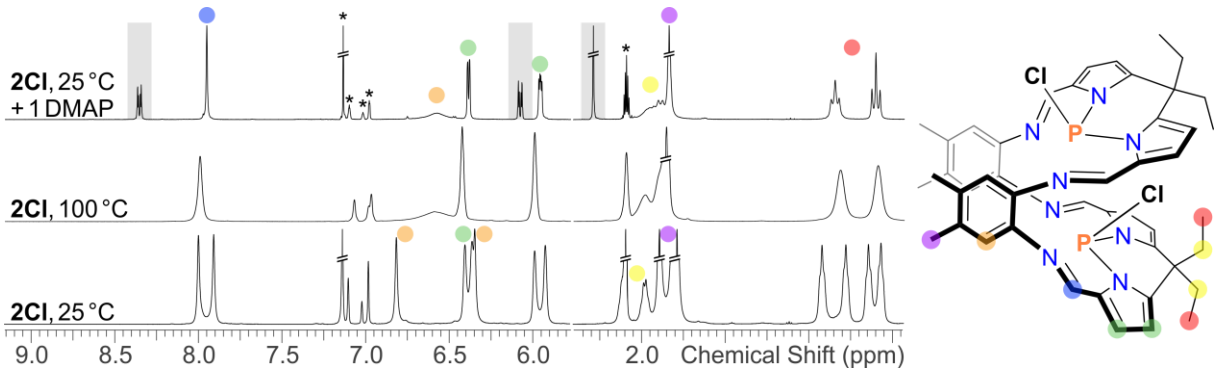

Figure 8. ^{1}H NMR spectra of **2Cl** in toluene at 25 °C (bottom) and 100 °C (middle) and with addition of one equiv. DMAP (top). Signals assigned to DMAP are marked in grey. Solvent signals indicated by asterisks.[43]

To investigate how these formal inversions can be explained, we calculated different reaction pathways. Relevant transition states and intermediates are depicted in Figure 9. The first process we investigated was an actual inversion on the phosphorus atoms. We were not able to find a transition state in which both phosphorus atoms invert simultaneously. Regarding the inversion of the phosphorus atoms in a stepwise process, the inversion barrier amounts to 205.5 kJ·mol^{-1} (Figure 9; calculation method: DLPNO-CCSD(T)/*m*TZVP), so that an actual inversion cannot explain the observed dynamic effect.[43]

Other possible explanations for the dynamic behaviour include the dissociation of the *exo*-P-Cl bond, so that either a radical or cation is formed as intermediate (Figure 9). The dissociated chlorine atom or chloride ion can attack the intermediate at both phosphorus atoms. If the recombination takes place on the original phosphorus atom, this leads to retention of the original structure. However, if the chlorine atom attacks the *endo*-substituted phosphorus atom, forming a new *exo*-orientated P-Cl bond, the *endo*-chlorine atom can be transferred to the opposite phosphorus atom resulting in the inverted isomer. Unfortunately, the dissociation of the P-Cl-bond is very disfavoured with Gibbs free reaction energies of 284.0 kJ·mol^{-1} for the homolytic and 197.6 kJ·mol^{-1} for the heterolytic bond dissociation (calculation method: DLPNO-CCSD(T)/*m*TZVP, the latter includes solvation correction for toluene). In addition, we measured EPR spectra of a solution of **2Cl** in toluene at 25 °C and at 100 °C, which did not

show any signals.[43] Overall, the reaction pathways including P-Cl bond dissociation were excluded as explanation for the dynamic behaviour.

As a third alternative, we took a look at an associative reaction mechanism, in which a chloride ion attacks the *endo*-substituted phosphorus atom in **2Cl**. In the resulting anionic intermediate, each phosphorus atom is included in an *exo*-P-Cl bond (Figure 9). Including solvation in toluene, the formation of the anionic intermediate is slightly exergonic compared to **2Cl** and free chloride ($\Delta_R G° = -1.6$ kJ·mol^{-1}, calculation method: DLPNO-CCSD(T)/*m*TZVP). In this intermediate, the *endo*-chlorine atom can easily switch between both phosphorus atoms with a maximum activation barrier of approx. 20 kJ·mol^{-1} (PBE-D3/*m*TZVP).[43] Therefore, depending on which *exo*-P-Cl bond of the intermediate is dissociated, **2Cl** is recovered in its original or inverted orientation. The crucial question concerning this reaction pathway was the origin of enough chloride ions to reach the observed reaction rate, but according to estimations based on simulation of the NMR spectra and the quantum chemical results, already chloride concentrations in the order of 10^{-6} mol·L^{-1} are sufficient. These can partly result from the dissociation of **2Cl** forming the cationic intermediate and a chloride ion, but probably also small amounts of impurities play a role (e.g. NEt_3·HCl from the synthesis).[43]

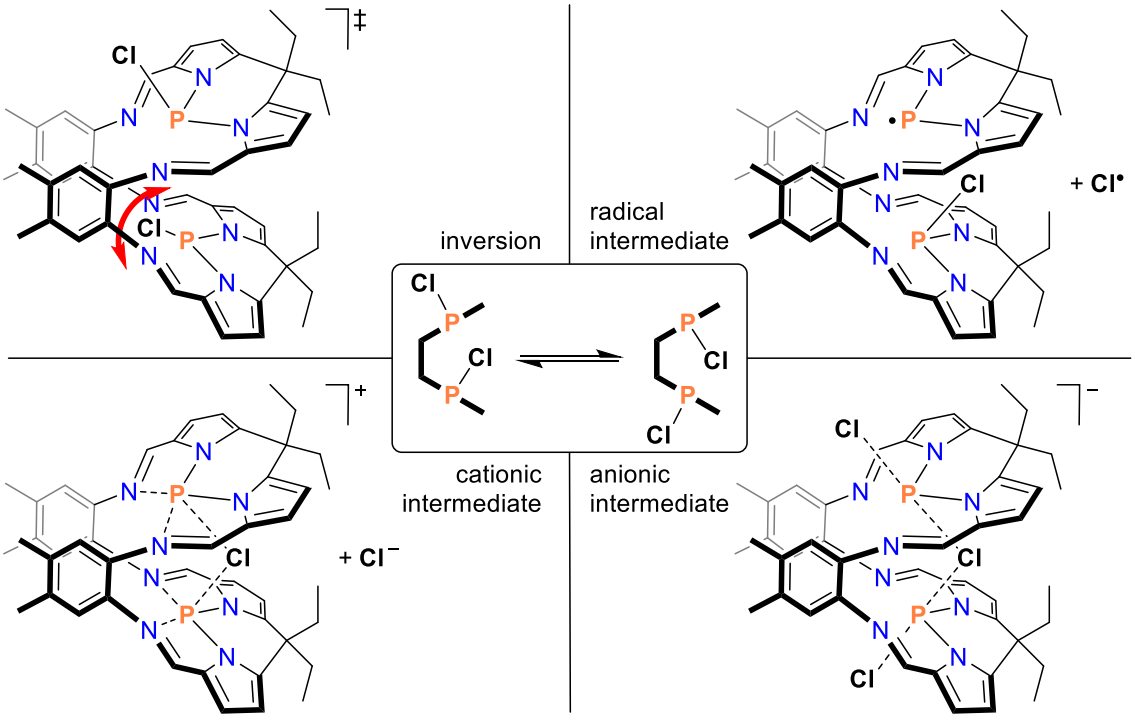

Figure 9. Possible transition states and intermediates for the inversion of **2Cl**.[43]

To test the assumption of an associative mechanism, two experiments were run. In the first one, one equivalent of DMAP (4-dimethylaminopyridine) was added to the solution of **2Cl** in

toluene to stabilize the cationic intermediate (Figure 9) and consequently receive a higher chloride concentration. As shown in Figure 8 (top), a very sharp NMR spectrum resulted from this mixture.[43] Only one set of signals was observed and it shows the same chemical shifts as the high temperature NMR spectrum of **2Cl**. In addition, the chemical shifts of DMAP are identical to pure DMAP. This shows that no significant amount of an adduct of **2Cl** and DMAP is formed, but that in the mixture the inversion of **2Cl** is strongly accelerated. In the second experiment, we added one equivalent of $[PPh_4]Cl$ as direct chloride source to a solution of **2Cl**, however, in the NMR spectra we did not see any effect, which we attributed to a very low solubility of $[PPh_4]Cl$ in toluene.[43]

For further investigation, we changed the solvent. In dichloromethane, NMR spectra of **2Cl** show separate signals for the *endo*- and *exo*-half of the molecule which are even less broadened, compared to toluene (Figure 10, bottom).[43] Nevertheless, a dynamic behaviour can be observed, which has been demonstrated e.g. by NMR studies at low temperature. At −40 °C even a small coupling of 3.2 Hz in-between the two phosphorus atoms is resolved.[41] Although in the more polar solvent, a higher concentration of chloride ions and therefore faster dynamic behaviour can be expected, the sharp NMR spectra are in line with the associative mechanism for the inversion. Applying solvent correction for dichloromethane in the calculations, the formation of the anionic intermediate (Figure 9) is disfavoured compared to **2Cl** and chloride by approx. 30 $kJ \cdot mol^{-1}$ (calculation method: DLPNO-CCSD(T)/*m*TZVP), leading to a slower exchange rate.[43]

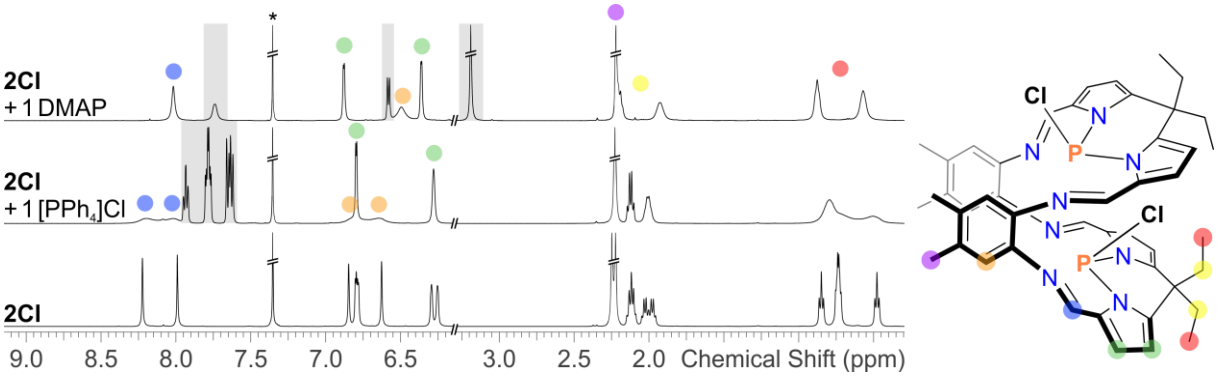

Figure 10. ^1H NMR spectra of **2Cl** in dichloromethane without (bottom) and with addition of one equiv. $[PPh_4]Cl$ (middle) or DMAP (top). Signals assigned to $[PPh_4]^+$ or DMAP are marked in grey, remaining benzene indicated by asterisk.[43]

In contrast to toluene, dichloromethane dissolves $[PPh_4]Cl$ and the addition of one equivalent to **2Cl** led to pronounced signal broadening in the NMR spectrum (Figure 10, middle).[41,43]

This indicates acceleration of the inversion behaviour and corroborates the associative reaction mechanism. The addition of DMAP to **2Cl** was repeated in dichloromethane, too. Unlike in toluene, significant changes in the chemical shifts of DMAP as well as **2Cl** (Figure 10, top) revealed the formation of a new species e.g. a DMAP adduct of **2Cl**, which has not yet been further characterized.[43] Further calculations and experiments excluded a significant role of bimolecular mechanisms or intermediate dicationic species (chapter 0; for further information, see ref. [43]).

Taking together all results, we are convinced that small amounts of chloride ions can induce the formal inversion of the two phosphorus centres in **2Cl** by the formation of an anionic intermediate.

During the high temperature NMR experiments with **2Cl** in toluene, we observed that NMR spectra measured at 25 °C *after* heating the solution to 100 °C are much sharper than spectra of untreated **2Cl**. The signals in the NMR spectra continuously broaden again, leading back to the original broad line width after approx. three weeks.[43] In Figure 11, a section of the ^{1}H NMR spectra of **2Cl** over the broadening period is depicted. It is clearly visible, that only sample signals (CH_2 and phenylene-CH_3 groups) and not the solvent are affected. Broken down to the molecular level, these observations mean that the inversion of the phosphorus centres is significantly slower after the sample was heated and only very slowly increases afterwards. An explanation for this behaviour are possible side reactions of chloride ions at high temperature, leading to lower chloride concentration and a slower exchange reaction. Over time, free chloride ions are reformed e.g. by P-Cl bond dissociation of **2Cl**.

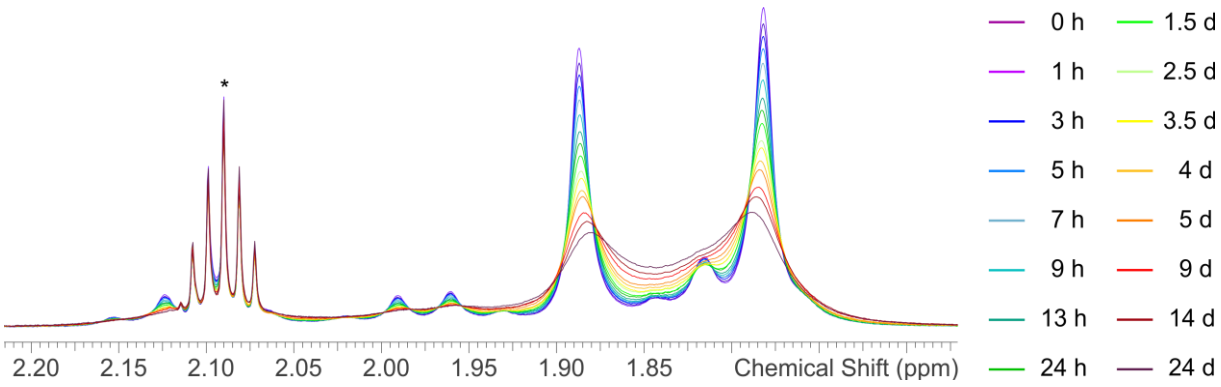

Figure 11. ^{1}H NMR spectra of **2Cl** (CH_2 and phenylene-CH_3 groups) in toluene at 25 °C after heating to 100 °C. Solvent signal (Ph-CD_2H) indicated by asterisk.[43]

In addition to **2Cl**, we synthesized Pacman phosphanes with organic substituents on the phosphorus atoms. Although these are not predestined for further functionalization due to a missing leaving group, their investigation can increase the general understanding of Pacman phosphanes.

3.1.3 Further Pacman Phosphanes

Using dichlorophosphanes $RPCl_2$ instead of PCl_3 in the reaction with Pacman ligand **1**, allowed the synthesis of Pacman phosphanes with organic substituents. By base assisted HCl elimination under reaction conditions very similar to those for **2Cl**, planar phenyl or more bulky diisopropylamino substituents were introduced, yielding the Pacman phosphanes **2Ph** and **2N^{i}Pr$_2$** (Scheme 2). For the synthesis of the latter, dichloromethane was used as solvent instead of THF to achieve reasonable reaction times.[44] In addition to the successful introduction of phenyl and diisopropylamino groups, we reacted Pacman ligand **1** with ^{t}BuPCl$_2$ but unselective product formation was observed.[45]

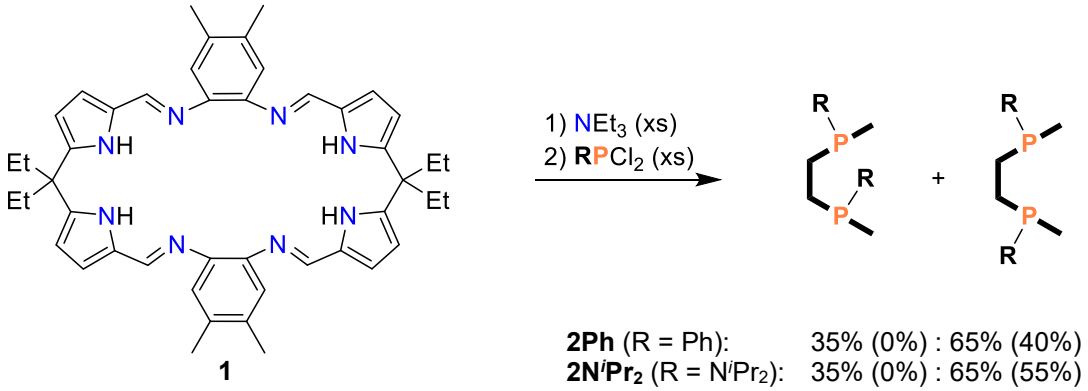

Scheme 2. Synthesis of **2Ph** and **2N^{i}Pr$_2$** (isolated yields in parentheses).[44]

$^{31}P\{^1H\}$ NMR spectra of the raw products of **2Ph** and **2N^{i}Pr$_2$** show three main signals. Two of them have a 1:1 ratio (**2Ph**: 57.7 ppm and 60.8 ppm; **2N^{i}Pr$_2$**: 70.1 ppm and 80.8 ppm) while the third one has a higher integral and is shifted slightly downfield (**2Ph**: 68.1 ppm; **2N^{i}Pr$_2$**: 83.2 ppm). In analogy to **2Cl**, the two signals in 1:1 ratio belong to the respective *endo-exo*-isomer. Due to the higher steric demand of the organic substituents in **2Ph** and **2N^{i}Pr$_2$** additionally the *exo-exo*-isomer is formed, causing the third signal. In both cases, the *endo-exo*:*exo-exo* ratio is approx. 1:2 (Scheme 2). The more symmetric *exo-exo*-isomer can be crystallized selectively enabling the isolation of pure *exo-exo*-**2Ph** (40%) and *exo-exo*-**2N^{i}Pr$_2$**

(55%).[44] Until now, we have not been able to isolate the *endo-exo*-isomers. Therefore, if not stated otherwise, the notations **2Ph** and **2N^{i}Pr$_2$** only refer to the *exo-exo*-isomers.

In solid state, **2Ph** forms a very symmetric cavity, although the overall symmetry is reduced to C_1 by a twisted ethyl group (Figure 12, left). The P···P-distance of 4.2368(6) Å is shorter than in **2Cl** where the *endo*-chlorine substituent widens in the cavity.[44]

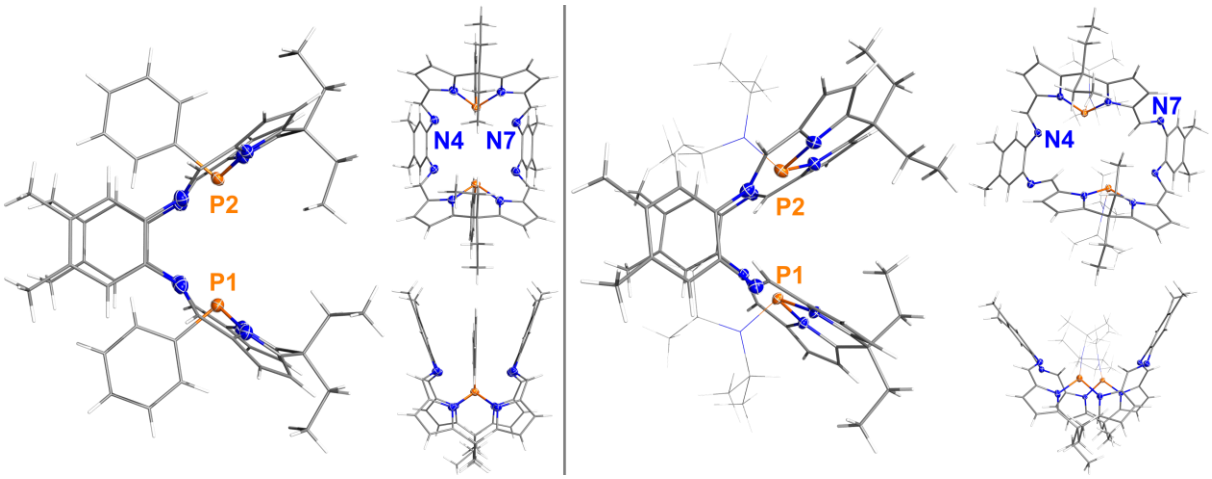

Figure 12. Side, front and top view on the molecular structures of **2Ph** (left) and **2N^{i}Pr$_2$** (right) in the crystal. Ellipsoids set at 50% probability at 203(2) K (**2Ph**) or 123(2) K (**2N^{i}Pr$_2$**). Solvent and disorder of one N^{i}Pr$_2$-group omitted for clarity.[44]

The structure of **2N^{i}Pr$_2$** is significantly distorted (Figure 12, right). Compared to **2Ph**, the distance between the two phenylene linkers in the backbone of the molecule is extremely widened. Additionally, two imine nitrogen atoms are rotated out of the molecule cavity (cf. N7 in Figure 12). These atoms interact with C-H atoms of pyrrole units in neighbouring **2N^{i}Pr$_2$** molecules.[44] Interestingly, the P···P distance (4.281(2) Å) is not much elongated by the distortion. In solution, **2N^{i}Pr$_2$** adopts a higher symmetry (C_{2v}), visible in the NMR spectra, where one sharp set of signals is observed. This means that all imine functions of the molecule become equivalent in solution or that their rotation is faster than the NMR time scale.[44]

Neither for **2Ph** nor for **2N^{i}Pr$_2$** any sign of dynamic inversion processes regarding the phosphorus centres like in **2Cl** was observed. In addition, we did not find evidence of an interconversion of the two isomers (*exo-exo* to *endo-exo* or the other way around) for these Pacman phosphanes.

Due to the *exo-exo* orientation of the substituents in **2Ph** and **2N^{i}Pr$_2$**, the free electron pairs of both phosphorus atoms are directed inside the Pacman cavity. This is an outstanding

qualification to use these molecules as bidentate phosphane ligands for the coordination of metals in the Pacman cavity. First examples for this application are presented in chapter 3.3.

The different substituents of the three Pacman phosphanes presented in this chapter were introduced together with the phosphorus atom. In the next chapter the reactivity of the chlorinated Pacman phosphane **2Cl** is presented, which *inter alia* allowed the synthesis of further Pacman phosphanes by halogen exchange reactions.

3.2 Reactivity of Pacman Phosphanes

3.2.1 Halogen Exchange Reactions of **2Cl**

Having seen the inversion of the phosphorus centres in **2Cl**, which was not observed for the Pacman phosphanes with organic substituents **2Ph** and **2N^{i}Pr$_2$**, we wanted to investigate the effects on the dynamic behaviour upon exchange of the chlorine by lighter and heavier halogens.

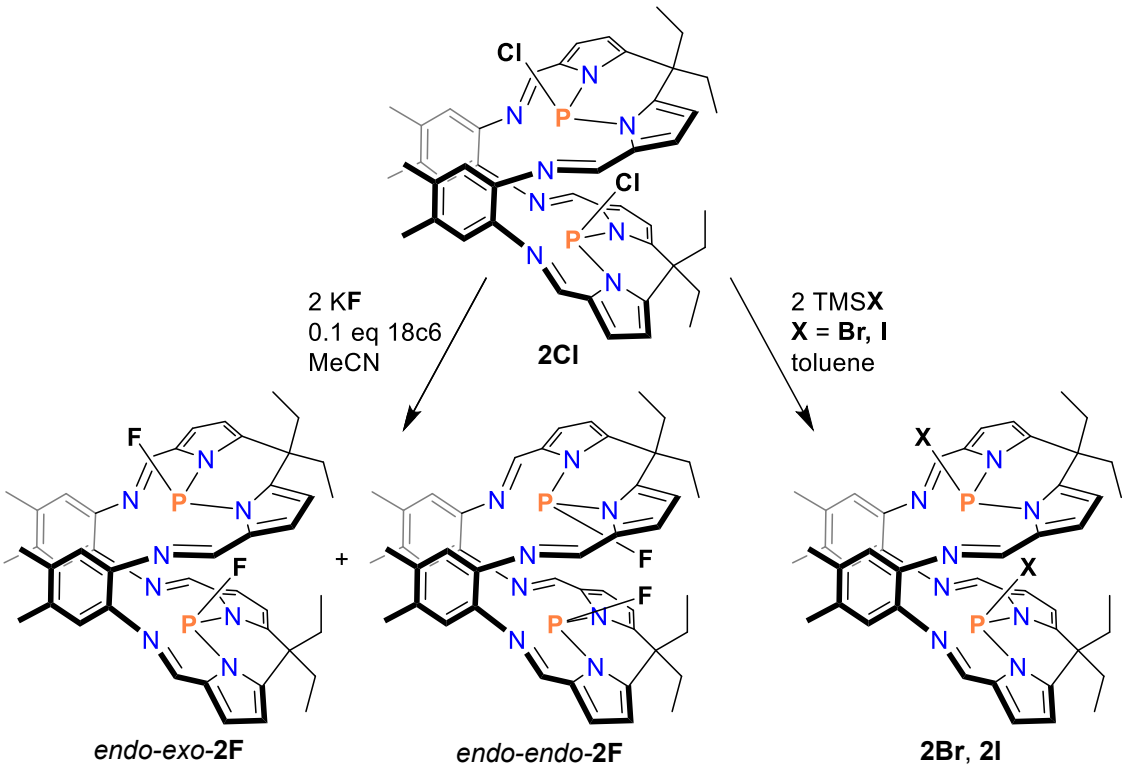

Scheme 3. Halogen exchange reactions of **2Cl** yielding *endo-exo*-**2F** and *endo-endo*-**2F** as well as **2Br** and **2I**.[43]

Because the introduction of a PF function analogously to the synthesis of **2Cl** would have afforded working with gaseous, toxic PF_3, we decided to use **2Cl** as precursor and exchange the chlorine by fluorine atoms. Therefore, we tried different fluorination agents (SbF_3,[46] $AgBF_4$[47] and KF[47]) of which KF in combination with 18-crown-6 delivered a complete and selective exchange (Scheme 3). Depending on the amount of crown ether (0.1 or 1 equiv.), the reaction took between five days and a few hours. Without crown ether, no exchange reaction was observed.[43]

Although the ^{31}P chemical shifts were not much affected in this reaction, ^{31}P-^{19}F couplings proved successful chlorine-fluorine exchange. Like in the syntheses of **2Ph** and **2N^{i}Pr$_2$**, upon halogen exchange two different isomers of **2F** are formed. From NMR spectra, one can be identified as the *endo-exo* isomer due to two inequivalent phosphorus and fluorine atoms. The second isomer is a symmetric one, in which the phosphorus and fluorine atoms are equivalent, respectively. Due to better solubility of the *endo-exo*-isomer in acetonitrile, it can be extracted from the mixture and crystallized selectively (molecular structure comparable to Figure 13, middle, without dichloromethane molecules or displayed in ref. [43]).[43]

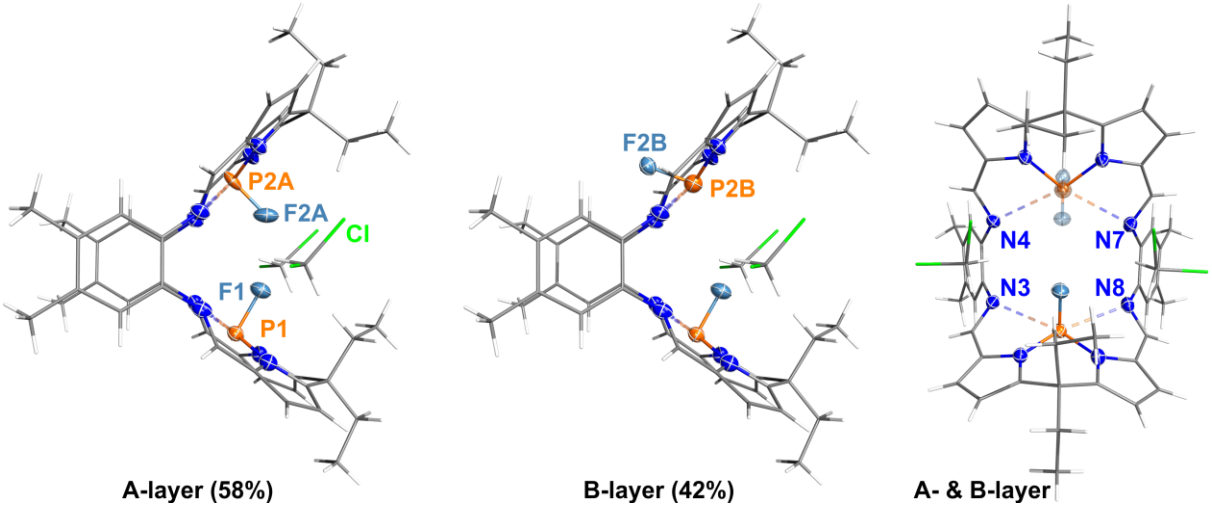

Figure 13. Side view on the A-layer (left) and the B-layer (middle) as well as front view on both layers (right) of the molecular structure of **2F** in the crystal. Ellipsoids set at 50% probability at 173(2) K. Additional solvent and disorder of one ethyl group omitted for clarity.[43]

Crystallization of the residue (after extraction of *endo-exo*-**2F** from the mixture) from dichloromethane yielded crystals in which both isomers co-crystallized including 42% of the *endo-exo*-isomer. In contrast to **2Ph** and **2N^{i}Pr$_2$**, **2F** does not form the *exo-exo*-isomer but the sterically crowded *endo-endo*-isomer (Figure 13). Two dichloromethane molecules are located in the Pacman cavity widening the P···P-distance by 0.182(9) Å compared to isomeric pure

endo-exo-**2F**. Coupled cluster calculations predict *endo-exo*-**2F** as energetically most favoured, followed by the *exo-exo*-isomer ($\Delta G° = 23.8$ kJ·mol^{-1}) while *endo-endo*-**2F** is highest in energy (32.2 kJ·mol^{-1}, calculation method: DLPNO-CCSD(T)/*m*TZVP). Including the two dichloromethane molecules observed in the single-crystal structure (Figure 13) in the calculations, the energetic relation of the observed isomers changes dramatically. While the *exo-exo*-isomer stays significantly higher in energy, e*ndo-endo*-**2F** and *endo-exo*-**2F** become nearly degenerate with the *endo-endo*-isomer even slightly favoured (−4.5 kJ·mol^{-1}; calculation method: DLPNO-CCSD(T)/*m*TZVP).[43]

In solution, both isomers display the distinct coupling patterns of an ABXY (*endo-exo*-**2F**) and AA'XX' spin system (*endo-endo*-**2F**) in the $^{31}P\{^{1}H\}$ and $^{19}F\{^{1}H\}$ NMR spectra (Figure 14). Besides the direct coupling within each P-F unit of approx. 1300 Hz significant through-space couplings in-between the two P-F functions are visible. In the *endo-exo*-isomer, the through space coupling of P^X and F^B (Figure 14) amounts to 132 Hz, very comparable to the coupling of the two fluorine atoms in *endo-endo*-**2F** of 128 Hz.[43] It should be noted, that the AA'XX' coupling pattern of the *endo-endo*-isomer does not contain triplets. The "side bands" have slightly different distances to the central signals parts.

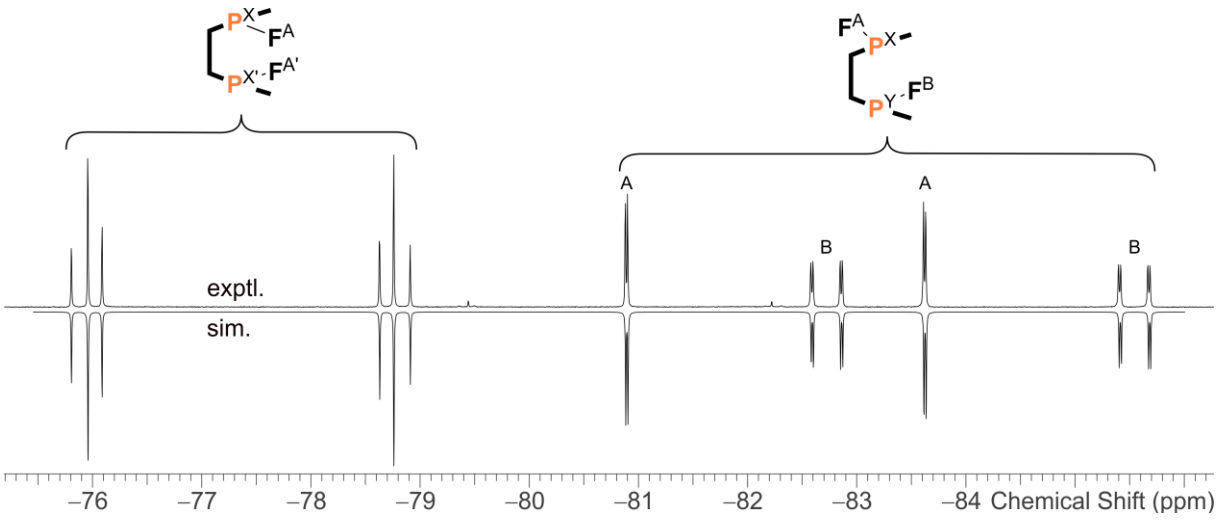

Figure 14. Experimental (top) and simulated (bottom) $^{19}F\{^{1}H\}$ NMR spectrum of the isomeric mixture of **2F** in dichloromethane.[43]

For both isomers, no fast inversion of the phosphorus centres as known from **2Cl** was observed. But if pure *endo-exo*-**2F** or the crystallized isomeric mixture with a ratio of 58:42 (*endo-endo*:*endo-exo*) were dissolved in dichloromethane, slow interconversion of the two isomers was found. After several days, both solutions reached the equilibrium ratio of approx. 1:4,

showing that in the presence of dichloromethane, both isomers are nearly degenerate in energy, although in contrast to the calculations (see above) *endo-exo*-**2F** is slightly preferred. DMAP and especially fluoride ions accelerated the interconversion in dichloromethane, while no change in the concentrations was observed in toluene.[43]

Since the reaction of **1** with PBr_3 was unselective, the heavier halogens bromine and iodine were introduced to **2Cl** by halogen exchange, too. As exchange reagents the TMS-halides (TMS = trimethylsilyl) were used, added slowly to a cooled solution of **2Cl** in toluene (Scheme 3). In NMR spectra of the raw products received after drying of the reaction solutions, a downfield shift of the ^{31}P signals was observed, indicating successful exchange reactions to **2Br** and **2I**. Unfortunately, crystallisation and further purification of both compounds was impossible. Therefore, information about the structure of these two Pacman phosphanes was only obtained from the collected NMR spectra. The ^{1}H NMR spectrum of **2Br** resembles the one of **2Cl**, although the signals are broader, suggesting that the overall structure remains intact upon the exchange reaction. The two signals in the ^{31}P NMR spectrum (81.6 pm and 83.5 ppm) additionally prove the *endo-exo*-structure. The NMR spectra of **2I** are further broadened compared to **2Cl** and **2Br**, impeding their interpretation. Nevertheless, the overall picture including ^{31}P NMR shifts of 106.4 ppm and 108.5 ppm indicates the formation of **2I**.[43]

The increasing broadening of the NMR spectra from **2F** over **2Cl** and **2Br** to **2I** due to accelerated inversion on the phosphorus atoms emphasizes the crucial role of the halogen on the dynamic behaviour. Additionally this trend confirms the assumption of an associative mechanism for the dynamic process (cf. chapter 0), because due to less strong phosphorus-halogen bonds and increasing stability of the halide ions going from fluorine to iodine, the concentration of halide ions is supposed to be higher in solutions of the heavier Pacman halophosphanes enabling higher inversion rates.[43]

During NMR experiments and crystallization attempts of **2Br** and **2I** we noticed that in polar solvents both Pacman phosphanes are converted into a new, ionic species by phosphorus halogen bond dissociation. The dicationic reaction product is presented in detail in the following section.

3.2.2 Halide Abstraction from **2Cl**, **2Br** and **2I**

Having in mind small-molecule activation with Pacman phosphanes, one possibility of transformation into a more reactive species is the generation of electron deficient phosphorus centres. Phosphorus cations are e.g. known to react with different E-H (E = B, C, Si, N, O),[48–50] C-F[51] or C-Si[51] bonds. Using **2Cl** as starting material, electron deficiency can be achieved by chloride abstraction from the phosphorus atoms, which should lead to two cationic phosphorus centres in an overall dicationic Pacman phosphane $\mathbf{2}^{2+}$ (Figure 15). The donor-acceptor interactions of the lone pairs of the imine nitrogen atoms, as observed for **2Cl** and other Pacman phosphanes, could partly compensate the electron deficiency of the phosphorus atoms.

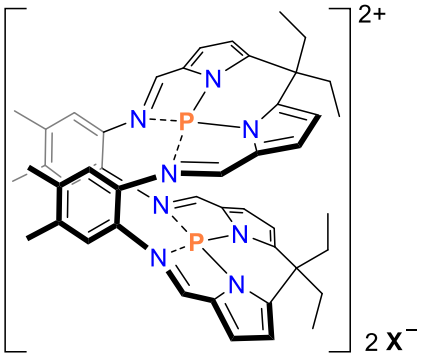

[2]X₂

Figure 15. Structure of the assumed dication $\mathbf{2}^{2+}$ formed upon halide abstraction from **2Cl**.

To realize this reaction experimentally, **2Cl** was reacted with two equivalents of AgOTf in dichloromethane or acetonitrile using the formation of AgCl as driving force (Scheme 4). Upon the reaction, the solution turned dark red and the ^{31}P NMR signals shifted significantly upfield to −81.4 ppm corresponding to the reaction product **[3][OTf]₂**.[41] Alternatively, we observed that the heavier halophosphanes **2Br** and **2I** undergo phosphorus-halogen bond dissociation in polar solvents (**2Br**: acetonitrile; **2I**: dichloromethane, acetonitrile) without any further reagent, forming **[3]Br₂** and **[3]I₂**, respectively (Scheme 4). NMR tracing of the dissociation reactions revealed concentration changes in line with first order kinetics and activation barriers of approx. 100 kJ·mol^{-1}, in line with reaction times of several hours to days.[43]

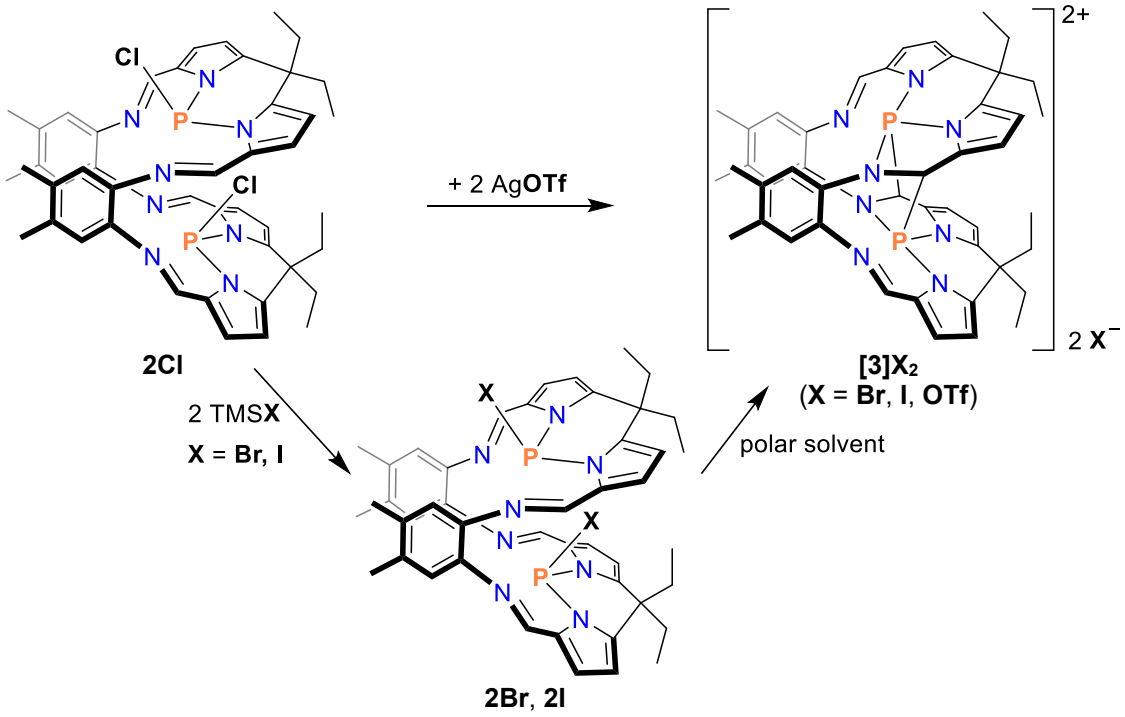

Scheme 4. Two reaction pathways to ionic **[3]X₂** (X = Br, I, OTf).[41,43]

The NMR spectra of the reaction products already indicated that not the desired dication $\mathbf{2}^{2+}$ was formed upon halide abstraction. This presumption was confirmed by SCXRD of all three ionic species **[3]X₂** (X = Br, I, OTf). The molecular structure of the dication $\mathbf{3}^{2+}$ is very similar in all three salts, indicating only weak interaction with the counterions.[41,43] Therefore, in the following, the molecular structure of **[3]Br₂** is discussed exemplarily for all salts **[3]X₂**.

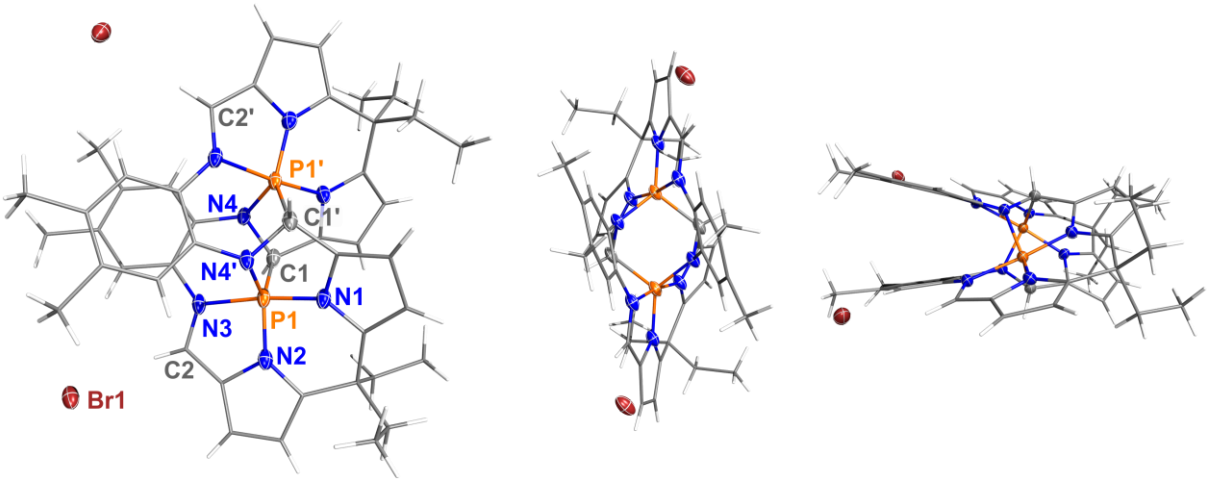

Figure 16. Side, back and top view on the molecular structure of **[3]Br₂** in the crystal. Ellipsoids set at 50% probability at 123(2) K. Solvent omitted for clarity. Symmetry code (‘): −x, y, ½−z.[43] For a better impression of this complex structure, we recommend the 3D model available at the CCDC data base (www.ccdc.cam.ac.uk/structures/) under the CCDC number 2204016 (**[3]Br₂**) or 2095508 (**[3][OTf]₂**).

Although the successful phosphorus-halogen bond dissociation is clearly evident from the molecular structure of **[3]Br$_2$** (Figure 16), the phosphorus centres in the resulting C_2-symmetric dication **3**$^{2+}$ are not only stabilized by donor-acceptor interactions with the imine nitrogen atoms (cf. Figure 15). Instead, in the strongly distorted Pacman structure, two newly formed P-C bonds (P1-C1, 1.875(3) Å) connect the two molecule halves. In the starting materials, these carbon atoms were part of imine double bonds which have only single bond character in **3**$^{2+}$ (C1-N4, 1.502(4) Å). The respective nitrogen atom is now bound to the phosphorus atom in its own molecule half (P1'-N4, 1.711(2) Å). A trigonal bipyramidal environment of the phosphorus atoms is completed by a short contact to the still iminic nitrogen atom in the respective molecule half (P1···N3, 1.895(2) Å).[43]

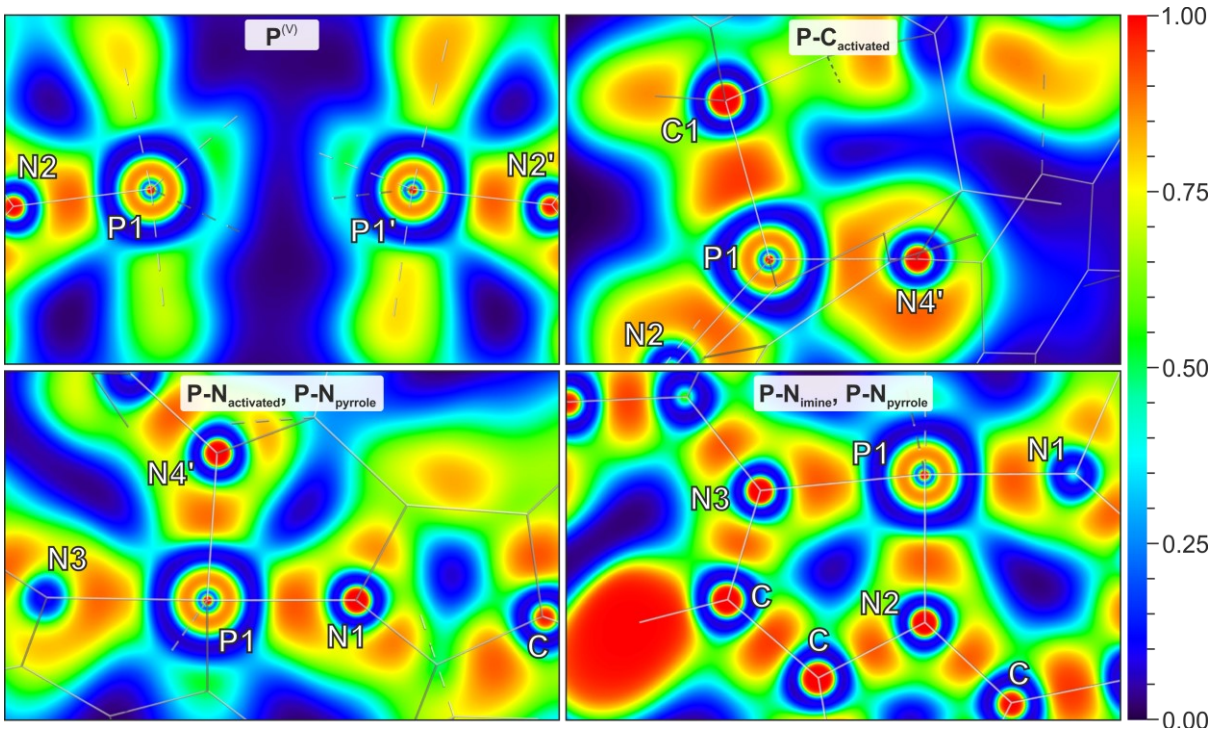

Figure 17. ELF of **3**$^{2+}$ around phosphorus atom P1 with focus on different interactions (PBE-D3/*m*TZVP; for atom assignment, see Figure 16).[41] ELFs plotted using the program *Multiwfn*.[52]

Regarding the bonding situation of the phosphorus atoms in **3**$^{2+}$, according to calculations the P-C bond can be regarded as nearly unpolarised covalent bond (calculation method: PBE-D3/*m*TZVP). Among the P-N-bonds, three are very similar. The interaction of the phosphorus atom with the two pyrrole nitrogen atoms (N1, N2) and the former iminic, now activated nitrogen atom N4' can be described as polarized covalent bonds. The interaction with the still iminic nitrogen atom N3 has to be treated separately. As indicated by the elongated distance compared to the other P-N bonds, the Wiberg bond index for the bond including N3 is the

lowest (0.52 vs. 0.64-0.78). Additionally, the electron density in the electron localization function (ELF) shows a strong deformation of the electron density towards the nitrogen atom (Figure 17). Overall, the P1-N3 interaction should not be interpreted as classical covalent bond but shows a strong donor-acceptor character. Regarding the phosphorus atoms themselves, lone pairs were found neither in the NBO analysis nor in the ELF (Figure 17), confirming an oxidation state of +V for the phosphorus atoms, in line with their trigonal bipyramidal environment.[41]

Compared to the desired dication $\mathbf{2}^{2+}$, $\mathbf{3}^{2+}$ is energetically favoured by 72.9 kJ·mol^{-1} (calculation method: DLPNO-CCSD(T)/*m*TZVP). For the conversion of one isomer to the other, a single transition state for a concerted mechanism was found. This is thermally accessible starting from $\mathbf{2}^{2+}$ ($\Delta_r G^{\ddagger}$ = 92.0 kJ·mol^{-1}) but regarding the energy difference between the isomers, the reverse reaction starting from $\mathbf{3}^{2+}$ is hardly possible ($\Delta_r G^{\ddagger}$ = 164.9 kJ·mol^{-1}).[41] Mechanistically, we therefore conclude that first, double halide abstraction of the Pacman halophosphanes **2Cl**, **2Br** or **2I** occurs, leading to intermediate formation of $\mathbf{2}^{2+}$. In a following concerted oxidative addition, the cationic phosphorus centres cooperatively attack one imine C-N bond in each molecule half, each forming a new P-C and P-N bond to the different imine units. This reaction step includes the oxidation of the phosphorus atoms from oxidation state +III to +V, so that it can be regarded as redox-isomerism, as also discussed e.g. for the antimony-calix[4]pyrrole presented in the introduction (cf. Figure 4d).[38,43]

Due to the high oxidation state of the phosphorus atoms and their poor accessibility for substrates due to the numerous bonding partners, $\mathbf{3}^{2+}$ does not seem as suitable for activation chemistry as $\mathbf{2}^{2+}$. Therefore, we investigated different approaches to synthesize $\mathbf{2}^{2+}$ or related species. The energy profile of the oxidative addition raised the question whether intermediately formed $\mathbf{2}^{2+}$ is accessible at low temperatures. We therefore performed a low-temperature NMR experiment to trace the reaction of **2Cl** with an excess of AgOTf (> 2 equivalents) at −30 °C. At this temperature, full conversion of **2Cl** and formation of multiple intermediates but not $\mathbf{3}^{2+}$ was observed. Although these species seemed to be stable up to −20 °C according to the measurements, a reaction in higher scale did not allow the isolation of any intermediate, hampering their identification.[45] A different approach to produce $\mathbf{2}^{2+}$, was to heat a solution of $\mathbf{3}^{2+}$ to reverse the oxidative addition process *in situ*. In a respective NMR experiment, no broadening or shift of the signals was observed, verifying the high barrier calculated for the reverse reaction (see above).[41]

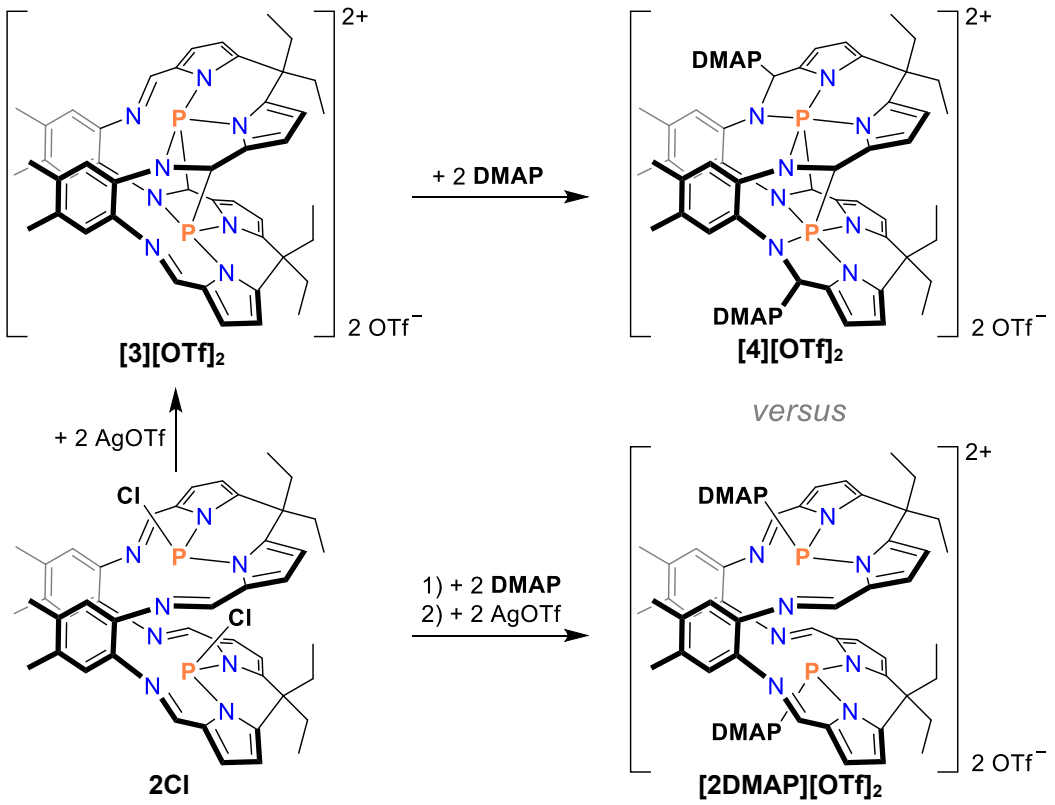

Scheme 5. Formation of **[4][OTf]$_2$** (top) or **[2DMAP][OTf]$_2$** (bottom) depending on the order of addition of AgOTf and DMAP.[45]

In order to lower the barrier for the reverse reaction of the oxidative addition process, stabilization of the phosphorus centres by a Lewis base (LB) was considered. Therefore, **[3][OTf]$_2$** was reacted with two equivalents of DMAP (Scheme 5), leading to an orange solution (in contrast to dark red **[3][OTf]$_2$**). Unfortunately, the ^{31}P NMR shift of the product resembled the shift of **3**$^{2+}$ (−85.4 ppm vs. −81.4 ppm), indicating minimal influence of the reaction on the phosphorus atoms. This was confirmed by SCXRD, demonstrating that the DMAP is not bound to the phosphorus, but to the carbon atom of the imine bond in **3**$^{2+}$ yielding dication **4**$^{2+}$. The molecular structure of **[4][OTf]$_2$** is depicted in Figure 18 (left) and very much resembles **3**$^{2+}$. The main difference of **4**$^{2+}$ compared to **3**$^{2+}$ is the interaction of the former planar, imine carbon atom C2 with the DMAP molecule (C2-N9: 1.498(4) Å) leading to a quarternization of C2. The former imine C2-N3 double bond is significantly elongated to 1.443(6) Å (**3**$^{2+}$: 1.315(4) Å) but still shorter than the comparable C1-N4 distance (1.500(5) Å). The bonding situation around the phosphorus atoms is only slightly affected by the addition of the DMAP. Due to a shortening of the P1-N3 distance by 0.110(6) Å to 1.785(3) Å, it is now in the same region as the other P-N interactions. At the same time, the opposite P1-N1 distance is slightly elongated by 0.040(6) Å, while all other bonds of the phosphorus atoms do not significantly change.[45]

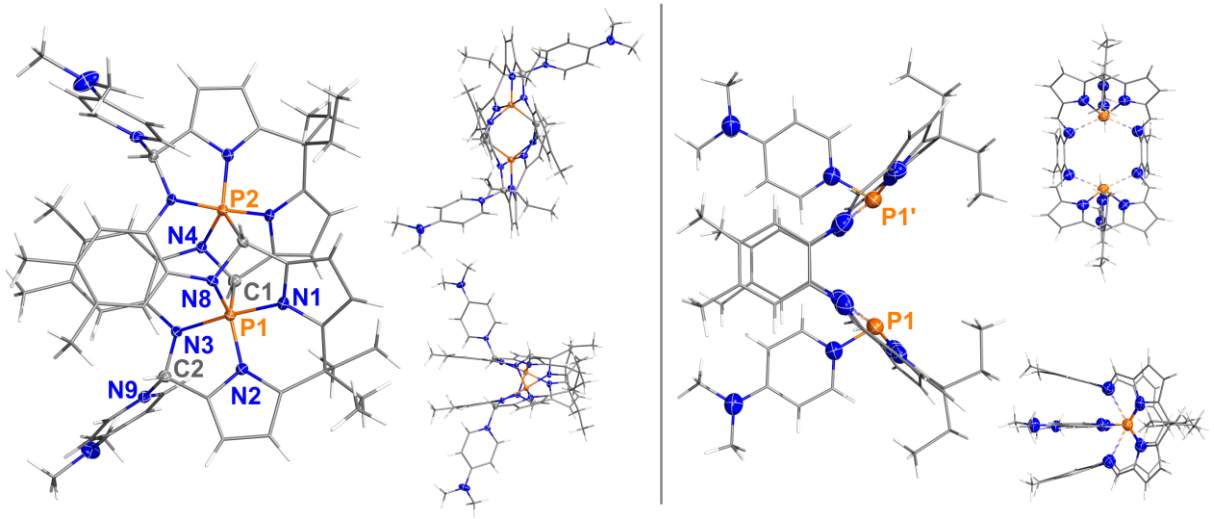

Figure 18. Side, top and back or front view on the molecular structures of **[4][OTf]$_2$** (left) and **[2DMAP][OTf]$_2$** (right) in the crystal. Ellipsoids set at 50% probability at 123(2) K. Solvent omitted for clarity. Symmetry code (‘): 1/2−x, 3/2−x, z. Structure of **[2DMAP][OTf]$_2$** results of low quality data set (see appendix for crystallographic details).[45]

The reaction of $\mathbf{3}^{2+}$ with DMAP did not lead to the desired reversion of the inner redox reaction. Hence, in a next step, we decided to trap the putative *in-situ* formed dication $\mathbf{2}^{2+}$ before the oxidative addition can take place. Therefore, **2Cl** was mixed with DMAP before the halide abstraction by addition of AgOTf. During the reaction, the yellowish/orange colour was maintained, indicating that no dark red $\mathbf{3}^{2+}$ was formed. In addition, a ^{31}P NMR shift of 67.9 ppm in the reaction solution suggested the formation of a different adduct than $\mathbf{4}^{2+}$ with phosphorus in the oxidation state +III rather than +V. SCXRD showed that halide abstraction in the presence of DMAP indeed prohibits the oxidative addition process, yielding the desired dication $\mathbf{2}^{2+}$ as its DMAP-stabilized adduct **[2DMAP][OTf]$_2$** (Figure 18, right). Due to low quality of the X-ray data, no metrical parameters of **[2DMAP][OTf]$_2$** will be discussed here but the overall structure of the dication $\mathbf{[2DMAP]}^{2+}$ is clearly evident from the measurement. The DMAP molecules are attached to the phosphorus atoms, leading to a structure very similar to the phenyl-substituted Pacman phosphane **2Ph**. According to computations, $\mathbf{[2DMAP]}^{2+}$ is 25.8 kJ·mol^{-1} higher in energy than $\mathbf{4}^{2+}$ and therefore probably kinetically stabilized (calculation method: DLPNO-CCSD(T)/*m*TZVP).[45]

The reactivity of $\mathbf{2DMAP}^{2+}$ towards substrates has not yet been tested but this will follow soon. Besides the formation of dications, there are other possibilities to increase the reactivity of Pacman phosphanes. Therefore, in the following chapter first attempts to reduce **2Cl** are presented.

3.2.3 Reduction of **2Cl**

The aim of the reduction of **2Cl** is the abstraction of the two chlorine atoms and the consequential formation of a radical centre on each phosphorus atom as depicted in Scheme 6. The biradical $\mathbf{2}^{2\cdot}$ should be able to react with a wide scope of substrates, as known from other biradical species.[28]

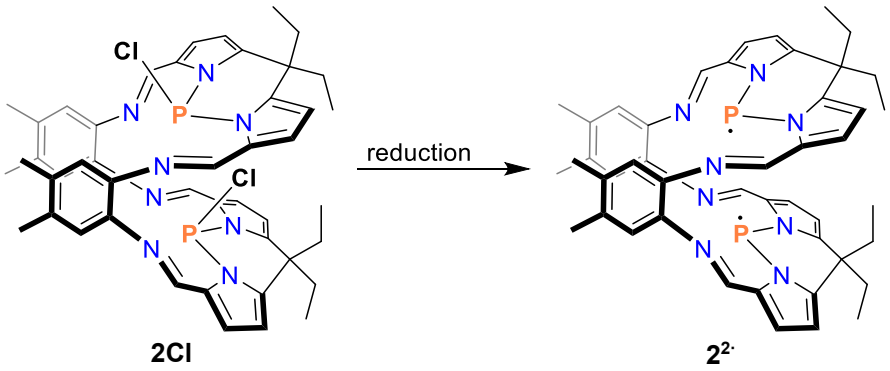

Scheme 6. Attempted reduction of **2Cl**.[45]

For first reduction experiments with **2Cl**, we used different reducing agents known for their ability to reduce P-Cl bonds (Mg,[53] Zn,[54] KC_8,[55] 1,4-bis(TMS)-1,4-dihydropyrazine[56]). In most cases, the reactions led to diminishing NMR signals of the starting material without formation of new signals. Because no significant amount of precipitation was observed during these reactions, it was assumed that indeed a radical species is formed, however, it still must be verified by EPR spectroscopy.[45]

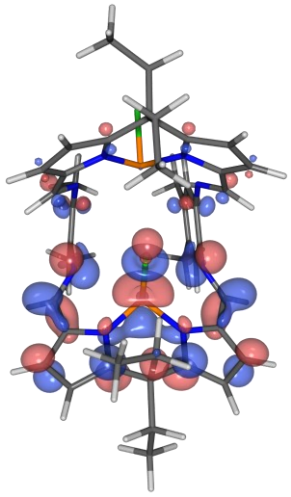

Figure 19. Lowest unoccupied molecular orbital (LUMO) of **2Cl** (calculation method: PBE-D3/*m*TZVP).[45]

The LUMO of **2Cl** is delocalized over the complete *endo*-substituted molecule half (Figure 19). Therefore, not only the reduction by chlorine abstraction but e.g. also a reduction of the imine function has to be considered as possible reaction outcome, as well as intramolecular reactions in analogy to the formation of dication $\mathbf{3}^{2+}$ instead of $\mathbf{2}^{2+}$.[45]

In addition to the development of a metal-free system for small-molecule activation, we investigated the potential of Pacman phosphanes as bidentate ligands for transition metals, which is presented in the following chapter.

3.3 Pacman Phosphane Complexes

As described in chapter 0, the Pacman phosphanes **2Ph** and **2N^{i}Pr$_2$** form *exo-exo*-isomers, making them predestined as bidentate phosphane ligands because the free electron pairs of both phosphorus atoms are directed inside the cavity of the molecule. The coordination of metals in the pocket of the Pacman phosphanes provides a defined environment around the metal centres, which is a good feature for potentially highly selective catalytic reactions of those complexes. This coordination mode is in contrast to Pacman ligands, which do not bear phosphorus atoms and usually coordinate a metal atom in each molecule half (cf. Figure 3).[2,57] To distinct Pacman phosphanes coordinating metal centres from Pacman complexes, the first will be called Pacman phosphane complexes.

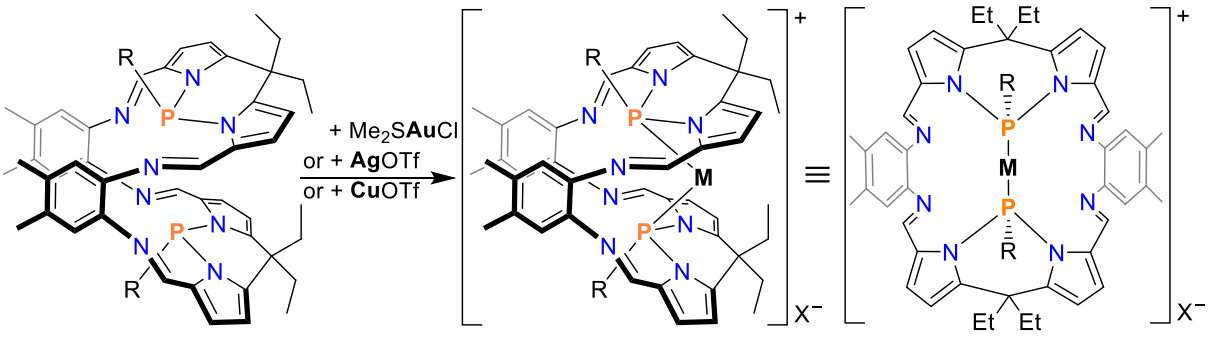

Scheme 7. Syntheses of Pacman phosphane coinage metal complexes **[5M]X** and **[6M]X**.[44]

As proof of principle, we started with the coordination of gold(I) ions and subsequently investigated the lighter coinage metals silver and copper. Dissolving the Pacman phosphane ligands **2Ph** and **2N^{i}Pr$_2$** together with one equivalent of a coinage metal salt (L)MX

(Me_2SAuCl, AgOTf or CuOTf) in dichloromethane yielded the corresponding complexes **[5M]X** (complexes of **2Ph**) and **[6M]X** (complexes of **2N^{i}Pr$_2$**, Scheme 7).[44]

NMR spectra of the complexes show highly symmetric structures in solution. In the ^{1}H NMR spectra only one signal is observed for each type of protons (e.g. imine protons or phenylene CH_3-groups), proving that the molecules contain four equivalent quarters. This is supported by the $^{31}P\{^1H\}$NMR spectra. In most cases, only one signal is present here. The only exception are the spectra of the silver complexes **[5Ag]OTf** and **[6Ag]OTf** in which two ^{31}P signals are present because either silver isotope ^{107}Ag or ^{109}Ag is coordinated. Additionally, both signals split to doublets due to P-Ag coupling constants of approx. 700 Hz (^{107}Ag) and 800 Hz (^{109}Ag). Altogether, this clearly indicates, that the metal ions are indeed coordinated in the middle of the Pacman phosphane ligands.[44]

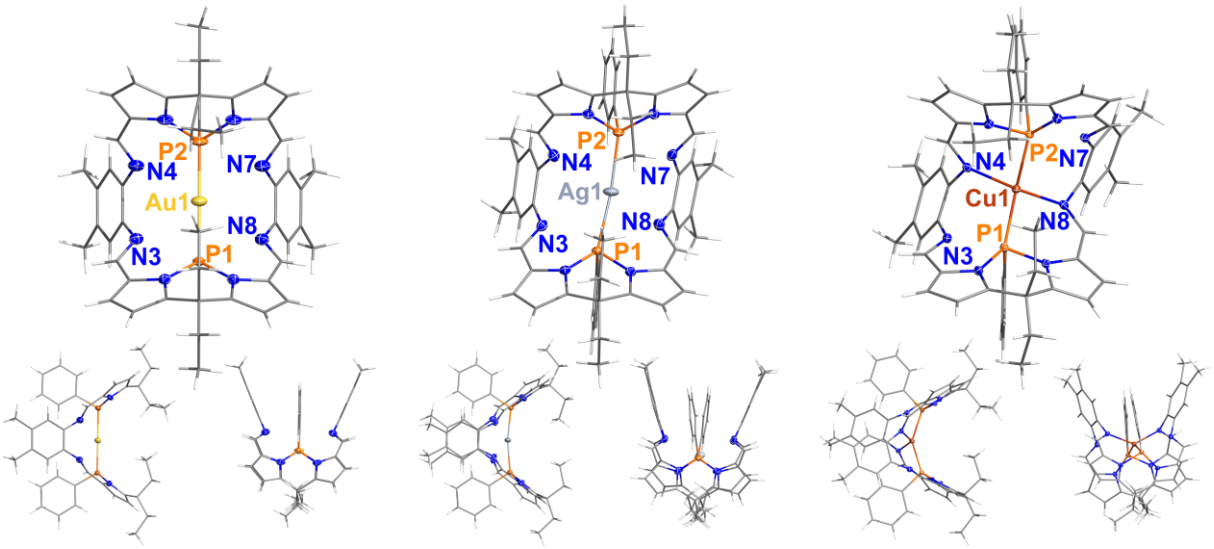

Figure 20. Front, side and top view on the molecular structures of **[5Au]Cl** (left), **[5Ag]OTf** (middle) and **[5Cu]OTf** (right) in the crystal. Ellipsoids set at 50% probability at 123(2) K. Solvent and counterions omitted for clarity.[44]

Most of the complexes were crystallized directly from the reaction solution (dichloromethane), THF or a mixture of THF with either dichloromethane or toluene. SCXRD confirmed that the metals are located in the pocket of the Pacman phosphane ligands but the coordination modes depend on the ligand and the metal and partly differ significantly from the symmetric structures observed in solution (**[5M]X**: Figure 20; **[6M]X**: Figure 21). Generally, the complexes **[5M]X** are more symmetric than **[6M]X**, just like the ligands **2Ph** and **2N^{i}Pr$_2$** themselves (cf. Figure 12). The most symmetric complex is **[5Au]Cl** in which the gold ion is coordinated almost perfectly linearly (P1-Au1-P2: 179.54(5)°). In this complex, the P···P distance (4.566(2) Å) is

elongated by approx. 0.33 Å compared to the free ligand **2Ph**.[44] This confirms that the concept of Pacman flexibility known from Pacman ligands is applicable to Pacman phosphane ligands, too. Going on to the lighter metals, the P-M-P angle becomes more acute (**[5Ag]OTf**: 168.95(6)°; **[5Cu]OTf**: 145.44(2)°) and the overall structure more distorted (Figure 20). While the distances between the metal and the nitrogen atom N3 or N7 lie in-between 3.0 – 3.2 Å for all complexes **[5M]X**, the M-N distances including N4 or N8 decrease significantly (e.g. M-N8: **[5Au]Cl**: 3.071(3) Å; **[5Ag]OTf**: 2.580(1) Å; **[5Cu]OTf**: 2.120(2) Å). In line with this, in NBO analyses of the cationic complexes increasing donor-acceptor energies between the metal and the nitrogen atoms were found (**5Au**$^+$: 21.7 kJ·mol^{-1}; **5Ag**$^+$: 37.5 kJ·mol^{-1}; **5Cu**$^+$: 118.9 kJ·mol^{-1}; calculation method: PBE-D3/*m*TZVP). At the same time, the donor-acceptor energies between the phosphorus atoms and the metal decrease from 781.7 kJ·mol^{-1} (**5Au**$^+$) over 296.0 kJ·mol^{-1} (**5Ag**$^+$) to 238.9 kJ·mol^{-1} in **5Cu**$^+$. While the silver ion in the distorted linear coordination is still mainly coordinated by the phosphorus atoms, in **5Cu**$^+$ the nitrogen atoms significantly contribute to the coordination, in line with a distorted tetrahedral coordination environment.[44]

For the complexes **[6M]X** of Pacman phosphane ligand **2N^{i}Pr$_2$**, bearing the bulkier diisopropylamino-groups, various differences were observed. In the case of the gold complex, the reaction of **2N^{i}Pr$_2$** with one equivalent of Me_2SAuCl led to complete complexation of the ligand, according to NMR spectra. Nevertheless, upon crystallization a mixture of the complexes **[6Au]Cl** and **[6Au][AuCl$_2$]** was received, while uncoordinated **2N^{i}Pr$_2$** remained in the supernatant. This problem was overcome by usage of a 1:2 ratio, yielding pure **[6Au][AuCl$_2$]**. The structure of the complex is much more distorted than **[5Au]Cl** (Figure 21). Two of the nitrogen atoms are twisted out of the cavity, of which N3 interacts with a pyrrole C-H function of a neighbouring molecule. A comparable arrangement is also observed for the free ligand **2N^{i}Pr$_2$** (cf. chapter 0). Additionally, the gold atom is not linearly coordinated by the two phosphorus atoms. With an angle of 165.06(3)°, the coordination is comparable to that in **[5Ag]OTf**. However, no significant interaction between the gold and any nitrogen atom was found in an NBO analysis of **6Au**$^+$, in accord with rather large Au-N distances of 2.910(3) Å (N7) and 3.005(4) Å (N8).

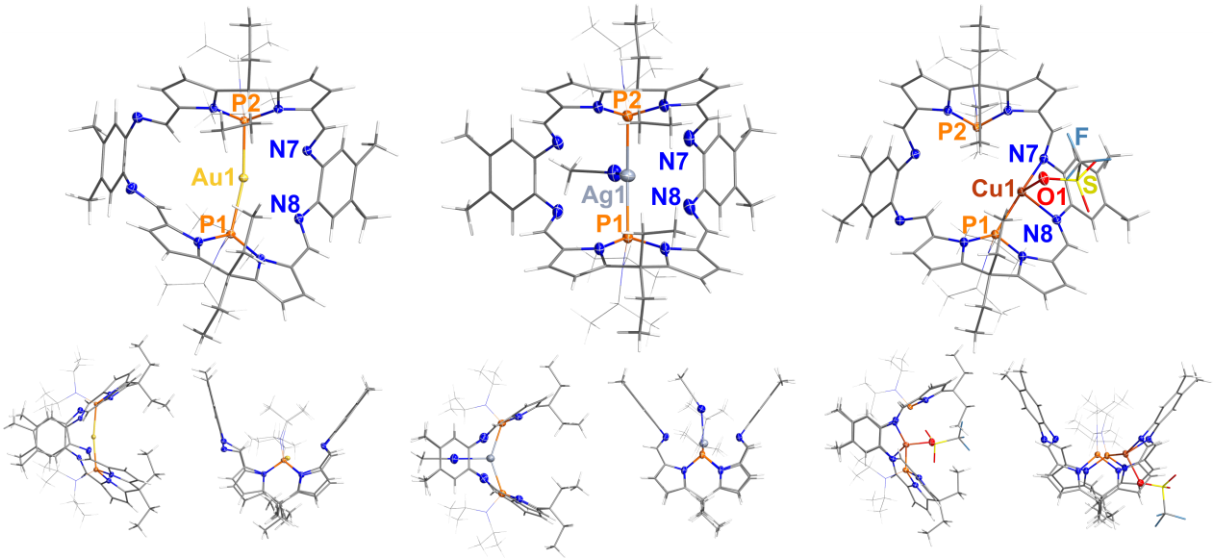

Figure 21. Front, side and top view on the molecular structures of **[6Au][AuCl$_2$]** (left), **[6Ag·MeCN]OTf** (middle) and **6Cu·OTf** (right) in the crystal. Ellipsoids set at 50% probability at 123(2) K. Solvent and counterions omitted for clarity. N^{i}Pr$_2$ groups displayed thinly for clarity.[44]

The silver complex **[6Ag]OTf** was isolated and characterized after precipitation from a dichloromethane/THF mixture but single crystals suitable for SCXRD could only be received from acetonitrile. In this complex, the silver ion is coordinated not only by the Pacman phosphane ligand but additionally by one acetonitrile forming **[6Ag·MeCN]OTf**. The overall structure of this complex is more symmetric than of the gold complex. For all complexes discussed so far, both phosphorus atoms interact with the metal centre and no significant influence of the anion on the complexation is found. In contrast to this, the copper ion in **[6Cu]OTf** is coordinated by only one phosphorus atom (P1-Cu1: 2.191(1) Å; P2-Cu1: 3.391(1) Å) but additionally by an oxygen atom of the triflate anion (O1-Cu1: 2.144(2) Å). Two nitrogen atoms complete the seesaw-like coordination environment in the solid state.[44]

In addition to the coinage metals, we also investigated the coordination of the catalytically more relevant palladium. Analogously to the coordination experiments above, the Pacman phosphane ligand **2Ph** or **2N^{i}Pr$_2$** was dissolved together with one equivalent of (COD)PdCl$_2$ (COD: cyclooctadiene). In the case of **2Ph**, we have not yet been able to isolate the reaction product, but ^{31}P{^{1}H} NMR spectra of the reaction solution indicate full conversion of the ligand. The main signal is shifted significantly upfield compared to the free ligand (−26.9 ppm vs. 80.8 ppm). Overall, the NMR spectra indicate a symmetric structure, in which both phosphorus atoms are involved in the coordination. Additionally, **2Ph** coordinating a Pd-Cl fragment was detected by mass spectrometry.[58] Further investigations of this reaction are in progress.

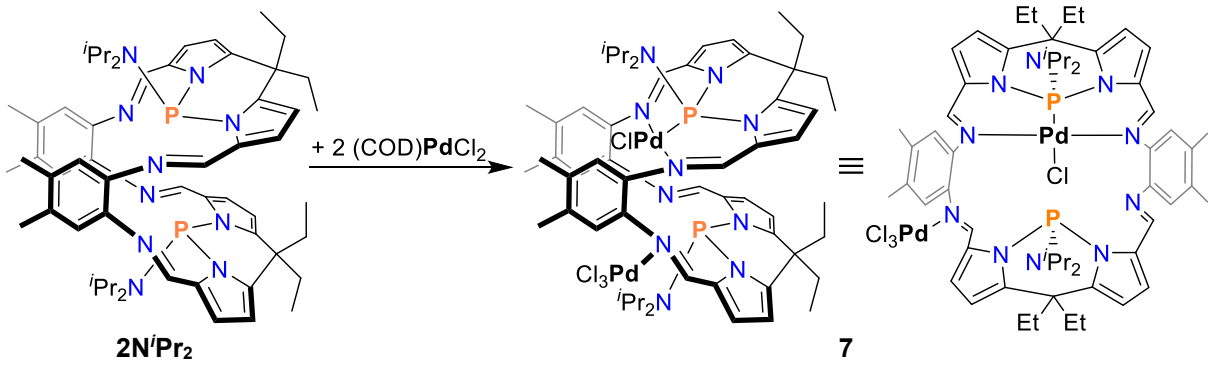

Scheme 8. Synthesis of Pacman phosphane palladium complex **7**.[58]

The coordination of palladium by **2N^{i}Pr$_2$** was more successful. Although in a reaction with 1:1 ratio, half of the ligand remained unreacted, addition of a second equivalent of (COD)$PdCl_2$ led to full conversion to **7** (Scheme 8).[58] NMR spectra of **7** revealed a more complex structure than for the complexes discussed so far. In addition to two inequivalent phosphorus atoms (59.0 ppm; 64.6 ppm), four chemically inequivalent quarters of the ligand scaffold are represented in the ^{1}H NMR spectrum, meaning that all protons in **7** are inequivalent (except for those bound to the same carbon atom).

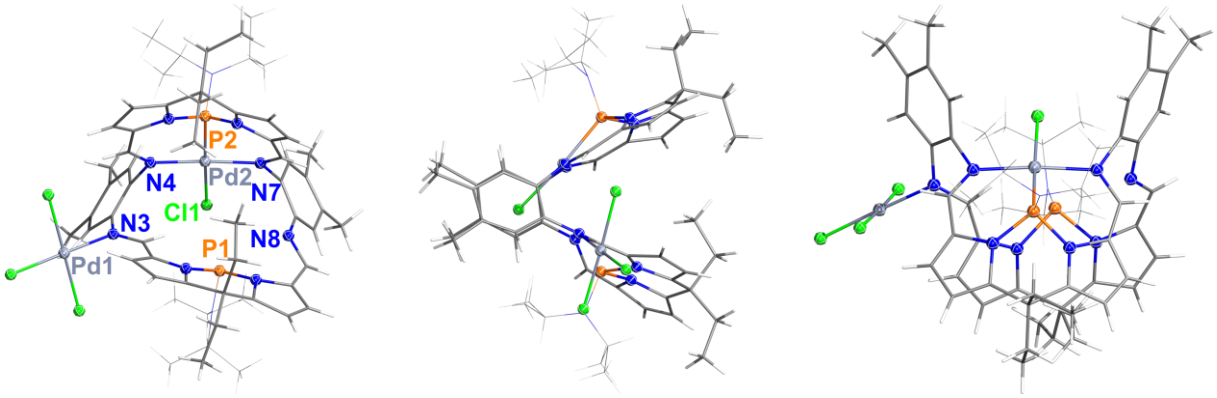

Figure 22. Front, side and top view on the molecular structure of **7** in the crystal. Ellipsoids set at 50% probability at 123(2) K. Solvent omitted for clarity.[58]

The structure was resolved by SCXRD (Figure 22). As indicated by the 1:2 stoichiometry in the synthesis, two palladium centres are coordinated by the Pacman phosphane ligand. One of them is coordinated to the phosphorus and the two imine nitrogen atoms in the respective molecule half. Its square planar environment is completed by a chlorine atom. The second palladium ion is bound to an imine nitrogen atom, which is twisted out of the molecules cavity and additionally coordinated by three chlorine atoms, leading to an overall neutral complex. The second phosphorus atom is not involved in the coordination. The additional coordination

of the $PdCl_3$ unit entails the inequivalence of all four quarters of the ligand observed in the ^{1}NMR spectrum. Moreover, it introduces chiral information to the Pacman cavity, increasing the relevance of this complex regarding possible catalytic applications. The second enantiomer ($PdCl_3$ bound to N8 instead of N3) crystallizes in the same unit cell as the enantiomer depicted in Figure 22. The sharp NMR spectra of **7** indicate, that both enantiomers are not easily interconverted but further investigation regarding this process or the separation of the enantiomers have not yet been done.[58]

Overall, the first coordination experiments with **2Ph** and **2N^{i}Pr$_2$** show the high adaptability of the Pacman phosphane ligands towards the coordinated metal. On one hand, this is realized by distortion of the ligand enabling coordination of the imine nitrogen atoms in addition to the phosphorus atoms. Moreover, the ligand **2N^{i}Pr$_2$**, widened by the bulkier N^{i}Pr$_2$-substitutents, allows the coordination of additional donors to the metal centres, so that multiple coordination modes can be realized: from pure, linear bidentate phosphane coordination over distorted tetrahedral to seesaw or square planar coordination.[44,58]

3.4 Comparison of Pacman Phosphanes

During this project, different Pacman phosphanes of the type **2R** have been synthesized. In the following, some parameters of these compounds are compared to find out whether conclusions about the influence of the different substituents at the P atom on the Pacman phosphanes can be drawn.

The most apparent difference related to the substituent on the phosphorus atoms is the formation of different isomers. The *endo-exo* isomer is observed for all neutral species of **2R**.[41,43,44] Additionally, **2F** forms the sterically crowded *endo-endo* isomer, while with phenyl- and diisopropylamine-substituents, the *exo-exo* orientation is favoured.[43,44] This displays the expected trend, that for higher steric demand, the *exo*-orientation of the P-R unit is preferred due to the limited space inside the Pacman cavity. However, the dicationic **[2DMAP]$^{2+}$** purely forms the *exo-exo* isomer.[45] On the one hand, this can be an effect of the additional *para*-substitution of DMAP compared to **2Ph**. Another explanation would be that the reaction of the substituents with dication **2^{2+}**, which has already adapted Pacman structure, leads to a selective formation of the thermodynamically favoured isomer. In contrast, the introduction of the P-R units to the flexible Pacman ligand **1** (e.g. synthesis of **2Ph**) additionally leads to the formation of the *endo-exo* isomer, probably due to kinetic reaction control. These conclusions still have to be investigated experimentally and/or by mechanistic calculations.

Table 1: P···P distances, ^{31}P chemical shifts and natural charges q_{nat}(P) of the phosphorus atoms characterizing the Pacman phosphanes **2R**.

Compound	d_{exp}(P···P) [Å]	$\delta(^{31}P)$[a] [ppm]	q_{nat}(P)[b] [e]
endo-endo-**2F**	4.834(6)	81.6	1.49
endo-exo-**2F**	4.653(2)	83.2[c]; 83.5[d]	1.49[c]; 1.51[d]
2Cl	4.6383(9)	81.6; 83.5	1.23[c]; 1.24[d]
2Br	–	90.8; 91.6	1.18[c]; 1.17[d]
2I	–	106.4; 108.5	1.08[c]; 1.06[d]
2N^{i}Pr$_2$	4.282(2)	83.2	1.37
2Ph	4.2368(6)	68.1	1.23
[2DMAP]$^{2+}$	–[f]	67.9[g]	1.41

[a] In dichloromethane. [b] calculation method: PBE-D3/*m*TZVP. [c] *endo*-P. [d] *exo*-P. [f] not given due to low quality SCXRD data set. [g] preliminary values due to small amount of impurity after isolation (see appendix for further details).

The P···P-distances (Table 1) are closely related to the isomeric structure and behave as expected. They are longest for *endo*-*endo*-**2F** and shortest for the *exo*-*exo*-substituted Pacman phosphane ligands **2Ph** and **2N^{i}Pr$_2$**.[43,44] The overall difference of nearly 0.6 Å again demonstrates the Pacman flexibility also known for Pacman ligands themselves.

Dynamic behaviour of the P-R units is only observed for the halogenated Pacman phosphanes. While **2F** only shows slow interconversion of its two isomers, the heavier homologues show increasing inversion rates of the phosphorus centres (cf. chapters 0 and 0).[43] **2Ph** and **2N^{i}Pr$_2$** show no sign of dynamic behaviour.[44] Whether **[2DMAP]$^{2+}$** shows dynamic coordination/dissociation of the DMAP-substituents still needs to be investigated.

A characteristic property of the Pacman phosphanes are their ^{31}P chemical shifts (Table 1). For the derivatives **2Cl**, **2F** and **2N^{i}Pr$_2$** they all lie between 80 and 85 ppm, for heavier halogens the signals are shifted downfield (90 – 110 ppm) while **2Ph** gives a signal at only 68.1 ppm.[41,43,44] Interestingly, the latter is very similar to the shift of the dication **[2DMAP]$^{2+}$** (67.9 ppm). As indicator for the electron density on the phosphorus atoms, the respective natural charges are given in Table 1. No correlation between both parameters can be identified but it is well known, that ^{31}P chemical shifts do not only depend on electronic parameters but are also strongly geometry dependent e.g. on bond angles. Therefore, no reliable information about the electronic situation at the phosphorus atoms can be drawn from the ^{31}P NMR shifts.

Besides the information about the isomer of the Pacman phosphane and possible dynamic behaviour, the ^{1}H NMR spectra contain some additional information about the structure of the Pacman phosphanes in solution. Figure 23 depicts the aromatic section of the ^{1}H NMR spectra of the different Pacman phosphanes. The chemical shifts of the pyrrole C-H protons (marked in green) are very similar for all Pacman phosphanes **2R**, which is explained by the comparably large distance to the substituents R. The imine protons and especially the phenylene C-H units lie closer to R (regarding the "trough space"-distance and not the number of bonds) and are therefore more influenced by changes of the substituents. The halogenated Pacman phosphanes **2F**, **2Cl** and **2Br** have very similar chemical shifts. The only difference in the spectra is the increasing linewidth for the heavier analogues.[41,43] Regarding the Pacman phosphanes with organic substituents **2Ph** and **2N^{i}Pr$_2$**, two main differences attract the attention. The first is the strong downfield shift of the imine protons (Figure 23, marked in blue) of **2N^{i}Pr$_2$**.[44] Whether this is an effect of the widened structure of this compound and a possibly fast rotation of the imine functions (cf. twisted imine functions observed only in the solid state structures of this

compound (Figure 12) and its complexes (Figure 21)), has not yet been further investigated, though.

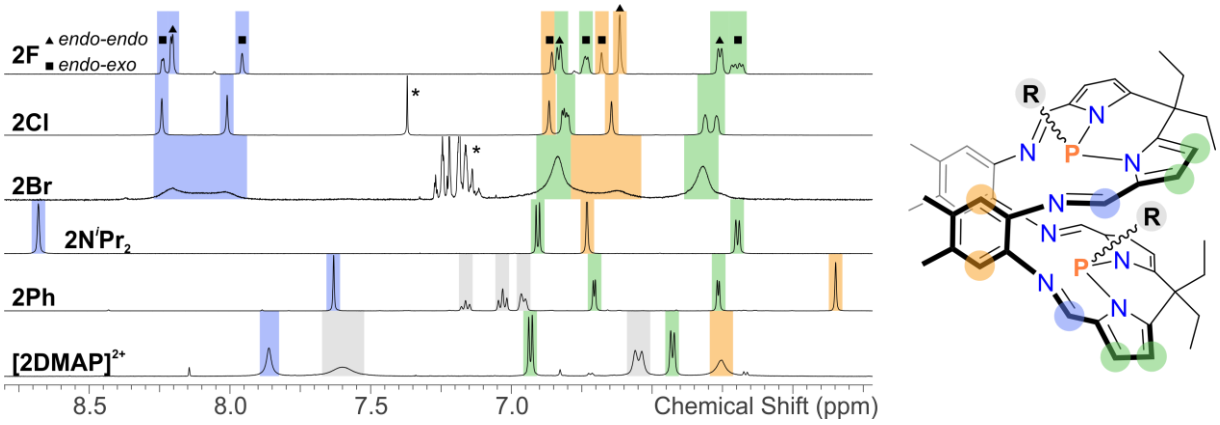

Figure 23. Aromatic region of the ^{1}H NMR spectra of the synthesized Pacman phosphanes **2R** in dichloromethane. Signals of remaining solvents indicated by asterisks. **2I** is left out due to broad linewidth. **[2DMAP]$^{2+}$** spectrum from reaction solution.

The second highlight is the strong upfield shift of the phenylene C-H protons (marked in yellow) in **2Ph**.[44] We attribute this to an anisotropic influence of the phenyl substituents, which are located in-between the two phenylene units of the Pacman scaffold (cf. Figure 12). The spectrum of the dication **[2DMAP]$^{2+}$** is very similar to that of **2Ph** but every signal is shifted downfield. This is in line with the similar solid state structures of both compounds and with the positive charge of **[2DMAP]$^{2+}$**.[45]

As already discussed for **2Cl** in chapter 0, we expect the imine nitrogen atoms of the Pacman scaffold to play a beneficial role in the stabilization of reactive intermediates or transition states in the follow-up chemistry of the Pacman phosphanes **2R**. Therefore, the donor-acceptor energies for the interaction of the imine lone pair with the opposite P-N bond of all synthesized Pacman phosphanes are listed in Table 2. These values should be understood as approximations because they are calculated for the optimized gas-phase structures and the distances between the imine nitrogen atoms and the phosphorus atom are significantly shortened for the gas-phase structures compared to the experimental solid state data (Table 2). (Optimizations started from the molecular structure in solid state, where available; for **2Br** and **2I**, which could not be crystallized, the halogen atoms were exchange starting from the optimized structure of **2Cl**.) The situation in solution may differ from both structures; nevertheless, some trends can be concluded from the data. In general, the energy gain for the described donor-acceptor interactions lies in the same range as (weak) hydrogen bonds.[59] Interestingly, for the *endo-exo*

isomers, the donor-acceptor energies in the *exo* half are nearly twice as high as in the *endo* half and additionally depend on the nature of the substituent (increasing for heavier halogens) while they are nearly equal for all *endo*-halves of the halogenated **2R**. This correlates with shorter P-N-distances in the *exo*-halves but whether the latter are an effect of higher flexibility or only coincidence still has to be investigated. For **2N^{i}Pr$_2$** only a very small donor-acceptor energy is observed, in accordance with its widened structure and the therefore long P-N-distances. This indicates that in general low donor-acceptor interactions can be expected for Pacman phosphanes bearing bulky substituents. Interestingly, although a strong stabilization was expected for the dicationic Pacman phosphane **[2DMAP]$^{2+}$**, the donor-acceptor energies are very similar to neutral **2Ph**. This might be due to strong stabilization of the phosphorus centres by the DMAP substituents, which is additionally indicated by the natural charge of the phosphorus atoms of 1.41 which is very comparable to the equally nitrogen substituted phosphorus atoms in neutral **2N^{i}Pr$_2$** (1.37; Table 1). Another explanation would be that the role of the imine nitrogen atoms in the stabilization of the phosphorus atoms is less important than initially assumed. To estimate whether this is really the case, the synthesis of further, differently Lewis base-stabilized dications of the type **[2LB]$^{2+}$** is necessary.

Table 2: Averaged experimental and calculated P-N_{imine} distances of the Pacman phosphanes **2R** as well as the respective averaged donor-acceptor energies E_{DA} between the lone pair of the imine nitrogen atoms and the σ*-orbitals of the opposite P-N bonds. For *endo-exo* isomers, all values are averaged separately for the *endo* and *exo* half.

Compound	*endo*			*exo*		
	d_{exp}(P-N_{imine}) [Å]	d_{calc}(P-N_{imine})[a] [Å]	E_{DA}[a] [kJ/mol]	d_{exp}(P-N_{imine}) [Å]	d_{calc}(P-N_{imine})[a] [Å]	E_{DA}[a] [kJ/mol]
endo-endo-**2F**	2.79(3)	2.65(1)	28.5	–	–	–
endo-exo-**2F**	2.85(11)	2.611	33.0	2.84(10)	2.500(1)	54.6
2Cl	2.871(5)	2.682(5)	31.3	2.82(7)	2.549(2)	59.1
2Br	–	2.692(2)	32.4	–	2.544(2)	65.1
2I	–	2.694(1)	34.3	–	2.533(6)	70.9
2N^{i}Pr$_2$	–	–	–	2.99(3)[b]	2.894(3)[b]	8.3[b]
2Ph	–	–	–	2.74(2)	2.712(4)	32.4
[2DMAP]$^{2+}$	–	–	–	–[c]	2.668	33.3

[a] calculation method: PBE-D3/*m*TZVP. [b] imine nitrogen atoms twisted out of molecular cavity not included. [c] not given due to low quality SCXRD data set (see appendix for further details).

4 Summary and Outlook

In the course of my PhD thesis, we successfully developed the new compound class of Pacman phosphanes (Scheme 9). They contain two phosphorus atoms in close proximity (4.24 Å to 4.83 Å), which makes them promising precursors for cooperative metal-free activation chemistry. During our investigation of this compound class, first evidence for cooperative behaviour of both phosphorus atoms was found. The proposed intermediate of the dynamic behaviour of the Pacman chlorophosphane **2Cl**, chloride adduct **2Cl·Cl**$^{-}$, in which the *endo*-chlorine atom is easily transferred from one phosphorus atom to the other, is one example for the cooperative potential of this molecule class. Furthermore, in the redox-isomerisation process in which the heavier halogenated Pacman phosphanes **2Br** and **2I** form the dicationic species **3**$^{2+}$, not only the phosphorus-halide bond dissociation but also the cooperative oxidative addition of the phosphorus atoms to two imine C-N bonds plays a significant role. Beside this phosphorus(V) species, dication **[2DMAP]**$^{2+}$ with phosphorus in the oxidation state +III can be trapped by addition of DMAP during the halide abstraction reaction. Attempts to form further reactive Pacman species by reduction of **2Cl**, e.g. a biradical, have not been successful yet but will be further investigated in combination with the reduction of the dications **3**$^{2+}$ and **[2DMAP]**$^{2+}$.

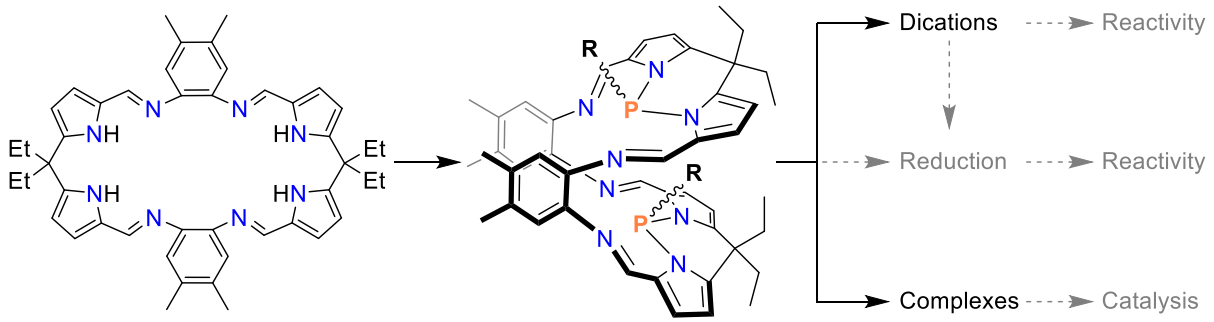

Scheme 9. Synthesis of Pacman phosphanes and related topics investigated in this work as well as future projects (grey).

Nevertheless, the most important future experiments will be reactions of **3**$^{2+}$ and **[2DMAP]**$^{2+}$ as well as possible reduced species with small molecules to find out whether both phosphorus atoms undergo cooperative activation reactions and whether this brings advantages compared

to mono-functionalized systems. Therefore, it might be beneficial to trap the dication $\mathbf{2}^{2+}$ with different Lewis bases to find an adduct $\mathbf{[2LB]}^{2+}$, in which the reactivity of $\mathbf{2}^{2+}$ is best maintained, but the redox-isomerisation to $\mathbf{3}^{2+}$ is prohibited. Regarding this, we already know that MeCN is not capable of stabilizing $\mathbf{2}^{2+}$ as upon reaction of **2Cl** with AgOTf in MeCN dication $\mathbf{3}^{2+}$ is formed instead of $\mathbf{[2MeCN]}^{2+}$. Trapping or *in-situ* reactions can also help identify reduction products of **2Cl** or other Pacman compounds. Additionally, we want to investigate the potential of Pacman phosphane complexes in catalysis. Our first complexation experiments revealed the high adaptivity of the Pacman phosphanes towards different metal ions. Due to the defined environment around the metal centre in the Pacman cavity, we expect high selectivity in catalytic reactions e.g. by size exclusion of substrates. Moreover, the chirality of the palladium complex **7** is promising regarding catalytic applications. Nevertheless, complexation of further metals and/or oxidation states will be necessary for catalytic investigations.

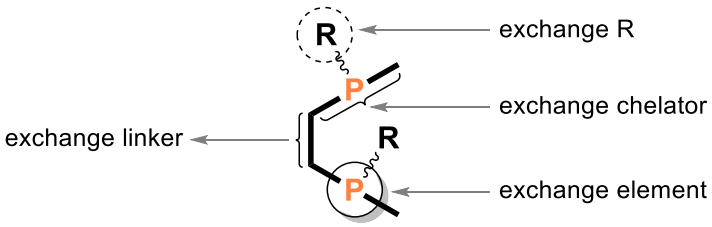

Figure 24. Possibilities to adapt main-group Pacman molecules.

Besides these ideas, there are multiple possibilities for the long-term development of Pacman phosphanes (Figure 24). In this work, we already showed that a variation of the substituent R on the phosphorus atoms strongly influences the structure of the Pacman phosphane, e.g. forming different isomers (*endo*- vs. *exo*-orientation of the P-R units) or by distortion of the Pacman scaffold. Especially regarding Pacman phosphane complexes, the investigation of further substituents might be advantageous. Using other linkers than phenylene (e.g. anthracene[60]) for the Pacman scaffold will affect the P···P distance and therefore influence the size of tolerated substrate molecules. Additionally, chiral linkers can be introduced. If further reduction experiments reveal problematic influences of the imine functions of the linkers, it might become necessary to use other chelating units in the Pacman ligands. Last but not least, the exchange of phosphorus to other non-metal elements could open further activation possibilities (e.g. a mixed P-B-species for FLP chemistry). If synthetic challenges are overcome, Pacman phosphanes promise a flourishing future.

5 References

[1] J. P. Collman, P. S. Wagenknecht, J. E. Hutchison, *Angew. Chem. Int. Ed. Engl.* **1994**, *33*, 1537–1554.

[2] J. B. Love, *Chem. Commun.* **2009**, 3154–3165.

[3] P. Lang, M. Schwalbe, *Chem. Eur. J.* **2017**, *23*, 17398–17412.

[4] H. Bisswanger, *Enzyme - Struktur, Kinetik Und Anwendungen*, Wiley-VCH, Weinheim, **2015**.

[5] H. Morrison, *Enzyme Active Sites and Their Reaction Mechanisms*, Elsevier, **2021**.

[6] D. L. Purich, R. D. Allison, *The Enzyme Reference: A Comprehensive Guidebook to Enzyme Nomenclature, Reactions, and Methods*, Academic Press, **2002**.

[7] M. D. Wodrich, X. Hu, *Nat. Rev. Chem.* **2017**, *2*, 0099.

[8] J. Campos, *Nat. Rev. Chem.* **2020**, *4*, 696–702.

[9] M. Navarro, J. J. Moreno, M. Pérez-Jiménez, J. Campos, *Chem. Commun.* **2022**, *58*, 11220–11235.

[10] J. I. van der Vlugt, *Eur. J. Inorg. Chem.* **2012**, *2012*, 363–375.

[11] J. M. Gil-Negrete, E. Hevia, *Chem. Sci.* **2021**, *12*, 1982–1992.

[12] J. P. Collman, C. M. Elliott, T. R. Halbert, B. S. Tovrog, *Proc. Natl. Acad. Sci. U. S. A.* **1977**, *74*, 18–22.

[13] H. Ogoshi, H. Sugimoto, Z. ichi Yoshida, *Tetrahedron Lett.* **1977**, *18*, 169–172.

[14] N. E. Kagan, D. Mauzerall, R. B. Merrifield, *J. Am. Chem. Soc.* **1977**, *99*, 5484–5486.

[15] C. K. Chang, M.-S. Kuo, C.-B. Wang, *J. Heterocycl. Chem.* **1977**, *14*, 943–945.

[16] C. K. Chang, I. Abdalmuhdi, *J. Org. Chem.* **1983**, *48*, 5388–5390.

[17] T. Iwatani, *Pac-Man*, Midway Games, Chicago, **1980**.

[18] J. Uppenbrink, *Science* **2000**, *287*, 769.

[19] P. D. Harvey, C. Stern, C. P. Gros, R. Guilard, *Coord. Chem. Rev.* **2007**, *251*, 401–428.

[20] P. D. Harvey, N. Proulx, G. Martin, M. Drouin, D. J. Nurco, K. M. Smith, F. Bolze, C. P. Gros, R. Guilard, *Inorg. Chem.* **2001**, *40*, 4134–4142.

[21] T. Kajiwara, T. Yamaguchi, H. Kido, S. Kawabata, R. Kuroda, T. Ito, *Inorg. Chem.* **1993**, *32*, 4990–4991.

[22] R. D. Sommer, A. L. Rheingold, A. J. Goshe, B. Bosnich, *J. Am. Chem. Soc.* **2001**, *123*, 3940–3952.

[23] W. Dammann, T. Buban, C. Schiller, P. Burger, *Dalton Trans.* **2018**, *47*, 12105–12117.

[24] J. Rosenthal, D. G. Nocera, in *Prog. Inorg. Chem.* (Ed.: K.D. Karlin), John Wiley & Sons, Inc., Hoboken, NJ, USA, **2008**, pp. 483–544.

[25] G. Givaja, A. J. Blake, C. Wilson, M. Schröder, J. B. Love, *Chem. Commun.* **2003**, 2508–2509.

[26] J. L. Sessler, W.-S. Cho, S. P. Dudek, L. Hicks, V. M. Lynch, M. T. Huggins, *J. Porphyrins Phthalocyanines* **2003**, *07*, 97–104.

[27] A. R. Jupp, D. W. Stephan, *Trends Chem.* **2019**, *1*, 35–48.

[28] J. Bresien, L. Eickhoff, A. Schulz, E. Zander, in *Comprehensive Inorganic Chemistry III* (Eds.: J. Reedijk, K. Poeppelmeier), Elsevier, **2023**, pp. 165–233.

[29] L. Greb, F. Ebner, Y. Ginzburg, L. M. Sigmund, *Eur. J. Inorg. Chem.* **2020**, *2020*, 3030–3047.

[30] M. Hasenbeck, U. Gellrich, *Chem. Eur. J.* **2021**, *27*, 5615–5626.

[31] R. Guilard, M. A. Lopez, A. Tabard, P. Richard, C. Lecomte, S. Brandes, J. E. Hutchison, J. P. Collman, *J. Am. Chem. Soc.* **1992**, *114*, 9877–9889.

[32] R. Guilard, S. Brandes, C. Tardieux, A. Tabard, M. L'Her, C. Miry, P. Gouerec, Y. Knop, J. P. Collman, *J. Am. Chem. Soc.* **1995**, *117*, 11721–11729.

[33] J. W. Leeland, A. M. Z. Slawin, J. B. Love, *Organometallics* **2010**, *29*, 714–716.

[34] N. L. Bell, P. L. Arnold, J. B. Love, *Dalton Trans.* **2016**, *45*, 15902–15909.

[35] H. Spinney, D. Richeson, T. Burchell, T. Jurca, S. Gorelsky, I. Mallov, *Inorg. Chim. Acta* **2012**, *392*, 5–9.

[36] R. Sharma, M. Ravikanth, *J. Porphyrins Phthalocyanines* **2016**, *20*, 895–917.

[37] T. Higashino, A. Osuka, *Chem. Sci.* **2012**, *3*, 103–107.

[38] M. Schorpp, R. Yadav, D. Roth, L. Greb, *Angew. Chem. Int. Ed.* **2022**, *61*, e202207963.

[39] M. Pawlicki, A. Kędzia, D. Bykowski, L. Latos-Grażyński, *Chem. Eur. J.* **2014**, *20*, 17500–17506.

[40] A. Idec, J. Skonieczny, L. Latos-Grażyński, M. Pawlicki, *Eur. J. Org. Chem.* **2016**, *2016*, 3691–3695.

[41] L. Eickhoff, L. Ohms, J. Bresien, A. Villinger, D. Michalik, A. Schulz, *Chem. Eur. J.* **2022**, *28*, e202103983.

[42] M. Mantina, A. C. Chamberlin, R. Valero, C. J. Cramer, D. G. Truhlar, *J. Phys. Chem. A* **2009**, *113*, 5806–5812.

[43] L. Eickhoff, P. Kramer, J. Bresien, D. Michalik, A. Villinger, A. Schulz, *Inorg. Chem.* **2023**, DOI: 10.1021/acs.inorgchem.3c00481.

[44] L. Ohms, L. Eickhoff, P. Kramer, A. Villinger, J. Bresien, A. Schulz, *Chem. Commun.* **2023**, DOI: 10.1039/D3CC01174G.

[45] Unpublished results. Synthetic, crystallographic and computational details outlined in the appendix.

[46] S. Borucki, Z. Kelemen, M. Maurer, C. Bruhn, L. Nyulászi, R. Pietschnig, *Chem. Eur. J.* **2017**, *23*, 10438–10450.

[47] F. Reiß, A. Schulz, A. Villinger, *Eur. J. Inorg. Chem.* **2012**, *2012*, 261–271.

[48] S. Volodarsky, D. Bawari, R. Dobrovetsky, *Angew. Chem. Int. Ed.* **2022**, *61*, e202208401.

[49] N. Đorđević, R. Ganguly, M. Petković, D. Vidović, *Inorg. Chem.* **2017**, *56*, 14671–14681.

[50] A. Kroll, H. Steinert, M. Jörges, T. Steinke, B. Mallick, V. H. Gessner, *Organometallics* **2020**, *39*, 4312–4319.

[51] J. M. Bayne, D. W. Stephan, *Chem. Eur. J.* **2019**, *25*, 9350–9357.

[52] T. Lu, F. Chen, *J. Comput. Chem.* **2012**, *33*, 580–592.

[53] J. Bresien, D. Michalik, A. Schulz, A. Villinger, E. Zander, *Angew. Chem. Int. Ed.* **2021**, *60*, 1507–1512.

[54] E. Zander, J. Bresien, V. V Zhivonitko, J. Fessler, A. Villinger, D. Michalik, A. Schulz,

2023, Manuscript in preparation.

[55] D. Rottschäfer, B. Neumann, H. G. Stammler, R. S. Ghadwal, *Chem. Eur. J.* **2017**, *23*, 9044–9047.

[56] L. P. Ho, M.-K. Zaretzke, T. Bannenberg, M. Tamm, *Chem. Commun.* **2019**, *55*, 10709–10712.

[57] P. L. Arnold, N. A. Potter (née Jones), C. D. Carmichael, A. M. Z. Slawin, P. Roussel, J. B. Love, *Chem. Commun.* **2010**, *46*, 1833.

[58] L. Ohms, Master Thesis, University of Rostock, **2022**.

[59] K. Bläsing, J. Bresien, R. Labbow, A. Schulz, A. Villinger, *Angew. Chem. Int. Ed.* **2018**, *57*, 9170–9175.

[60] C. Finn, J. B. Love, J. R. Pankhurst, D. Betz, T. Cadenbach, *Dalton Trans.* **2015**, *44*, 2066–2070.

[61] L. Teichmeier, Bachelor Thesis, University of Rostock, **2022**.

[62] W. Kaim, *J. Am. Chem. Soc.* **1983**, *105*, 707–713.

6 Publications

This chapter contains the three publications about Pacman phosphanes originating from my PhD phase.

For the whole project, Axel Schulz, my PhD supervisor, provided the infrastructure and coordinated the research. We regularly discussed results and further research steps and he revised all three manuscripts.

All authors discussed results and revised a finalized version of the manuscript before submission.

The contributions of all other authors to the papers are outlined below.

1. **A Phosphorus-Based Pacman Dication Generated by Cooperative Self-Activation of a Pacman Phosphane** (L. Eickhoff, L. Ohms, J. Bresien, A. Villinger, D. Michalik, A. Schulz, *Chem. Eur. J.* **2022**, *28*, e202103983.)

I carried out the computations and most of the experimental work for this publication. The synthesis of the less soluble Pacman chlorophosphane (in the paper: compound **2b**) was part of my Master thesis. All other experimental work was performed during my PhD. The synthesis of the Pacman chlorophosphane (in the paper: compound **2a**) by deprotonation of the Pacman ligand with KH was carried out by Leon Ohms during his Bachelor thesis under my supervision. Jonas Bresien supported and supervised the experimental and especially the theoretical work and revised the manuscript and Supporting Information. Alexander Villinger determined and refined the solid state structures from SCXRD experiments. Dirk Michalik performed the NMR measurements including several non-standard experiments. I wrote the manuscript as well as the Supporting Information. My overall contribution amounts to approx. 75%.

2. **On the Dynamic Behaviour of Pacman Phosphanes – A Case of Cooperativity and Redox Isomerism** (L. Eickhoff, P. Kramer, J. Bresien, D. Michalik, A. Villinger, A. Schulz, *Inorg. Chem.* **2023**, DOI:10.1021/acs.inorgchem.3c00481.)

First experiments regarding the chlorine-fluorine exchange as well as the synthesis of the iodinated Pacman phosphane and corresponding dication (in the paper: compounds **2Br** and **[3]Br$_2$**) were carried out by Pascal Kramer in the course of his Bachelor thesis under my

supervision. All other experiments as well as the computations and NMR simulations were performed by me. Jonas Bresien supported and supervised the experimental and especially the theoretical work and revised the manuscript and Supporting Information. Dirk Michalik performed the NMR measurements including several non-standard experiments. Alexander Villinger determined and refined the solid state structures from SCXRD experiments. I wrote the manuscript and Supporting Information of this publication. My own contribution amounts to approx. 75%.

3. **Coinage metal complexes of multidentate Pacman phosphane ligands** (L. Ohms, L. Eickhoff, P. Kramer, A. Villinger, J. Bresien, A. Schulz, *Chem. Commun.* **2023**, DOI: 10.1039/D3CC01174G.)

I supervised the experimental and computational work for this paper which was performed by Pascal Kramer in the course of his Bachelor thesis (syntheses of Pacman phosphanes ligands) and by Leon Ohms during his Master thesis (all complexation reactions and computations). In this function, my contributions to the publication were *inter alia* planning of the general synthetic strategy and of specific reaction conditions for the performed syntheses, supervision of the experimental work, assistance in the interpretation of analytical data and instructions regarding the computations that were carried out. Alexander Villinger determined and refined the solid state structures from SCXRD experiments. Jonas Bresien additionally supported and supervised the experimental and theoretical work. The manuscript and supporting information were co-written from Leon Ohms and me. Overall, my own contribution amounts to approx. 40%.

6.1 A Phosphorus-Based Pacman Dication Generated by Cooperative Self-Activation of a Pacman Phosphane

L. Eickhoff, L. Ohms, J. Bresien, A. Villinger, D. Michalik, A. Schulz*

Chem. Eur. J. **2022**, *28*, e202103983.

DOI: 10.1002/chem.202103983

Chemistry–A European Journal
Research Article
doi.org/10.1002/chem.202103983
Chemistry Europe
European Chemical Societies Publishing
www.chemeurj.org

A Phosphorus-Based Pacman Dication Generated by Cooperative Self-Activation of a Pacman Phosphane

Liesa Eickhoff,[a] Leon Ohms,[a] Jonas Bresien,[a] Alexander Villinger,[a] Dirk Michalik,[a, b] and Axel Schulz*[a, b]

Abstract: Formal coordination of phosphorus(III) by a calix[4]pyrrole Schiff base ligand was achieved through the reaction of this ligand with PCl_3 under basic conditions. The reaction product adopts a Pacman conformation with two P–Cl moieties, one in *exo* and one in *endo* position. It represents the first non-metal compound of calix[4]pyrrole Schiff base ligands and of Pacman ligands in general. The spatial neighborhood of the two phosphorus atoms enables cooperative reactions. As a first example, the chloride abstraction with AgOTf is presented, yielding a macrocyclic dication with two embedded phosphorus(III) monocations, which both undergo a cooperative, internal activation reaction with an adjacent C=N double bond. This intramolecular redox process affords two pentacoordinated phosphorus(V) centers within the Pacman dication. All reaction products were fully characterized and all results are supported by computations.

So-called Pacman ligands and their transition metal complexes have been known since 1983.[1] They are related to cofacial ligands;[2,3] however, in contrast to the latter, the parallel arrangement of the two chelating units in Pacman ligands is enforced by a rigid connection on only one side of the molecule, resulting in a more flexible metal-metal distance. In 2003, the groups of Love and Sessler independently introduced calix[4]pyrrole Schiff base ligands (**1**, cf. Scheme 1), a new type of Pacman ligands easily synthesized in high yields.[4,5] Ever since, numerous metal complexes have been reported (e.g. **A**, Figure 1).[4,6,15–19,7–14] Due to the spatial proximity of two metal centers, Pacman complexes are used to investigate and mimic highly efficient reaction centers of enzymes, for example by using energy and electron transfer upon irradiation for molecule activation.[20–24]

The concept of two cooperative reaction centers is also widely spread in metal-free molecule activation (e.g. in FLPs or biradicals).[25–30] To the best of our knowledge, Pacman complexes of phosphorus or non-metals in general have not yet been described, except for the free ligands with hydrogen atoms on the pyrrolic nitrogen atoms.[4,15,16,31,32]

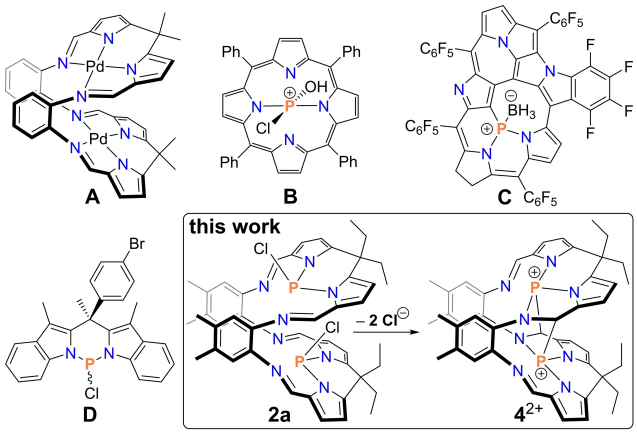

Figure 1. Literature examples for a calix[4]pyrrole Schiff base complex (**A**) and P containing compounds **B** - **D** related to the molecules presented in this work.

If only one half of Pacman ligands is regarded, porphyrins are structurally closely related and can therefore be seen as model substances. Several $P^{(V)}$ containing porphyrins were reported, mostly cations (e.g. **B**, Figure 1).[33–35] The first $P^{(III)}$ porphyrinoid (**C**, Figure 1) was synthesized in 2012 by Osuka and coworkers[36] and, to our knowledge, Latos-Grażyński, Pawlicki and coworkers reported the only two further examples.[37,38] Both types of $P^{(III)}$ porphyrinoids were structurally characterized but due to missing leaving groups on the $P^{(III)}$ atoms, they are not predestined for follow up chemistry. A calix[2]pyrrole binding a P-Cl moiety (**D**, Figure 1) was synthesized by the group of Richeson in 2012.[39] In contrast to these examples containing only one P center, here, we present a

[a] L. Eickhoff, L. Ohms, Dr. J. Bresien, Dr. A. Villinger, Dr. D. Michalik, Prof. Dr. A. Schulz
Institut für Chemie
Universität Rostock
Albert-Einstein-Str. 3a, 18059 Rostock (Germany)
E-mail: jonas.bresien@uni-rostock.de
axel.schulz@uni-rostock.de
Homepage: http://www.schulz.chemie.uni-rostock.de/
[b] Dr. D. Michalik, Prof. Dr. A. Schulz
Leibniz-Institut für Katalyse e. V.
Albert-Einstein-Str. 29a, 18059 Rostock (Germany)

Supporting information for this article is available on the WWW under https://doi.org/10.1002/chem.202103983

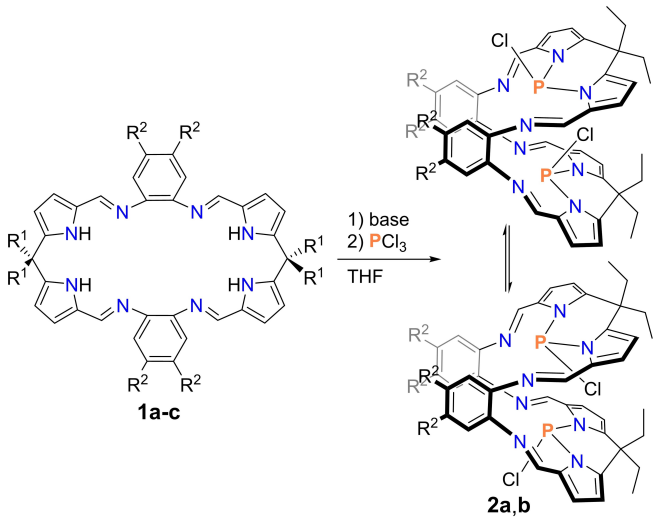

Scheme 1. Synthesis of **2** and its equilibrium with respect to the *exo*/*endo* Cl positions (**a**: R^1=Et, R^2=Me, **b**: R^1=Et, R^2=H, **c**: R^1=Ph, R^2=H; base = KH, NEt_3).

Pacman compound binding *two* P–Cl moieties as a promising synthon for versatile reactive species containing P atoms in an enforced neighborhood.[40] The concept of cooperative reactivity is demonstrated by the synthesis of a P based Pacman dication.

For the synthesis, we started from calix[4]pyrrole Schiff base ligands **1a–c** (Scheme 1) of which **1b** has not been reported before (see Supporting Information).[4,14] **1a–c** were synthesized according to modified literature procedures.[4,5,14,16,41–43] Base assisted HCl elimination upon treatment of **1** with PCl_3 allowed for the introduction of P–Cl moieties and led to the isolation of the first metal-free Pacman complexes **2a,b** (Scheme 1). Due to severe solubility problems, a reaction product of **1c** (R^1=Ph, R^2=H) could never be isolated. The replacement of the Ph substituents in R^1-position by Et groups enabled us to isolate **2b** but low yields and bad reproducibility prevented further investigations. Only the introduction of additional methyl groups on the phenylene linkers (R^2) allowed for the reliable synthesis of **2a** as yellow to orange crystals. Here, using KH as base (the potassium complex **3** was also isolated and fully characterized, Figure S7) entailed an easier separation of the product from the byproduct (KCl) but only the less reactive NEt_3 led to reasonable yields of 26% for crystalline **2a** (raw product 54%).

Inserting two P–Cl moieties in a Pacman ligand can theoretically lead to three different isomers - *endo-endo*, *exo-endo* and *exo-exo* - depending on the position of the Cl substituents outside or inside the cavity of the complex. In single crystals received from benzene and dichloromethane, respectively, **2a** and **2b** reveal the *exo-endo* orientation of the P–Cl moieties within the Pacman structure (Figure 2; due to the resemblance of the structural parameters, only **2a** is discussed here, for **2b** see Figures S5 and S6).[44] Each $P^{(III)}$ atom in **2a** is embedded in a distorted trigonal pyramidal coordination environment including one Cl atom and two pyrrolic N atoms

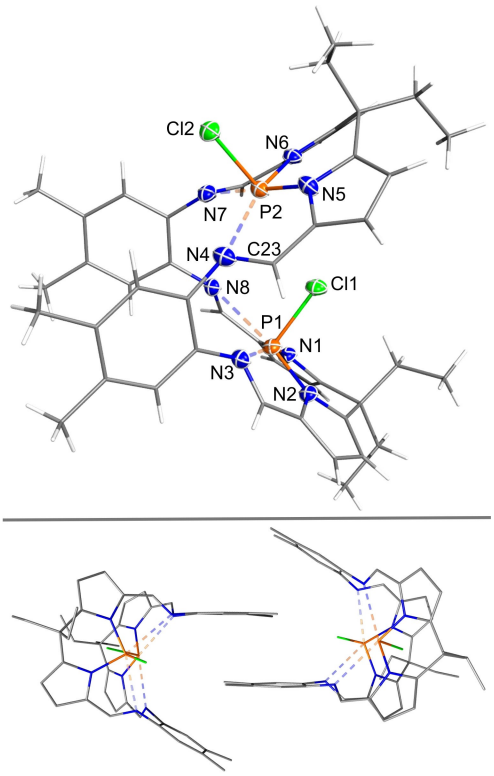

Figure 2. Top: Molecular structure of **2a** (crystallized from benzene) in the solid state. Ellipsoids are drawn at 50% probability at 123(2) K. Solvent omitted for clarity. Selected distances (Å) and angles (°): P1–Cl1 2.0965(8), P1–N1 1.743(2), P1–N2 1.736(2), P1–N3 2.866(2), P1–N8 2.874(2), P2–Cl2 2.1016(8), P2–N4 2.881(2), P2–N5 1.741(2), P2–N6 1.746(2), P2–N7 2.743(3), N4–C23 1.277(3); N1–P1–Cl1 98.90(6), N2–P1–N1 94.86(8), N1–P1–N3 165.62(8) N5–P2–Cl2 100.18(6), N5–P2–N6: 94.18(9), N5–P2–N7 167.06(8). Bottom: π-stacking between two molecular entities of **2a** in the crystal. Hydrogen atoms omitted for clarity.

($d_{ø}$(P–N_{pyr}) = 1.742(3) Å). Additionally, the distances between the P atoms and iminic N atoms $d_{ø}$(P–N_{imin}) = 2.86(3) Å (Table S4) are significantly shorter than the sum of the van der Waals radii (Σr_{vdW}(N···P) = 3.35 Å).[45] This interaction was examined by NBO (Natural bond orbital)[46,47] analysis (see Supporting Information, p. S62 ff). It reveals donor-acceptor energies of about 30 and 60 kJ mol^{-1} (*endo* and *exo* half, respectively; Table S6) for the donation of the lone pairs of the iminic N atoms into the σ* orbitals of the opposite P–$N_{pyrrole}$ bonds. Although these interactions are rather weak (the values correspond to the strength of typical hydrogen bonds),[48] they indicate that the structural motif is capable of stabilizing reactive compounds in follow-up reactions. Regarding the N_4 planes formed by the pyrrolic and iminc N atoms in each half of the molecule, the P atoms are slightly bent out of the plane towards the respective chlorine atom by 0.140(1) Å (*exo*) and 0.190(1) Å (*endo*). Moreover, the carbon-nitrogen framework in the upper and lower half of the molecule of **2a** is not planar but bent away from the respective P–Cl bond.

Both P–Cl bonds are in the expected range for covalent single bonds ($d_{ø}$(P–Cl) = 2.099(3) Å, cf. Σr_{cov}(P–Cl) = 2.04 Å).[49] In contrast, the intramolecular distance between the *endo* Cl atom

Cl1 and the *exo* substituted P2 atom is slightly smaller than the sum of the van der Waals radii (d(P2···Cl1) = 3.3552(8) Å, Σr_{vdW}(P···Cl) = 3.55 Å)[45] but still longer than previously reported distances for Cl atoms bridging two P atoms (e.g. d(P···Cl) = 2.602(1) Å).[50] The overall coordination around the $P^{(III)}$ atom could also be regarded as strongly distorted square pyramidal. The lone pair of the P2 atom, however, does not point away from the base of an imagined square pyramid but rather intersects it while sitting on top of the trigonal pyramid formed by the P atom and the Cl as well as pyrrolic nitrogen atoms (Figure 3). Therefore, the P atoms are better described as trigonal pyramidally surrounded with additional stabilization by two weak interactions with the iminic N atoms (3 + 2 coordination). A close look at the intermolecular distances in crystalline **2a** indicates significant face-to-face π-π-interactions between four phenyl rings of two neighboring **2a** molecules (Figure 2, bottom).

$^{31}P\{^{1}H\}$ NMR spectra of the reaction solution and isolated **2a** show two singlets at δ = 80.8 ppm and δ = 82.6 ppm, proving that the *exo-endo* isomer is formed selectively. Due to the inequivalency of the *exo* and *endo* halves of the molecule, each half produces a separate set of signals in the ^{1}H NMR spectra of **2a**, too (Figure 4a). Interestingly, the C*H* protons of the phenylene backbone seem to be most influenced by the orientation of the P–Cl moieties, showing the largest chemical shift difference between their two signals (δ = 6.34, 6.81 ppm; Figure 4a, blue dots). This is explained by their spatial proximity to either the *exo* Cl atom or the lone pair of electrons of the *endo* substituted P atom. Due to the additional *exo* and *endo* orientation of the ethyl groups in each half of the molecule, all ethyl groups are inequivalent. The broad linewidth, both in ^{1}H and $^{31}P\{^{1}H\}$ NMR spectra, already indicated a dynamic behavior of **2a** in solution. High temperature NMR spectra confirmed this assumption, showing only a single set of signals for **2a** at 100 °C (Figure 4b; Figures S20 and S21). On the other hand, cooling down a solution of **2a** led to sharp signals (Figure S22). In the $^{31}P\{^{1}H\}$ spectrum at −40 °C even a small coupling of 3.2 Hz between the *exo* and *endo* P atom could be observed (Figure S23). The dynamic behavior is explained by the exchange of the *exo* and *endo* orientation of the P-Cl moieties, which can be regarded as their formal inversion. The addition of $[PPh_4]Cl$ to an NMR sample of **2a** in dichloromethane (Figures S24 and S25) had the same effect as heating, leading to only a single set of signals in the NMR spectra. This makes us propose a central role of chloride ions in the inversion of the P–Cl orientation. Further investigations concerning the mechanism are in progress and will be published separately.

After observing the dynamic behavior of the P–Cl bonds and the interactions between the iminic N atoms and the P atoms, we decided to attempt the abstraction of chloride ions from **2a** to form the corresponding dication. Therefore, 2 equivalents of AgOTf were added to **2a** in the dark, resulting in a red suspension. Extraction with acetonitrile gave the dark red salt [**4**][OTf]$_2$ (Scheme 2). We expected each P^+ cation in $\mathbf{4}^{2+}$ to be surrounded by the two pyrrolic and two iminic N atoms in a square planar coordination mode, by analogy with related square planar calix[4]pyrrole complexes of aluminum[51] and silicon,[52] recently published by the group of Greb. Instead, the P^+ atoms in $\mathbf{4}^{2+}$ undergo an internal redox reaction with two of the adjacent iminic C=N double bonds, affording a cationic cage compound as depicted in Figure 5. In each half of dication $\mathbf{4}^{2+}$, the N atom of one former iminic C–N moiety is now covalently bound to the P atom in the same half of the molecule. The carbon atom of the same C–N moiety is also covalently bound to a P atom, however, of the opposite half, creating a six-membered [PNC]$_2$ ring with P in the oxidation state +V. Only few examples for the synthesis of [PNC]$_2$ rings

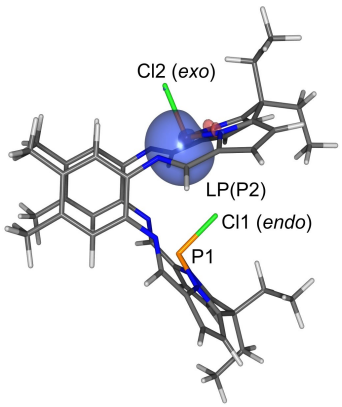

Figure 3. Natural Localized Molecular Orbital (NLMO) of the lone pair (LP) localized at the *exo*-substituted P2 atom in **2a** (PBE-D3/*m*TZVP).

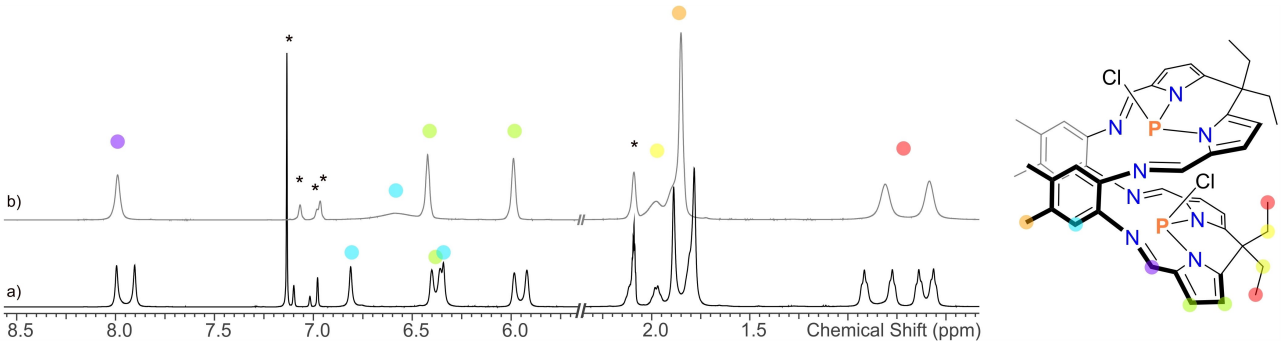

Figure 4. ^{1}H NMR spectra of crystalline **2a** dissolved in toluene-d_8; a) at 25 °C, b) at 100 °C (solvent signals indicated by asterisks).

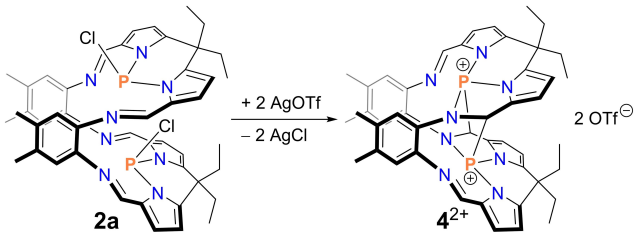

Scheme 2. Synthesis of [**4**][OTf]$_2$.

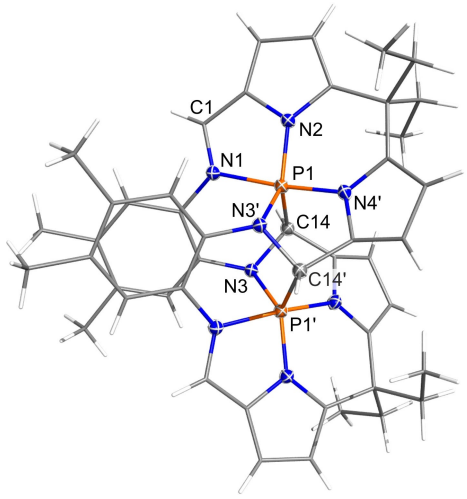

Figure 5. Molecular structure of $\mathbf{4}^{2+}$ in the solid state. Ellipsoids are drawn at 50% probability at 173(2) K. Counterions and solvent omitted for clarity. Symmetry code: 1-x, y, $^1/_2$-z. Selected distances (Å) and angles (°): P1–N1 1.9019(9), P1–N2 1.687(1), P1–N3′ 1.7028(9), P1–N4′ 1.7362(9), P1–C14 1.889(2), N1–C1 1.308(2), N3–C14 1.500(2); N1–P1–N4′ 172.85(4), N1–P1–N2 84.43(4), N2–P1–C14 124.35(5).

by the activation of iminic C=N double bonds by P cations have been reported and to our knowledge, never as an intramolecular reaction.[53–55] In $\mathbf{4}^{2+}$ the oxidative addition of the formal two P^+ ions to the C=N double bonds can be regarded as a cooperative process. The reaction of **2a** with one equivalent of AgOTf did not lead to the formation of the monocation but also to the dication $\mathbf{4}^{2+}$ in the mixture with excess **2a**.

The crystal structure of [**4**][OTf]$_2$ reveals a C_2 symmetric macrocyclic dication with two monocationic, trigonal bipyramidally surrounded $P^{(V)}$ atoms (Figure 5). Radosevich and coworkers observed a square pyramidally surrounded $P^{(V)}$ atom in a related corrole monocation.[56] In $\mathbf{4}^{2+}$, the bonds of the P1 atom to the two pyrrolic N atoms (N2, N4′) as well as to the former iminic N3′ and C14 atoms lie in the expected range for covalent single bonds ($d_{\varnothing}$(P–N) = 1.71(2) Å, cf. Σr_{cov}(P–N) = 1.76 Å; d(P1–C14) = 1.889(2) Å, cf. Σr_{cov}(P–C) = 1.87 Å).[49] The N3–C14 distance in $\mathbf{4}^{2+}$ (d(N3–C14) = 1.500(2) Å) is strongly elongated compared to **2a** (d(N4–C23) = 1.277(3) Å, double bond) indicating only a N3–C14 single bond. The P–N distance to the iminic N1 atom (d(P1–N1) = 1.9019(9) Å) is approx. 0.2 Å longer than the other P–N bonds.

According to NBO analysis, electron localization function (ELF) and the Laplacian of the electron density,[57] all four P–N interactions can be described as strongly polarized bonds while the P–C bond is almost non-polarized (see Supporting Information, p. S67 ff). Furthermore, as expected for a formal $P^{(V)}$ center, no lone pair was found at either P atom. For the elongated P1–N1 distance, the Wiberg bond index is smallest (0.52), whereas the values for all other P–N and P–C bonds range from 0.64 to 0.78 (Table S7). Together, they add to a total Wiberg bond index of 3.79 for each P center in accord with tetravalent $P^{(V)}$.

To address the question of why the *N*-tetracoordinated dication ("open structure" **min1** in Figure 6) is not observed experimentally but internal oxidation occurs to the $\mathbf{4}^{2+}$ ion ("closed" structure, **min0**), quantum chemical calculations were performed at the DLPNO-CCSD(T)[58–62]/*m*TZVP//PBE-D3/*m*TZVP level of theory, including correction terms for the solvation in MeCN (SMD[63] model, computed using DFT, cf. Supporting Information). These computations reveal a concerted reaction mechanism with only one transition state for the intramolecular bond formations, confirming the cooperative nature of the reaction. Furthermore, they indicate that the "open" structure lies significantly higher in energy and the transition state of 164.9 kJ mol^{-1} for the reverse "opening" reaction becomes hardly accessible, which is in accord with our experimental observations. NMR spectra of [**4**][OTf]$_2$ show only one product: one singlet in the $^{31}P\{^1H\}$ NMR spectrum and sharp signals including several $^1H,^{31}P$ couplings in the ^1H NMR spectrum (Figure S26). Also, upon heating neither additional nor significantly broadened signals are observed (Figure S27). Nevertheless, we are confident that the addition of appropriate Lewis bases will facilitate the "opening" (cleavage of the P–C bond) which is part of an ongoing project.

In summary, we were able to synthesize the first Pacman complex of phosphorus by reaction of PCl_3 with calix[4]pyrrole Schiff base ligands. The product also represents one of the rare examples of $P^{(III)}$ porphyrinoids. Since the Pacman ligand itself provides steric protection comparable to reaction centers of enzymes, implying high stability and selectivity, chloride abstraction in **2a** with AgOTf leads to the formation of a highly reactive macrocyclic dication with two monocationic P centers.

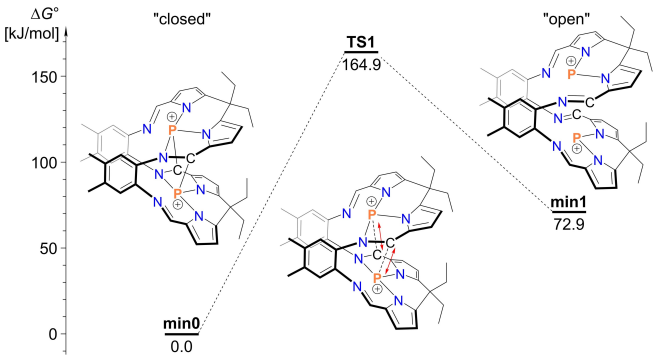

Figure 6. Energy profile of the P-C bond dissociation in $\mathbf{4}^{2+}$ in MeCN (DLPNO-CCSD(T)/*m*TZVP//PBE-D3/*m*TZVP) (see also Figure S28).

These undergo self-activation by cooperative internal redox reactions with C=N double bonds, resulting in C–N single bonds and phosphorus atoms in the oxidation state +V. This demonstrates the ideal pre-requirements in **2a**, such as the enforced neighborhood of two phosphorus atoms, for cooperative reactions and is part of ongoing reactivity studies of **2a** and [**4**][OTf]$_2$.

Acknowledgements

We gratefully acknowledge financial support by the Deutsche Forschungsgemeinschaft (DFG; SCHU 1170/12-2). L. E. gratefully acknowledges funding by the University of Rostock via the PhD Scholarship Program. Moreover, we wish to thank the ITMZ at the University of Rostock for access to the cluster computer, and especially Malte Willert for his assistance with the queuing system and software installations. We thank Dr. Wolfgang Baumann for support with NMR investigations. Open Access funding enabled and organized by Projekt DEAL.

Conflict of Interest

The authors declare no conflict of interest.

Data Availability Statement

The data that support the findings of this study are available in the supplementary material of this article.

Keywords: activation · macrocyle · Pacman · phosphorus cation · redox reaction

[1] C. K. Chang, I. Abdalmuhdi, *J. Org. Chem.* **1983**, *48*, 5388–5390.
[2] J. P. Collman, C. M. Elliott, T. R. Halbert, B. S. Tovrog, *Proc. Natl. Acad. Sci. USA* **1977**, *74*, 18–22.
[3] C. K. Chang, in *Advances in Chemistry - Inorganic Compounds with Unusual Properties-II* (Eds.: R. F. Gould, R. B. King), American Chemical Society, Washington, DC, **1979**, pp. 162–177.
[4] G. Givaja, A. J. Blake, C. Wilson, M. Schröder, J. B. Love, *Chem. Commun.* **2003**, 2508–2509.
[5] J. L. Sessler, W.-S. Cho, S. P. Dudek, L. Hicks, V. M. Lynch, M. T. Huggins, *J. Porphyrins Phthalocyanines* **2003**, *07*, 97–104.
[6] V. M. Lynch, J. L. Sessler, U. Mirsaidov, J. M. Veauthier, J. T. Markert, E. Tomat, *Inorg. Chem.* **2005**, *44*, 6736–6743.
[7] P. L. Arnold, A. J. Blake, C. Wilson, J. B. Love, *Inorg. Chem.* **2004**, *43*, 8206–8208.
[8] P. L. Arnold, N. A. Potter née Jones, C. D. Carmichael, A. M. Z. Slawin, P. Roussel, J. B. Love, *Chem. Commun.* **2010**, *46*, 1833.
[9] J. B. Love, *Chem. Commun.* **2009**, 3154–3165.
[10] S. D. Reid, M. Volpe, J. B. Love, C. Wilson, A. J. Blake, *Inorg. Chim. Acta* **2006**, *360*, 273–280.
[11] P. L. Arnold, N. A. Potter, N. Magnani, C. Apostolidis, J. C. Griveau, E. Colineau, A. Morgenstern, R. Caciuffo, J. B. Love, *Inorg. Chem.* **2010**, *49*, 5341–5343.
[12] J. W. Leeland, F. J. White, J. B. Love, *J. Am. Chem. Soc.* **2011**, *133*, 7320–7323.
[13] N. L. Bell, P. L. Arnold, J. B. Love, *Dalton Trans.* **2016**, *45*, 15902–15909.
[14] J. W. Leeland, A. M. Z. Slawin, J. B. Love, *Organometallics* **2010**, *29*, 714–716.
[15] G. Givaja, M. Volpe, J. W. Leeland, M. A. Edwards, T. K. Young, S. B. Darby, S. D. Reid, A. J. Blake, C. Wilson, J. Wolowska, et al., *Chem. Eur. J.* **2007**, *13*, 3707–3723.
[16] E. Askarizadeh, A. M. J. Devoille, D. M. Boghaei, A. M. Z. Slawin, J. B. Love, *Inorg. Chem.* **2009**, *48*, 7491–7500.
[17] E. A. Connolly, J. W. Leeland, J. B. Love, *Inorg. Chem.* **2016**, *55*, 840–847.
[18] C. J. Stevens, G. S. Nichol, P. L. Arnold, J. B. Love, *Organometallics* **2013**, *32*, 6879–6882.
[19] G. Givaja, M. Volpe, M. A. Edwards, A. J. Blake, C. Wilson, M. Schröder, J. B. Love, *Angew. Chem. Int. Ed.* **2007**, *46*, 584–586; *Angew. Chem.* **2007**, *119*, 590–592.
[20] P. D. Harvey, C. Stern, C. P. Gros, R. Guilard, *Coord. Chem. Rev.* **2007**, *251*, 401–428.
[21] A. Osuka, K. Maruyama, N. Mataga, T. Asahi, I. Yamazaki, N. Tamai, Y. Nishimura, *Chem. Phys. Lett.* **1991**, *181*, 413–418.
[22] J. P. Collman, P. S. Wagenknecht, J. E. Hutchison, *Angew. Chem. Int. Ed. Engl.* **1994**, *33*, 1537–1554.
[23] P. Lang, M. Schwalbe, *Chem. Eur. J.* **2017**, *23*, 17398–17412.
[24] P. Lang, M. Pfrunder, G. Quach, B. Braun-Cula, E. G. Moore, M. Schwalbe, *Chem. Eur. J.* **2019**, *25*, 4509–4519.
[25] M. Abe, *Chem. Rev.* **2013**, *113*, 7011–7088.
[26] G. C. Welch, R. R. S. Juan, J. D. Masuda, D. W. Stephan, *Science* **2006**, *314*, 1124–1126.
[27] J. Lam, K. M. Szkop, E. Mosaferi, D. W. Stephan, *Chem. Soc. Rev.* **2019**, *48*, 3592–3612.
[28] S. Ito, *Tetrahedron Lett.* **2018**, *59*, 1–13.
[29] J. Bresien, L. Eickhoff, A. Schulz, E. Zander, in *Comprehensive Inorganic Chemistry III* (Eds.: J. Reedijk, K. Poeppelmeier), Elsevier, **2021**, https://doi.org/10.1016/B978-0-12-823144-9.00029-7.
[30] S. González-Gallardo, F. Breher, in *Comprehensive Inorganic Chemistry II* (Eds.: J. Reedijk, K. Poeppelmeier), Elsevier, **2013**, pp. 413–455.
[31] J. M. Veauthier, W.-S. Cho, V. M. Lynch, J. L. Sessler, *Inorg. Chem.* **2004**, *43*, 1220–1228.
[32] C. Finn, J. B. Love, J. R. Pankhurst, D. Betz, T. Cadenbach, *Dalton Trans.* **2015**, *44*, 2066–2070.
[33] P. Sayer, M. Gouterman, C. R. Connell, *J. Am. Chem. Soc.* **1977**, *99*, 1082–1087.
[34] C. J. Carrano, M. Tsutsui, *J. Coord. Chem.* **1977**, *7*, 79–83.
[35] R. Sharma, M. Ravikanth, *J. Porphyrins Phthalocyanines* **2016**, *20*, 895–917.
[36] T. Higashino, A. Osuka, *Chem. Sci.* **2012**, *3*, 103–107.
[37] M. Pawlicki, A. Kędzia, D. Bykowski, L. Latos-Grażyński, *Chem. Eur. J.* **2014**, *20*, 17500–17506.
[38] A. Idec, J. Skonieczny, L. Latos-Grażyński, M. Pawlicki, *Eur. J. Org. Chem.* **2016**, *2016*, 3691–3695.
[39] H. Spinney, D. Richeson, T. Burchell, T. Jurca, S. Gorelsky, I. Mallov, *Inorg. Chim. Acta* **2012**, *392*, 5–9.
[40] A. Schulz, *Dalton Trans.* **2018**, *47*, 12827–12837.
[41] A. J. F. N. Sobral, N. G. C. L. Rebanda, M. Da Silva, S. H. Lampreia, M. Ramos Silva, A. Matos Beja, J. A. Paixão, A. M. D. A. Rocha Gonsalves, *Tetrahedron Lett.* **2003**, *44*, 3971–3973.
[42] T. Dubé, G. P. A. Yap, S. Gambarotta, D. M. M. Freckmann, C. D. Bérubé, *Organometallics* **2002**, *21*, 1240–1246.
[43] J. B. Love, A. J. Blake, C. Wilson, S. D. Reid, A. Novak, P. B. Hitchcock, *Chem. Commun.* **2003**, 1682–1683.
[44] Deposition Number(s) https://www.ccdc.cam.ac.uk/services/structures?id=doi:10.1002/chem.202103983 2095503 (for **1b**·4 HCl), 2095504 (for **2a**·benzene), 2095506 (for **2a**·THF), 2095505 (for **2b**), 2095507 (for **3**), 2095508 (for $\mathbf{4}^{2+}$), 2095509 (for **5b**), 2095510 (for **6a**) contain(s) the supplementary crystallographic data for this paper. These data are provided free of charge by the joint Cambridge Crystallographic Data Centre and Fachinformationszentrum Karlsruhe http://www.ccdc.cam.ac.uk/structures Access Structures service.
[45] M. Mantina, A. C. Chamberlin, R. Valero, C. J. Cramer, D. G. Truhlar, *J. Phys. Chem. A* **2009**, *113*, 5806–5812.
[46] E. D. Glendening, J. K. Badenhoop, A. E. Reed, J. E. Carpenter, J. A. Bohmann, C. M. Morales, C. R. Landis, F. Weinhold, *NBO 6.0*, Theoretical Chemistry Institute, University of Wisconsin, Madison, **2013**.
[47] F. Weinhold, C. R. Landis, E. D. Glendening, *Int. Rev. Phys. Chem.* **2016**, *35*, 399–440.
[48] K. Bläsing, J. Bresien, R. Labbow, A. Schulz, A. Villinger, *Angew. Chem. Int. Ed.* **2018**, *57*, 9170–9175; *Angew. Chem.* **2018**, *130*, 9311–9316.
[49] A. F. Holleman, N. Wiberg, E. Wiberg, *Holleman Wiberg, Lehrbuch Der Anorganischen Chemie, 102. Aufl.*, Walter De Gruyter, Berlin, **2007**.

[50] F. D. Henne, E.-M. Schnöckelborg, K.-O. Feldmann, J. Grunenberg, R. Wolf, J. J. Weigand, *Organometallics* **2013**, *32*, 6674–6680.
[51] F. Ebner, H. Wadepohl, L. Greb, *J. Am. Chem. Soc.* **2019**, *141*, 18009–18012.
[52] F. Ebner, L. Greb, *Chem* **2021**, *7*, 2151–2159.
[53] N. K. Maidanovich, S. V. Iksanova, Y. G. Gololobov, *Zh. Obshch. Khim.* **1982**, *52*, 930–931.
[54] A. M. Kibardin, T. K. Gazizov, K. M. Enikeev, A. N. Pudovic, *Izv. Akad. Nauk SSSR Ser. Khim.* **1983**, 432–434.
[55] A. M. Arif, A. H. Cowley, R. M. Kren, D. L. Westmoreland, *Heteroat. Chem.* **1990**, *1*, 117–122.
[56] J. C. Gilhula, A. T. Radosevich, *Chem. Sci.* **2019**, *10*, 7177–7182.
[57] T. Lu, F. Chen, *J. Comput. Chem.* **2012**, *33*, 580–592.
[58] F. Neese, J. Wiley, *WIREs Comput. Mol. Sci.* **2012**, *2*, 73–78.
[59] F. Neese, *WIREs Comput. Mol. Sci.* **2018**, *8*, e1327.
[60] C. Riplinger, F. Neese, *J. Chem. Phys.* **2013**, *138*, 034106.
[61] D. G. Liakos, M. Sparta, M. K. Kesharwani, J. M. L. Martin, F. Neese, *J. Chem. Theory Comput.* **2015**, *11*, 1525–1539.
[62] C. Riplinger, P. Pinski, U. Becker, E. F. Valeev, F. Neese, *J. Chem. Phys.* **2016**, *144*, 024109.
[63] A. V. Marenich, C. J. Cramer, D. G. Truhlar, *J. Phys. Chem. B* **2009**, *113*, 6378–6396.

Manuscript received: November 4, 2021
Accepted manuscript online: November 10, 2021
Version of record online: November 24, 2021

6.2 On the Dynamic Behaviour of Pacman Phosphanes – A Case of Cooperativity and Redox Isomerism

L. Eickhoff, P. Kramer, J. Bresien, D. Michalik, A. Villinger, A. Schulz*

Inorg. Chem. **2023**, accepted.

DOI: 10.1021/acs.inorgchem.3c00481

Inorganic Chemistry

pubs.acs.org/IC Article

On the Dynamic Behavior of Pacman Phosphanes—A Case of Cooperativity and Redox Isomerism

Liesa Eickhoff, Pascal Kramer, Jonas Bresien, Dirk Michalik, Alexander Villinger, and Axel Schulz*

Cite This: https://doi.org/10.1021/acs.inorgchem.3c00481 Read Online

ACCESS | Metrics & More | Article Recommendations | Supporting Information

ABSTRACT: In solution, the Pacman chlorophosphane (**2Cl**) shows fast exchange of the *endo*/*exo*-orientation of the two P−Cl bonds in the molecule featuring cooperativity. Experimental and quantum mechanical investigations of the inversion on the phosphorus(III) centers reveal a crucial role of chloride ions in the dynamic process. To confirm the results, the homologous Pacman halogen-phosphanes **2X** were prepared by halogen exchange reactions (X = F, Br, and I). Besides accelerated dynamic behavior for the heavier analogues, significant differences in the molecular structure are caused by the halogen exchange reactions, including the formation of an *endo*−*endo* substituted Pacman fluorophosphane as well as dicationic species by phosphorus halogen bond dissociation. The latter process can be regarded as redox isomerism since two P^{III} atoms in **2X** become P^{V} centers in the dications.

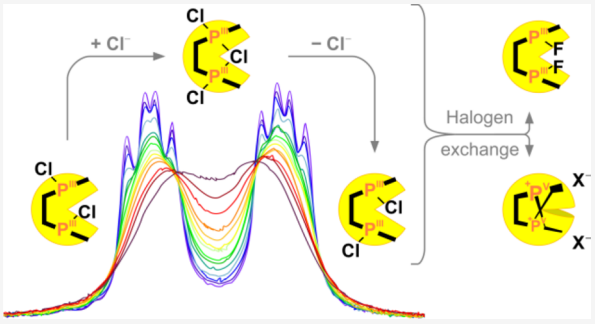

INTRODUCTION

In the last few years, bimetallic complexes opened a field for new, more selective or efficient pathways in activation chemistry, often inspired by nature.[1−5] Recently, growing interest in cooperative behavior of main group elements including even non-metals evolved.[6−8] A basic requirement for cooperative reactivity is close proximity of the interacting centers. Among several other systems, this can be achieved by the usage of Pacman ligands.[9−11]

Pacman ligands are built of two chelators and therefore able to coordinate two metal centers. A rigid linker connects the two chelators on one side of the molecule and forces them in a parallel position with a defined distance. The connection on only one side of the molecule allows for a small flexibility regarding the distance between the two chelators, referred to as opening and closing of the cavity in-between them. This flexibility is reminiscent of the eponymous video game figure; hence, the term "Pacman ligands" was coined.[12,13] Numerous metal complexes of Pacman ligands are known.[11,14,15] Recently, we were able to introduce the first non-metal into a Pacman ligand by reacting Schiff base imine ligand **1** with PCl_3 under basic conditions (Scheme 1).[16] The resulting chlorinated Pacman phosphane **2Cl** bears two P−Cl fragments, each bound to two pyrrolic nitrogen atoms in the respective half of the Pacman ligand. Compared to metal complexes of this ligand type, in which the imine nitrogen atoms strongly coordinate the metal centers, the imine nitrogen atoms only play a minor role in the binding of the non-metal.[16,17]

In the solid state as well as in solution, exclusively the *endo*−*exo* isomer of **2Cl** was observed. As expected for this isomer, all NMR spectra of **2Cl** showed a double set of signals, corresponding to the two molecule halves with the *endo*- and *exo*-P−Cl bonds, respectively (in the following referred to as

Scheme 1. Synthesis of 2Cl, Containing Two P^{III} Centers, and Chloride Abstraction by AgOTf To Give $[3][OTf]_2$ Exhibiting Two P^{V} Atoms

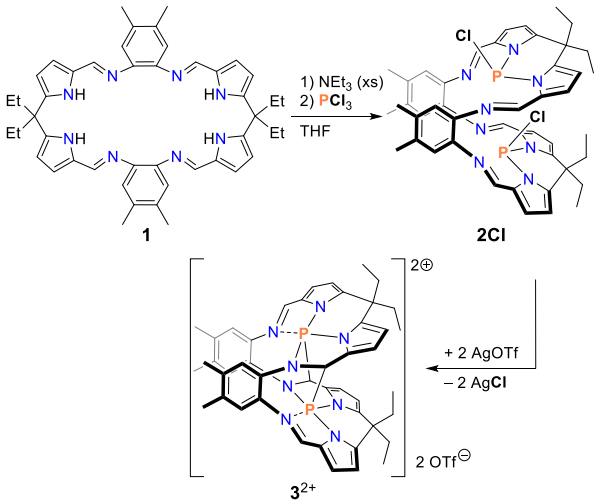

Received: February 13, 2023

Scheme 2. Halogen Exchange Reactions Starting from 2Cl To Introduce Fluorine (2F), Bromine (2Br), or Iodine (2I) to the Pacman Phosphane (TMS = Me_3Si)[a]

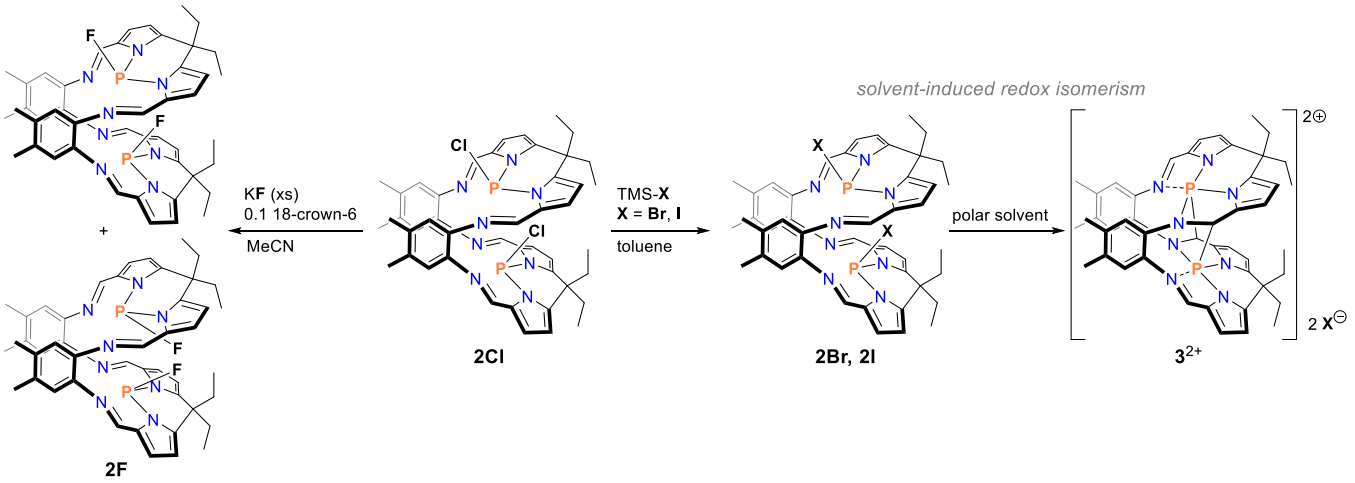

[a]For **2X** (X = Br and I), solvent-induced redox isomerism is observed leading to the formation of $[\mathbf{3}]X_2$.

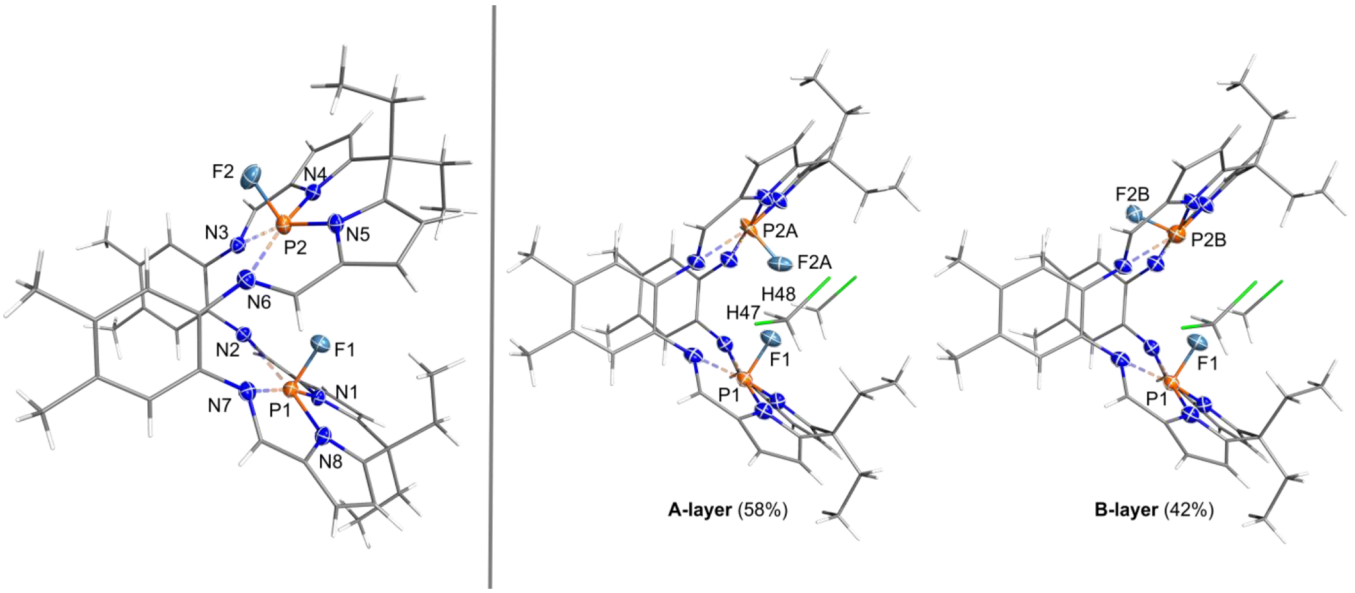

Figure 1. Left: Molecular structure of isomeric pure *endo*−*exo*-**2F** in the crystal. Single crystals obtained from acetonitrile. Ellipsoids are drawn at 50% probability at 123(2) K. Co-crystallized solvent molecules omitted for clarity. Selected distances (Å) and angles (°): P1−F1 1.588(2), P1−N1 1.745(2), P1−N2 2.942(2), P1−N7 2.735(2), P1−N8 1.736(2), P2−F1 3.450(2), P2−F2 1.594(2), P2−N3 2.968(3), P2−N4 1.752(2), P2−N5 1.731(2), P2−N6 2.774(2); N1−P1−F1 97.39(8), N1−P1−N7 169.57(8), N1−P1−N8 94.44(9), N4−P2−F2 95.82(9), N4−P2−N5 94.91(9), N4−P2−N6 169.45(8). Right: Molecular structure of the isomeric mixture of *endo*−*endo*-**2F** (A-layer, 58%) and *endo*−*exo*-**2F** (B-layer, 42%) in the crystal. Single crystals obtained from dichloromethane. Additional solvent molecules and disorder of one ethyl group are omitted for clarity. Ellipsoids are drawn at 50% probability at 173(2) K. Selected distances (Å) and angles (°): P1−F1 1.583(2), P1−N1 1.744(2), P1−N2 2.792(2), P1−N7 2.760(3), P1−N8 1.745(2), F1−F2A 2.382(3), P2A−F2A 1.519(6), P2B−F2B 1.538(9), P2A−N3 2.866(5), P2A−N4 1.738(5), P2A−N5 1.741(5), P2A−N6 2.877(5), F1−H47 2.607(2), F1−H48 2.669(2), F2A−H47 2.805(3), F2A−H48 2.825(3); N1−P1−F1 97.56 (9), N1−P1−N7 168.92(8), N1−P1−N8 94.22(9), N4−P2A−F2A 96.2(3), N4−P2−N5 95.4(2), N4−P2A−N6 169.6(3).

endo and *exo* halves). Furthermore, broad linewidths in the spectra indicated a dynamic process influencing the orientation of the chlorine substituents. In the first attempt to uncover the dynamics of the Pacman phosphane **2Cl**, it was, *inter alia*, reacted with AgOTf to abstract the two formal chloride ions. In the resulting dication, the positively charged phosphorus centers underwent inner redox reactions with adjacent C═N double bonds, forming cage compound $\mathbf{3}^{2+}$ (Scheme 1).[16]

Three questions arose from this earlier work: (1) the orientation of the P−Cl bonds is responsible for the observed dynamic of **2Cl** but how can it be explained mechanistically? (2) How do other substituents on the phosphorus atoms affect the dynamic behavior of Pacman phosphanes? (3) Since the introduction of OTf substituents led to the formation of $\mathbf{3}^{2+}$ bearing now two P^V centers, how do other substituents influence the bonding situation in Pacman phosphanes?

To answer these questions, we decided to replace the chlorine substituents in **2Cl** by the lighter halogen fluorine, as well as the heavier analogues bromine and iodine, taking advantage of the decreasing P−X bond dissociation energies along the 17th group (E_{diss}(P−F) = 496 kJ·mol^{-1}, E_{diss}(P−Cl) = 328 kJ·mol^{-1}, E_{diss}(P−Br) = 264 kJ·mol^{-1}, and E_{diss}(P−I) =

https://doi.org/10.1021/acs.inorgchem.3c00481
Inorg. Chem. XXXX, XXX, XXX−XXX

184 kJ·mol^{-1}) as well as the decreasing bond polarities.[18] Apart from complete characterization of the newly synthesized derivatives of **2Cl**, detailed NMR spectroscopic investigations and computational studies of the synthesized compounds were performed to shed light on the isomerization mechanism.

RESULTS AND DISCUSSION

Halogen Exchange Reactions. *Fluorine.* To avoid working with toxic, gaseous PF_3 in a reaction analogous to the synthesis of **2Cl** (cf. Scheme 1), we instead tested different fluorination reagents for a chlorine−fluorine exchange reaction starting from the chlorinated Pacman phosphane **2Cl**. After several unsuccessful attempts (Table S3), we found that reacting **2Cl** with KF in acetonitrile in the presence of 0.1 equiv of 18-crown-6 leads to complete conversion to **2F** within 5 days (Scheme 2). Although the addition of one equiv. of crown ether shortens the reaction time to a few hours, we decided to use the sub-stoichiometric route to minimize the effort of separating the crown ether from **2F**. $^{19}F\{^1H\}$ and $^{31}P\{^1H\}$ NMR spectra of the raw product of **2F** show an ABXY spin system as expected for the two chemically inequivalent P−F functions in *endo* and *exo* position. Additionally, an AA′XX′ spin system is present in the same $^{19}F\{^1H\}$ and $^{31}P\{^1H\}$ NMR spectra. This coupling pattern can only be explained by a symmetrical isomer of **2F**, meaning that in addition to *endo*−*exo*-**2F**, either the *endo*−*endo* or *exo*−*exo* isomer is formed upon halogen exchange.

The *endo*−*exo* isomer is better soluble than the symmetrical isomer so that it can be extracted from the mixture with acetonitrile and crystallized selectively (Figure 1, left). The residue of the extraction can be crystallized from dichloromethane. Single crystal X-ray analysis unequivocally proves the existence of the symmetrical isomer *endo*−*endo*-**2F** in which both fluorine atoms are located inside the pocket of the Pacman ligand (Figure 1). Additionally, *endo*−*exo*-**2F** co-crystallizes in a ratio of 58:42 (*endo*−*endo*:*endo*−*exo*).

In both isomers of **2F**, the phosphorus atoms are distorted trigonal pyramidally surrounded by two pyrrolic nitrogen atoms and a fluorine atom. While the P−N distances lie in the range of polar P−N single bonds, the P−F distances are significantly shortened. The different isomers of **2F** possess P−F distances from 1.519(6) to 1.594(2) Å. In related $F-P(NR_2)_2$ compounds, they are usually longer than 1.6 Å[19−24] with only one exception of d(P−F) = 1.588(2) Å[25] while the sum of the covalent radii for a polarized P−F single bond even amounts to 1.66 Å.[18] The averaged distance between the phosphorus atoms and the imine nitrogen atoms ($d_{Ø}$(P−N_{imine}) = 2.86(4) Å) lies significantly below the sum of their van der Waals radii (Σr_{vdW}(N···P) = 3.35 Å).[26] By analogy with **2Cl**, these are explained by small donor−acceptor interactions of the lone pairs of the imine nitrogen atoms and the anti-bonding σ^*-orbitals of the opposite P−N bonds, including the pyrrolic nitrogen atoms (Table S11).[16]

In the single crystals of the isomeric mixture of **2F** (Figure 1), two dichloromethane molecules are located inside the pocket of the Pacman ligand, widening the cavity and elongating the P···P-distance by approx. 0.18 Å (4.835(6) Å compared to 4.653(3) Å in pure *endo*−*exo*-**2F**). The shortest distances d(H···F) between the dichloromethane molecules and the *endo*-fluorine atoms of 2.6 to 2.8 Å are in the range of the sum of the van der Waals radii (Σr_{vdW}(H,F) = 2.56 Å).[26] The two fluorine atoms in *endo*−*endo*-**2F** come remarkably close with a distance of only 2.382(3) Å (Σr_{vdW}(F···F) = 2.94 Å).[26] Nevertheless, no significant donor−acceptor interaction between the two fluorine atoms was found in the NBO analysis[27,28] (NBO = natural bond orbital, Table S11).

Bromine. The attempt of introducing P−Br bonds by base assisted reaction of **1** with PBr_3 (cf. synthesis of **2Cl**, Scheme 1) led to a crude product mixture. As a more selective alternative, we decided to use TMS−Br (TMS = Me_3Si) to exchange the chlorine substituents in **2Cl** with bromine under elimination of TMS−Cl. The reaction in toluene runs smoothly showing only a slight color change from orange to a light red solution. A downfield shift of the two $^{31}P\{^1H\}$ NMR signals after the reaction (90.8 and 91.6 ppm compared to 81.6 and 83.5 ppm for **2Cl**) indicates the successful halogen exchange to the brominated Pacman phosphane **2Br** and clearly suggests that the phosphorus remains in the oxidation state +III. Additionally, the ^1H chemical shifts only change marginally compared to spectra of **2Cl**, proving that the overall structure of the ligand is not affected by the chlorine−bromine exchange reaction. Although isolating single crystals of **2Br** was impossible (crystallization attempts from CH_2Cl_2, THF, C_6H_6, and C_6H_5F), it can be assumed that upon the exchange reaction, the covalent species **2Br** with an analogous structure to **2Cl** is formed. To our surprise, when trying to crystallize **2Br** from acetonitrile over the course of several days, a color change from orange to a characteristic dark red and the deposition of crystals of the same color were observed. By single crystal X-ray analysis, the crystals could be identified as [**3**]Br_2 (Figure 2). Heterolytic dissociation of the P−Br bonds of **2Br** in the polar solvent leads to the same dication 3^{2+} as received by chloride abstraction from **2Cl**. Upon dissociation of the bromide ions, the highly electrophilic phosphenium centers attack their adjacent imine C═N bonds cooperatively,

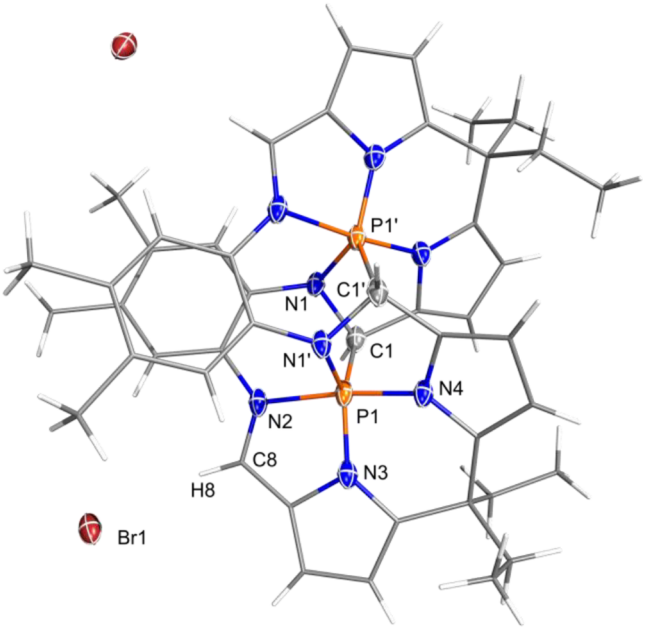

Figure 2. Molecular structure of [**3**]Br_2 in the crystal. Ellipsoids are drawn at 50% probability at 123(2) K. Co-crystallized solvent molecules omitted for clarity symmetry code (′): $-x, y, 1/2 - z$. Selected distances (Å) and angles (°): P1−N1′ 1.711(2), P1−N2 1.895(2), P1−N3 1.686(3), P1−N4 1.729(2), P1−C1 1.875(3), N1−C1′ 1.502(4), Br1−H8 2.5543(5); N1′−P1−N2 92.63(11), N1′−P1−N3 131.2(2), N1′−P1−C1 107.0(2), N2−P1−N4 171.6(2), Br1−H8−C8 151.3(2).

https://doi.org/10.1021/acs.inorgchem.3c00481
Inorg. Chem. XXXX, XXX, XXX−XXX

each forming a P−N bond to one former imine nitrogen atom and a P−C bond to the opposite molecule half. This induces an oxidation of both phosphorus(III) centers to phosphorus(V). This internal redox process may be referred to as a form of redox isomerism.[29−31] The structural parameters of $\mathbf{3}^{2+}$ are nearly identical in $[\mathbf{3}]Br_2$ and already known $[\mathbf{3}][OTf]_2$ (Table S7), indicating that both counter ions are nearly innocent with respect to the structural parameters of the dication.[16] Each phosphorus atom is distorted trigonal bipyramidally surrounded by two pyrrolic nitrogen atoms and the newly bound carbon and nitrogen atoms of the former imine C═N bonds. The fifth bonding partner is the remaining imine nitrogen atom in the same molecule half. Although this contact (d(P1−N2) = 1.895(2) Å) cannot be interpreted as a typical covalent bond,[16] the short distance proves a strong interaction. The bromide ions do not interact with the phosphorus atoms, and the closest contact is hydrogen atom H8 with a distance of d(Br1−H8) = 2.5543(5) Å (Figure 2, cf. Σr_{vdW}(H···Br) = 2.93 Å).[26]

Iodine. The halogen exchange of chlorine to iodine can be performed analogously to the synthesis of **2Br**, using TMS−I as exchange reagent. Compared to the bromination, a more intensive color change occurs during the reaction with TMS−I, ending up with a brown suspension. Heating the mixture to remove all volatiles after the reaction leads to decomposition. Keeping the reaction mixture at maximally ambient temperature allows for the isolation of the iodinated species **2I**. However, extremely broad NMR spectra of the raw product complicate the identification. The $^{31}P\{^1H\}$ NMR signals of **2I** (106.4 and 108.5 ppm) are shifted even further downfield compared to **2Br**. As in the case of **2Br**, we were not able to crystallize covalent **2I** but dissolving the raw product in dichloromethane leads to the deposition of small, dark red crystals within 5 h. Unfortunately, these, as well as crystals received from acetonitrile, only give a data set of poor quality in the X-ray single crystal analysis (Table S2). Nevertheless, the formation of the ionic species $[\mathbf{3}]I_2$ in the solid state can be derived from these X-ray studies as well as from the recorded NMR spectra for solution of $[\mathbf{3}]I_2$ in acetonitrile or DMSO (Figures S4 and S8). From these data, it can be concluded that in polar solvents, **2I** undergoes the same redox isomerization process as described above for **2Br**.

Exploration of the Dynamic Behavior of the Halogenated Pacman Phosphanes. *Overview.* The four halogenated Pacman phosphanes **2X** (X = F, Cl, Br, and I) show significant differences. As for **2F**, two covalent isomers are observed, *endo*−*exo*-**2Cl** is formed exclusively, and in **2Br** and **2I**, the P−X bonds dissociate to give the salt $[\mathbf{3}]X_2$ in a redox isomerism process. To understand these results, we calculated the three possible isomers of **2X** (*endo*−*endo*, *endo*−*exo*, and *exo*−*exo*) and the ionic species $\mathbf{3}X_2$ on DFT level using triple zeta basis sets; for halogen atoms, additional diffuse basis functions were used (PBE-D3/*m*TZVP, cf. SI, p. S76f).[32,33] Electronic energies were determined by single-point DLPNO-CCSD(T)[34−36] calculations on optimized structures. Where necessary, solvation in different solvents (SMD[37] model) was taken into account (for bromine and iodine, we used adapted Coulomb radii,[38] cf. SI, p. S84f).

The energy differences between the *endo*−*endo*-, *endo*−*exo*-, and *exo*−*exo*-isomers of **2X** can be found in Table 1 as well as the Gibbs free reaction energies for the reaction of *endo*−*exo*-**2X** to $[\mathbf{3}]X_2$. For all covalent Pacman phosphanes **2X**, the *endo*−*exo*-isomer is most favored. A benefit within this isomer is attractive dipole−dipole interactions in the Pacman cavity between the *endo*-orientated halogen atom and the *exo*-substituted phosphorus atom (Figure S74). As expected, the dissociation of two halide ions leading to $[\mathbf{3}]X_2$ is highly disfavored in the gas phase and unpolar solvents. In dichloromethane, only the formation of $[\mathbf{3}]I_2$ seems possible ($\Delta_rG°$ = 2 kJ·mol^{-1}), which is also observed experimentally. However, in acetonitrile reactions to $[\mathbf{3}]Cl_2$, $[\mathbf{3}]Br_2$ and $[\mathbf{3}]I_2$ are exergonic, while experimentally, we only observe the latter two. The formation of $[\mathbf{3}]Cl_2$ is probably kinetically hindered due to the stronger P−Cl bonds (also see SI, p. S86ff).

Table 1. Relative Gibbs Free Energies ($\Delta G°$) of the Different Isomers of 2X and Gibbs Free Reaction Energies ($\Delta_rG°$) for the Reaction of *endo*−*exo*-2X to $[\mathbf{3}]X_2$ (CCSD(T)/*m*TZVP)

	compound	solvent	X			
			F	Cl	Br	I
$\Delta G°$ [kJ·mol^{-1}]	*endo-endo*-**2X**	gas phase	32.2	59.1	58.2	69.1
	endo-exo-**2X**		0.0	0.0	0.0	0.0
	exo-exo-**2X**		23.8	20.9	14.6	14.1
$\Delta_rG°$ [kJ·mol^{-1}]	*endo-exo*-**2X** ↓ $[\mathbf{3}]X_2$	gas phase	1329.8	966.9	900.9	849.1
		toluene	620.2	360.2	317.6	299.6
		dichloromethane	238.5	39.1	11.6	2.0
		acetonitrile	137.2	−46.1	−69.1	−77.0

With the differently substituted Pacman phosphanes **2X** in hand, we took a closer look into their behavior in solution. The dynamic processes are investigated by combination of experimental NMR studies (high temperature measurement and addition of Lewis bases or halide ions) and quantum chemical calculations. The discussion starts with the results of detailed investigations on the dynamic behavior of **2Cl** and afterward analyses similarities and differences to **2F**, **2Br**, and **2I**.

Dynamic Behavior of 2Cl. Due to the orientation of the P−Cl bonds in **2Cl**, forming the *endo*−*exo* isomer, the molecule is divided into two chemically inequivalent halves—the *endo* and the *exo* half. At 25 °C, each half produces a separate set of signals in the NMR spectra (Figure 3a). Nevertheless, the broad linewidth of the signals already hints toward an ongoing dynamic process. As previously reported, heating of an NMR sample of **2Cl** to 100 °C leads to the formation of only one broad set of signals (Figure 3b).[16] Thus, an acceleration of the dynamic process at higher temperatures results in the loss of the information about the orientation of the two P−Cl bonds, which indicates a formal inversion on the phosphorus centers as shown in Scheme 3. For this behavior, different explanations can be considered, such as the influence of the inversion barrier, P−X bond dissociation, the role of halide ions, etc.

As our computations predict an extremely high inversion barrier at the phosphorus atoms of 205.5 kJ·mol^{-1}, an actual inversion at the phosphorus atoms can be ruled out (Figure S72). Other explanations for the dynamic behavior of **2Cl** include the dissociation of a P−Cl bond. Homolytic bond cleavage and therefore the formation of a chlorine radical are disfavored by more than 280 kJ·mol^{-1} (Figure S72). Additionally, no EPR signals could be detected at 25 and 100 °C and NMR spectra applying the Evans method only

https://doi.org/10.1021/acs.inorgchem.3c00481
Inorg. Chem. XXXX, XXX, XXX−XXX

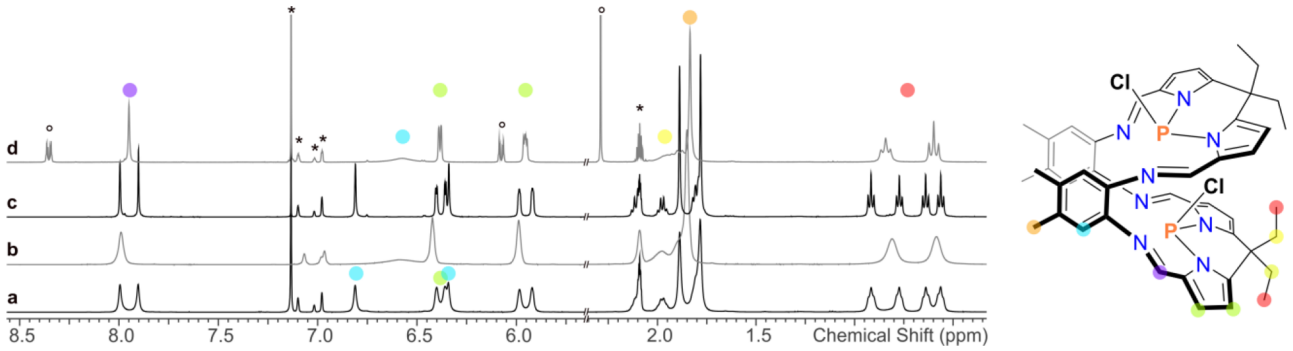

Figure 3. ^{1}H NMR spectra of **2Cl** in toluene-d_8; (a) **2Cl** at 25 °C, (b) **2Cl** at 100 °C, (c) **2Cl** at 25 °C after heating, and (d) **2Cl** + 1 equiv of DMAP at 25 °C (solvent signals indicated by asterisks, and DMAP signals indicated by circles).

Scheme 3. Simplified Notation of Pacman Phosphanes and the Dynamic Equilibrium of 2Cl in Solution via a Cationic (Top) or Anionic (Bottom) Intermediate

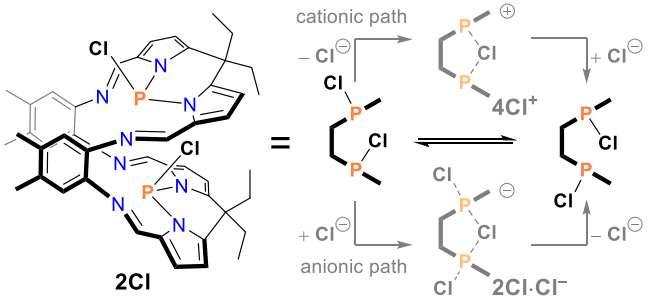

show diamagnetic influences on the chemical shift (Figure S46).[39] Heterolytic bond dissociation would lead to the monocation **4Cl**$^+$ and a free chloride ion (Scheme 3, "cationic path"), which can recombine to form either the original or the inverted structure of **2Cl**. Like the homolytic dissociation, this reaction is not favored ($\Delta G°$ = 197.6 kJ·mol^{-1} in toluene) and can therefore not explain the observed dynamic (Figure 4). In

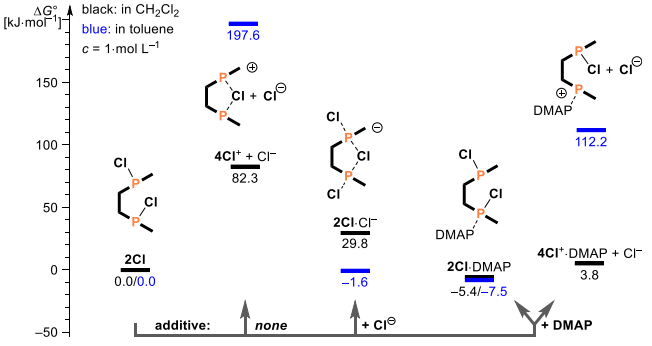

Figure 4. Possible intermediates for the chloride exchange on **2Cl**. Energies are given in relation to **2Cl** and respective additive (blue: in toluene, black: in dichloromethane; CCSD(T)/*m*TZVP).

contrast, the addition of a further chloride ion to **2Cl**, giving the complex **2Cl**·Cl$^-$ (Scheme 3, "anionic path"), is slightly favored in toluene by −1.6 kJ·mol^{-1} (Figure 4). With an additional chloride ion bound to the *endo* substituted phosphorus atom, the exchange of the *endo* chlorine between the two phosphorus atoms is nearly barrier-free (Figure S73). The dissociation of one *exo* chlorine atom from the **2Cl**·Cl$^-$ complex can therefore not only lead back to the original structure of **2Cl** but also to the inverted structure. Linewidth-based simulation of the broadened signals in the NMR spectrum of **2Cl** at 25 °C provided us with the reaction rate in the equilibrium between **2Cl** and its chloride adduct (p. S51).[40] Using this, we estimated that only a very small concentration of chloride ions on the order of ≤10^{-6} mol L^{-1} is necessary to cause the observed dynamic effect (p. S66 ff). Considering the high barrier for the chloride abstraction, the origin of the free chloride ions can only partly be explained by the dissociation of **2Cl**. Probably, additionally smallest amounts of impurities, e.g., [HNEt$_3$]Cl from the synthesis of **2Cl**, contribute to the dynamics. Formation of [**3**]Cl$_2$ as chloride source can be ruled out due to the highly endergonic reaction energy in toluene (Table 1).

Kee and co-workers investigated the dynamic behavior of a chiral chlorophosphane in which the P−Cl moiety is substituted by (1*R*,2*R*)-1,2-diaminocyclohexane (Scheme 4).[41] They likewise proposed a central role of chloride ions

Scheme 4. Dynamic Behavior of a P−Cl Bond and Reaction Pathways Postulated by Kee and Co-Workers (R = *p*-C$_4$H$_6$-*t*Bu)[41]

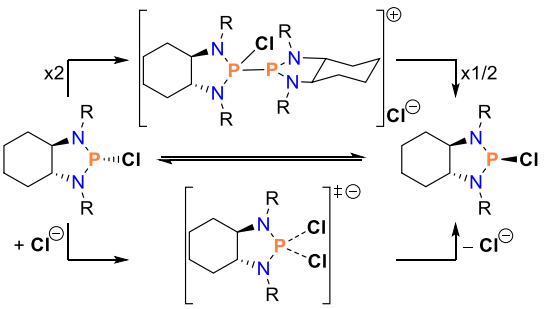

for the inversion. Moreover, they found a distinct correlation between the reaction rate and the squared concentration of the P−Cl functions. This suggests that in their system, the formation of dimers plays a significant role for the inversion on the phosphorus center. In our case, a bimolecular mechanism including intermediately formed dimers of **2Cl** for chlorine transfer cannot be excluded completely. Unfortunately, we were not able to investigate such reaction paths computationally due to the size of such dimeric species. Nevertheless, a significant contribution of a bimolecular inversion mechanism can be ruled out because of the low concentration dependency of the reaction rate (Figures S44 and S45). One explanation for the difference between Kee's and our system could be the Pacman structure of **2Cl**. It resembles a preformed dimer with

https://doi.org/10.1021/acs.inorgchem.3c00481
Inorg. Chem. XXXX, XXX, XXX−XXX

the second phosphorus atom having a beneficial effect on, e.g., the easy chloride transfer between both phosphorus atoms in **2Cl**·Cl^-. This also points out the possibility of cooperative behavior of the two phosphorus atoms of **2Cl**.

Although we cannot completely rule out other mechanisms, in summary, we propose that a constant, low concentration of chloride ions can attack compound **2Cl** and thus an inversion of **2Cl** occurs via the anionic pathway (cf. Scheme 3, bottom). The whole process can therefore formally be regarded as a chloride ion-catalyzed inversion. On the one hand, the necessary traces of chloride ions can be formed via the cationic reaction pathway (cf. Scheme 3, top), which itself is far too slow to cause the observed dynamics. On the other hand, a certain amount of chloride ions can also originate from the synthesis of **2Cl**.

To verify our proposed mechanism, we attempted to stabilize the possible cation **4Cl**$^+$ with a Lewis base, allowing for an easier P−Cl bond cleavage and therefore higher chloride concentration. In fact, the addition of 1 equiv of DMAP (4-(dimethylamino)pyridine) to an NMR sample of **2Cl** leads to very sharp NMR spectra with only one set of signals (Figures 3d and S9). Unfortunately, the addition of $[PPh_4]Cl$ to a solution of **2Cl** in toluene has no effect on the linewidth in the NMR spectra (Figures S25 and S26), which we attribute to the extremely low solubility of $[PPh_4]Cl$. Additionally, we performed the reaction with $[PPh_4]Cl$ in dichloromethane, which, like heating in toluene, results in the formation of a single broad set of signals (Figures S27 and S28) in accord with our proposed mechanism.

Notably, the NMR spectra of pure **2Cl** in dichloromethane are sharper than in toluene despite the fact that the dissociation into **4Cl**$^+$ and Cl^- is more favored in dichloromethane, which should result in a higher concentration of Cl^- in this more polar solvent. However, in contrast to toluene, the formation of the anionic intermediate **2Cl**·Cl^- is endergonic in dichloromethane (Figure 4), explaining the slower exchange reaction despite higher Cl^- concentrations. Upon addition of different amounts of DMAP to a sample of **2Cl** in dichloromethane, the signals in the NMR spectra of both compounds broaden but also shift significantly (Figures S11 and S12). This indicates the equilibrium formation of a **2Cl**·DMAP adduct and/or the corresponding cation **4Cl**$^+$·DMAP, which nicely correlates with calculated data (Figure 4). A similar behavior is observed upon the addition of DMAP to a solution of **2Cl** in acetonitrile. The formerly very broad signals transform to one sharp set of signals but with differing chemical shifts compared to free **2Cl** or DMAP. Unfortunately, no adduct could be crystallized from dichloromethane or acetonitrile. Aside from this, it is important to say that neither in dichloromethane nor in acetonitrile, the formation of the dicationic species $[\mathbf{3}]Cl_2$ is observed. Nevertheless, traces of $[\mathbf{3}]Cl_2$ could act as chloride source in polar solvents, especially in acetonitrile (Table 1).

During high temperature NMR investigations of **2Cl** in toluene, we observed that NMR spectra of **2Cl** in toluene at 25 °C become much sharper after the sample was heated to 100 °C (Figure 3, spectra a and c). Storing the sample at ambient temperature leads to broadening of the signals so that the initial broadness of the signals (i.e., before heating the sample) is recovered after approx. 3 weeks (Figures 5 and S36−S42). The observed effect is reproducible. After broadening, reheating of the sample led to sharp signals at ambient temperature again. The linewidth of the solvent signals

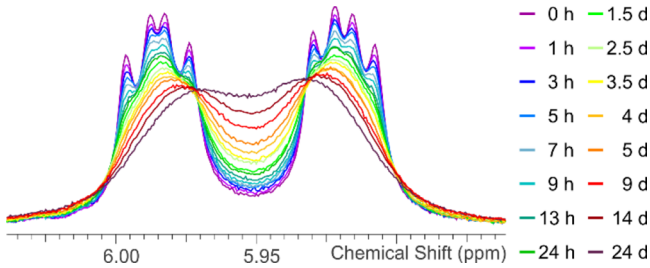

Figure 5. Time-dependent ^1H NMR spectra of a pyrrole C*H* in **2Cl** at 25 °C after short heating to 100 °C (for spectra of other signals, see Figures S36−S42).

remained constant throughout the whole experiment. In combination with the empty EPR spectra of **2Cl**, paramagnetic influences on the linewidth can be excluded. By ruling out other influences like concentration or light (Figures S43−S45), we are convinced that the change of linewidth is caused by changes in the chloride concentration. By heating, part of the free chloride is removed from solution (e.g., due to side reactions with **2Cl** or the solvent), causing slower exchange between the *exo* and *endo* orientation. The chloride concentration then increases slowly over time, e.g., by dissociation of **2Cl**.

Dynamic Behavior of 2F. In contrast to the chlorinated Pacman phosphane **2Cl**, the NMR spectra of **2F** show only sharp signals; in the ^1H NMR spectrum, even couplings of less than 2 Hz are resolved. This points out that the P−F bonds in **2F** do not undergo fast exchange. Even upon the addition of DMAP in toluene, the NMR signals neither broaden nor do the two sets of signals of the *endo*−*exo* isomer combine to give only one set of signals as observed for **2Cl**. The chemical shifts of both reagents do not change either (Figure S15). Quantum chemical calculations support these experimental results. Including solvation in polar solvents like dichloromethane, the abstraction of a fluoride ion from **2F**, forming cationic intermediate **4F**$^+$, is still thermodynamically disfavored by 180.1 kJ·mol^{-1} (Table S14). Without fluoride ions in solution, the anionic pathway for the isomerization of the P−F moieties can also be excluded, explaining why no dynamic behavior of **2F** is observed in solution. Even upon addition of fluoride ions, the NMR spectra do not show any sign of fast inversion of the P−F orientations comparable to **2Cl**. The formation of the anionic intermediate **2F**·F^- in dichloromethane is disfavored by more than 40 kJ·mol^{-1} (Table S13) so that the resulting exchange reaction is possibly too slow to show an effect on the NMR signals.

A further difference to the other halogenated Pacman phosphanes is that not only the *endo*−*exo* isomer of **2F** is formed but additionally a symmetrical isomer is also formed. As described above, in the solid state, *endo*−*endo*-**2F** is observed. To transfer these results to dissolved **2F**, the $^{19}F\{^1H\}$ and $^{31}P\{^1H\}$ NMR data of the isomers were calculated (Tables S5 and S6). The results resemble the experimental coupling patterns (Figures S47 and S48), and the measured NMR spectrum can be simulated for both isomers (Figure 6). Energetically, *endo*−*exo*-**2F** is the most favored isomer, followed by *exo*−*exo*-**2F** and *endo*−*endo*-**2F**, respectively, contradicting the experimental results (Table 1). Under solvent correction for dichloromethane, the energy differences do not change significantly (Table S10). Including two explicit dichloromethane molecules in the cavity of **2F**, as observed in

https://doi.org/10.1021/acs.inorgchem.3c00481
Inorg. Chem. XXXX, XXX, XXX−XXX

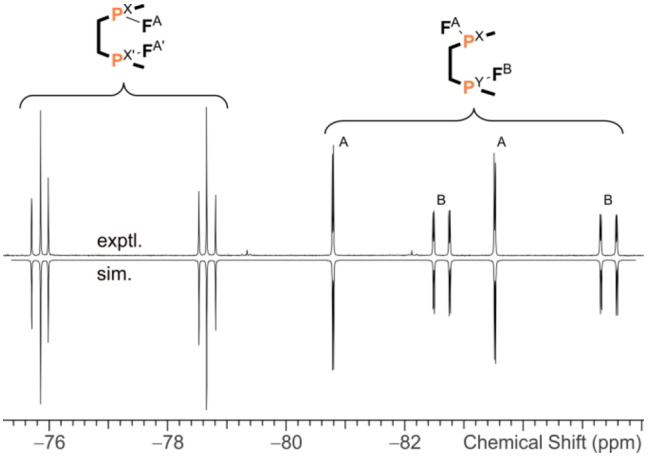

Figure 6. Experimental and simulated $^{19}F\{^1H\}$ NMR spectrum for the isomeric mixture of **2F** (CD_2Cl_2, 500 MHz).

the solid state for *endo*−*endo*- and *endo*−*exo*-**2F** (Figure 1), changes the energetic relation significantly. *Endo*−*endo*-**2F** becomes most favored ($\Delta G° = -4.5$ kJ·mol^{-1}), although nearly degenerate with *endo*−*exo*-**2F**, while the *exo*−*exo* isomer stays significantly higher in energy by 14.9 kJ·mol^{-1} (compared to *endo*−*exo*-**2F**).

To verify the calculated data experimentally, pure *endo*−*exo*-**2F** as well as the crystallized mixture of *endo*−*endo*-**2F** (58%) and *endo*−*exo*-**2F** (42%) were dissolved in dichloromethane. Both experiments resulted in a 1:4 mixture of the respective isomers after several days (Figures S53 and S54). This corresponds to a free reaction enthalpy of approx. 3.4 kJ·mol^{-1}. Although in the experiment, the *endo*−*exo* isomer is slightly favored with respect to *endo*−*endo*-**2F** and the experimental and calculated energy differences are still within the same order of magnitude. DMAP slightly accelerates the isomerization of the two isomers (Figure S16) while fluoride ions show an even larger influence. Already 15 min after the addition of $[Me_4N]F$ to a solution of *endo*−*exo*-**2F**, the equilibrium ratio is reached (Figures S29−S31). In toluene, *endo*−*endo*-**2F** is not converted to *endo*−*exo*-**2F**, which is also not affected by the addition of DMAP. Considering all the results, we are convinced that dichloromethane has a stabilizing effect on *endo*−*endo*-**2F**. Moreover, fluoride ions also play a role in the isomerization to *endo*−*exo*-**2F**, similarly to what was found for the inversion of **2Cl**.

*Dynamic Behavior of **2Br** and **2I**.* The Pacman phosphanes of the heavier halogens both behave similarly and are therefore discussed together. Upon halogen exchange, in both cases, the covalent compound **2Br** or **2I** is formed first as can be verified by the ^1H and $^{31}P\{^1H\}$ NMR shifts (see above). Both compounds show broad NMR signals, indicating faster dynamics than in **2Cl**. For **2Br**, a trend in the linewidth as a function of solvent polarity can be discerned, with a comparably sharp double set of signals in benzene, through broadened spectra in THF and dichloromethane, to one broad single set of signals in acetonitrile (Figures S55 and S56). Spectra of **2I** are even broader and additionally overlaid by impurities and signals of its rearrangement product $[3]I_2$ (Figures S57 and S58).

The addition of DMAP to solutions of **2Br** and **2I** in toluene in both cases instantly leads to significant precipitation, suggesting the formation of an ionic and therefore less soluble species. In dichloromethane, no precipitate is formed upon addition of DMAP to **2Br** and **2I**. In both cases, changes in the chemical shifts indicate the formation of a new species, e.g., a DMAP adduct (Figures S19 and S23). An isomerization reaction of **2I** to $[3]I_2$ is not observed after the addition of DMAP. Addition of $[PPh_4]Br$ to **2Br** leads to an acceleration of the dynamic process (Figures S32 and S33), whereas the addition of $[PPh_4]I$ to **2I** has no observable effect. This is likely due to the fast formation of $[3]I_2$ in dichloromethane, so a significant amount of iodide ions is already present in the sample of **2I**, leading to intrinsically accelerated dynamics, even without any additive (Figures S34 and S35).

To get a more detailed insight into the conversion of covalent **2I** to ionic $[3]I_2$, we traced the process by NMR spectroscopy. This redox isomerism reaction takes about 10 h in dichloromethane. In the $^{31}P\{^1H\}$ NMR spectra, two broad signals decrease in the manner of first-order reactions each, but with different reaction rates, implying the existence of two different isomers **2I** and **2I′** (Figure S59ff). Due to the broad NMR spectra of **2I** and missing single crystal data, we were not able to further investigate the nature of the second isomer. Repetition of the NMR experiment at different temperatures provided Gibbs free energies of activation at 25 °C for the two isomers of $\Delta G^{‡}$(**2I**) = (96 ± 14) kJ·mol^{-1} and $\Delta G^{‡}$(**2I′**) = (100 ± 30) kJ·mol^{-1} (for detailed information cf. SI p. S66ff). In acetonitrile, the same reaction is completed within minutes at ambient temperature.

In accordance with theoretical data (Table 1), the transformation of **2Br** to $[3]Br_2$ is significantly less favored. In dichloromethane, no evidence of the ionic species is detected. A solution of **2Br** in dichloromethane is orange instead of dark red as one would expect for 3^{2+}, and in the NMR spectra, the typical signal pattern is not visible even after several days. Nevertheless, in acetonitrile, the conversion is finally observed although it takes up to a whole week for completion. To verify the results of the kinetic NMR study of **2I**, we also investigated the dissociation of **2Br** but using acetonitrile as solvent and in a temperature range of 25 to 70 °C. The Gibbs free energy of activation at 25 °C amounts to $\Delta G^{‡}$(**2Br**) = (100 ± 17) kJ·mol^{-1} (SI, p. S71ff) in accord with the rather slow conversion.

CONCLUSIONS

Starting from Pacman chlorophosphane **2Cl**, the halogen substituents were successfully exchanged for fluorine, bromine, and iodine using KF, TMS−Br, and TMS−I as exchange reagents, respectively. While in the case of fluorine, an isomeric mixture of the fluorophosphanes **2F** was isolated, and for the heavy representatives, both, the halogen-phosphanes **2Br** and **2I** as well as the corresponding isomeric salts $3X_2$ are obtained.

For all Pacman phosphanes of the type **2X**, different isomers can formally be discussed, namely, *exo*−*exo*, *endo*−*exo*, and *endo*−*endo*. The *endo*−*exo* isomer is the most favored for all halogens. Only the small size of the fluorine in combination with the expansion of the Pacman cavity by dichloromethane molecules allows for the isolation of the sterically crowded *endo*−*endo*-isomer.

Moreover, the dynamic isomerization of the Pacman phosphanes **2X** was intensively studied experimentally and quantum mechanically. For the inversion of *endo*−*exo*-**2Cl**, it can be assumed that small amounts of chloride ions in solution accelerate the exchange of the P−Cl moieties in the molecule by the formation of an anionic intermediate via a cooperative mechanism between the two P−Cl groups.

https://doi.org/10.1021/acs.inorgchem.3c00481
Inorg. Chem. XXXX, XXX, XXX−XXX

In line with the decreasing P−X bond dissociation energy within the 17th group, for the fluorinated Pacman phosphane **2F**, no comparable dynamic behavior was observed. In contrast, it was even more distinct for the heavier analogues **2Br** and **2I**, which nicely correlates with the easy dissociation of the two halide ions observed by formation of the dication $\mathbf{3}^{2+}$. The latter process can be referred to as solvent-induced redox isomerism, a process rarely observed when main group atoms are involved, as in this case phosphorus.

The detailed understanding of the dynamic processes in the halogenated Pacman phosphanes will be utilized to explore the potential especially of **2Cl** regarding cooperative reaction behavior, e.g., in small molecule activation as well as for the generation of biradicals.

EXPERIMENTAL SECTION

All manipulations were carried out under oxygen- and moisture-free conditions under argon using standard Schlenk or glovebox techniques at room temperature [298(3) K] unless noted otherwise. Removal of volatile substances *in vacuo* was carried out at 1×10^{-3} mbar. Further information on experimental procedures, preparation of starting materials, data acquisition and processing, purification procedures, and a full set of analytical data for each compound as well as further details on the computations can be found in the Supporting Information (SI).

Synthesis of 2F. *Reaction.* **2Cl**·0.75 C_6H_6 (689 mg, 0.762 mmol), KF (180 mg, 3.10 mmol), and 18-crown-6 (24 mg, 0.091 mmol) are dissolved in MeCN (35 mL) at ambient temperature. Most of the potassium salt remains undissolved and suspended in the orange solution. The mixture is stirred for 5 days at ambient temperature until complete conversion of **2Cl** is achieved. Afterward, the solvent is removed and the residue is dried *in vacuo* (1×10^{-3} mbar) for 120 min at 50 °C. To make sure that all MeCN is removed from the product, the yellow powder is suspended in *n*-pentane (10 mL) and again dried *in vacuo* (1×10^{-3} mbar) for 20 min at 50 °C.

Separation from 18-Crown-6 and KF/KC. Most of the crown ether can be removed from the product by threefold extraction with *n*-pentane (20 mL, the solvent is re-condensed after each step). Afterward, the residue is dried *in vacuo* (1×10^{-3} mbar) for 20 min at 50 °C and suspended in benzene (12 mL). The orange solution is filtered off the colorless solids (pore 4), and the solids are washed with two additional amounts of benzene (5 mL, 1 mL; ambient temperature) to make sure all product is extracted from the KF and KCl. The filtrate is dried *in vacuo* (1×10^{-3} mbar) for 120 min at 50 °C.

Separation of the Isomers. This raw product contains both isomers of **2F**. To separate them, it is suspended in MeCN (20 mL) and the mixture is filtered through a pore 4 frit. The solid residue is again washed with MeCN (5 mL, ambient temperature). Due to significantly higher solubility of the *endo−exo*-isomer in MeCN, it is extracted from the mixture as orange filtrate (a), while the yellow residue (b) mainly consists of the *endo−endo* isomer.

Isolation of Endo−Exo-2F. The clear orange filtrate (a) is concentrated *in vacuo* (1×10^{-3} mbar). As soon as the solution turns slightly turbid, the mixture is warmed to approx. 80 °C and slowly cooled down to 5 °C, resulting in the deposition of orange blocks of the *endo−exo*-isomer. The supernatant is removed via syringe, and the crystals are washed with MeCN (0.5 mL, ambient temperature) and dried *in vacuo* (1×10^{-3} mbar) at 50 °C for 2 h. The second fraction can be received from the supernatant in the same manner. Yield (*endo−exo*-**2F**): 185 mg (0.227 mmol, 30%).

Isolation of Endo−Endo-2F and Endo−Exo-2F. The residue (b) is dried *in vacuo* (1×10^{-3} mbar) for 60 min at 50 °C and dissolved in dichloromethane (5 mL). The resulting yellow solution is concentrated *in vacuo* (1×10^{-3} mbar) to incipient crystallization and then slowly cooled to 5 °C and stored in the fridge overnight. On the next day, the supernatant is removed by syringe and the yellow crystals of a mixture of the *endo−endo* and *endo−exo* isomers are washed with dichloromethane (0.5 mL, ambient temperature) and dried *in vacuo* (1×10^{-3} mbar) at 50 °C for 2 h. After drying, 0.6 to 1 equiv dichloromethane remains in the product. The second fraction can be received from the supernatant and the washing solution in the same manner. Yield (*endo−endo*-**2F** and *endo−exo*-**2F** (58:42), incl. 0.6 equiv dichloromethane): 92 mg (0.107 mmol, 14%). Total yield (**2F**): 277 mg (0.334 mmol, 44%).

Endo−Exo-2F (for the Isomeric Mixture of Endo−Endo- and Endo−Exo-2F, See below). Mp 185 °C (dec.). **CHN** calcd (found) in %: C 67.97 (67.98), H 5.95 (6.05), N 13.78 (13.98). $^{19}F\{^1H\}$ NMR (toluene-d_8, 470.6 MHz): δ = −82.8 (dd, $^1J(^{19}F,^{31}P)$ =1297 Hz, $J(^{19}F,^{19}F)$ = 9 Hz, 1F, *exo*-P*F*), −84.9 ppm (ddd, $^1J(^{19}F,^{31}P)$ = 1337 Hz, $J(^{19}F,^{31}P)$ = 132 Hz, $J(^{19}F,^{19}F)$ = 9 Hz, 1F, *endo*-P*F*). $^{31}P\{^1H\}$ NMR (toluene-d_8, 202.5 MHz): δ = 82.4 (d, $^1J(^{31}P,^{19}F)$ = 1337 Hz, 1P, *endo*-P*F*), 82.1 ppm (dd, $^1J(^{31}P,^{19}F)$ =1297 Hz, $J(^{31}P,^{19}F)$ =132 Hz, 1P, *exo*-P*F*). ^1H NMR (toluene-d_8, 500.1 MHz): δ = 8.06 (d, J = 1.8 Hz, 2H, C*H* imine), 7.83 (d, J = 1.3 Hz, 2H, C*H* imine), 6.73 (s, 2H, C*H* phenylene), 6.43 (dd, $^3J(^1H,^1H)$ =3.5 Hz, J = 1.3 Hz, 2H, C*H* pyrrole), 6.39 (s, 2H, C*H* phenylene), 6.32 (d, $^3J(^1H,^1H)$ = 3.5 Hz, 2H, C*H* pyrrole), 5.93 (d, $^3J(^1H,^1H)$ = 3.5 Hz, 2H, C*H* pyrrole), 5.88 (d, $^3J(^1H,^1H)$ = 3.5 Hz, 2H, C*H* pyrrole), 1.99 (q, $^3J(^1H,^1H)$ = 7.5 Hz, 2H, CH_2), 1.87 (s, 6H, CCH_3), 1.84 (q, $^3J(^1H,^1H)$ = 7.3 Hz, 2H, CH_2), 1.80 (s, 6 H, CCH_3), 1.80 (q, $^3J(^1H,^1H)$ = 7.3 Hz, 2H, CH_2), 1.65 (q, $^3J(^1H,^1H)$ = 7.5 Hz, 2H, CH_2), 0.85 (t, $^3J(^1H,^1H)$ = 7.3 Hz, 3H, CH_2CH_3), 0.77 (t, $^3J(^1H,^1H)$ = 7.5 Hz, 3H, CH_2CH_3), 0.68 (t, $^3J(^1H,^1H)$ = 7.3 Hz, 3H, CH_2CH_3), 0.48 ppm (t, $^3J(^1H,^1H)$ = 7.5 Hz, 3H, CH_2CH_3).

Isomeric Mixture of Endo−Endo- and Endo−Exo-2F. Mp 170 °C (dec.). **CHN** (incl. 1 equiv CH_2Cl_2) calcd. (found) in %: C 62.88 (62.53), H 5.61 (5.68), N 12.48 (12.66). The NMR data is given separately for each isomer: $^{19}F\{^1H\}$ NMR (*endo−endo*-**2F**, CD_2Cl_2, 470.6 MHz): δ = −77.4 ppm (m). $^{19}F\{^1H\}$ NMR (*endo−exo*-**2F**, CD_2Cl_2, 470.6 MHz): δ = −82.4 (dd, $^1J(^{19}F,^{31}P)$ =1285 Hz, $J(^{19}F,^{19}F)$ = 10 Hz, 1F, *exo*-P*F*), −84.2 ppm (ddd, $^1J(^{19}F,^{31}P)$ = 1326 Hz, $J(^{19}F,^{31}P)$ = 127 Hz, $J(^{19}F,^{19}F)$ = 10 Hz, 1F, *endo*-P*F*). $^{31}P\{^1H\}$ NMR (*endo−endo*-**2F**, CD_2Cl_2, 202.5 MHz): δ = 81.6 ppm (m). $^{31}P\{^1H\}$ NMR (*endo−exo*-**2F**, CD_2Cl_2, 202.5 MHz): δ = 83.5 (dd, $^1J(^{31}P,^{19}F)$ =1285 Hz, $J(^{31}P,^{19}F)$ =127 Hz, 1 P, *exo*-P*F*) 83.2 ppm (d, $^1J(^{31}P,^{19}F)$ = 1326 Hz, 1P, *endo*-P*F*). ^1H NMR (*endo−endo*-**2F**, CD_2Cl_2, 500.1 MHz): δ = 8.21 (d, J = 2.0 Hz, 4 H, C*H* imine), 6.83 (d, $^3J(^1H,^1H)$ = 3.5 Hz, 4 H, C*H* pyrrole), 6.62 (s, 4H, C*H* phenylene), 6.26 (d, $^3J(^1H,^1H)$ =3.5 Hz, 4H, C*H* pyrrole), 5.33 (s, CH_2Cl_2), 2.23 (s, 12H, CCH_3), 2.14 (q, $^3J(^1H,^1H)$ = 7.2 Hz, 4H, CH_2), 1.93 (q, $^3J(^1H,^1H)$ = 7.5 Hz, 4H, CH_2), 0.80 (t, $^3J(^1H,^1H)$ = 7.2 Hz, 6 H, CH_2CH_3), 0.73 ppm (t, $^3J(^1H,^1H)$ = 7.5 Hz, 6H, CH_2CH_3). ^1H NMR (*endo−exo*-**2F**, CD_2Cl_2, 500.1 MHz): δ = 8.24 (d, J = 1.7 Hz, 2H, C*H* imine), 7.96 (s, 2H, C*H* imine), 6.86 (s, 2H, C*H* phenylene), 6.72−6.75 (m, 4H, C*H* pyrrole), 6.68 (s, 2H, C*H* phenylene), 6.20−6.23 (m, 2 H, C*H* pyrrole), 6.17−6.20 (m, 2H, C*H* pyrrole), 5.33 (s, CH_2Cl_2), 2.25 (s, 6H, CCH_3), 2.23 (s, 6H, CCH_3), 2.10 (q, $^3J(^1H,^1H)$ = 7.2 Hz, 2 H, CH_2), 2.04 (q, $^3J(^1H,^1H)$ = 7.3 Hz, 2H, CH_2), 2.01 (q, $^3J(^1H,^1H)$ = 7.3 Hz, 2H, CH_2), 1.74 (q, $^3J(^1H,^1H)$ = 7.5 Hz, 2 H, CH_2), 0.86 (t, $^3J(^1H,^1H)$ = 7.2 Hz, 3H, CH_2CH_3), 0.76 (t, $^3J(^1H,^1H)$ = 7.3 Hz, 3H, CH_2CH_3), 0.61 (t, $^3J(^1H,^1H)$ = 7.3 Hz, 3H, CH_2CH_3), 0.58 ppm (t, $^3J(^1H,^1H)$ = 7.5 Hz, 3H, CH_2CH_3).

Synthesis of [3]Br_2. **2Cl**·2/3 C_6H_6 (586 mg, 0.653 mmol) is dissolved in toluene (50 mL) giving an orange solution which is cooled to −80 °C. In a 1 mL syringe, TMS−Br (211 mg, 1.38 mmol) is mixed with toluene (0.5 mL) and added dropwise to the cooled, stirred solution of **2Cl** over a period of 5 min. To ensure complete addition of TMS−Br, the syringe is washed with toluene (2 × 0.5 mL) and the washing solutions are added to the reaction mixture. The solution is slowly warmed to ambient temperature over 80 min and further stirred at ambient temperature for 120 min during which a slight color change to red orange can be observed. All volatiles are removed *in vacuo* (1×10^{-3} mbar) at max. 30 °C, and the orange residue is dried *in vacuo* (1×10^{-3} mbar) at ambient temperature for 120 min resulting in a yellow powder. This raw product contains approx. 0.5 equiv toluene. Yield (of the raw product): 543 mg (0.548 mmol, 85%).

https://doi.org/10.1021/acs.inorgchem.3c00481
Inorg. Chem. XXXX, XXX, XXX−XXX

A part of this raw product (166 mg, 0.259 mmol) is dissolved in MeCN (15 mL) and filtered (pore 4). The resulting red brown solution is left to stand in the dark at ambient temperature for 8 days during which a color change to dark red can be observed, whereupon dark red crystals begin to precipitate. For isolation of the product, the supernatant is removed via syringe and the crystals are washed with MeCN (1 mL, ambient temperature) and dried *in vacuo* (1×10^{-3} mbar) at ambient temperature for 120 min. The product contains approx. 2/3 equiv of MeCN. Yield (for crystallization step, incl. 2/3 equiv MeCN): 66 mg (0.064 mmol, 26%).

Mp 165 °C (dec.). CHN calcd (found) in %: C 59.11 (59.24), H 5.18 (5.08), N 11.99 (12.29). $^{31}P\{^{1}H\}$ NMR (DMSO-d_6, 202.5 MHz): δ = −61.6 (s, 0.07 P, impurity), −81.5 (s, 2 P, *P* product), −84.1 ppm (s, 0.07 P, impurity). Small amounts of impurities in the NMR spectra can be attributed to decomposition traces of water in the DMSO-d_6. ^{1}H NMR (DMSO-d_6, 500.1 MHz): δ = 9.67−9.81 (m, 2H, C*H* imine), 7.97−8.08 (m, 2H, C*H* pyrrole), 7.13−7.18 (m, 4H, C*H* phenylene, C*H* pyrrole), 6.97 (br s, 2H, C*H* phenylene), 6.73−6.87 (m, 2H, P-C*H*), 5.96−6.04 (m, 2H, C*H* pyrrole), 5.86−5.91 (m, C*H* pyrrole), 2.18 (s, 6H, C-CH_3), 2.12−2.22 (m, 4H, CH_2-CH_3), 2.09 (s, 6H, C-CH_3), 2.07 (s, 2H, H_3CCN), 1.76−1.92 (m, 4H, CH_2-CH_3), 0.86 (t, $^{3}J(^{1}H,^{1}H)$ = 7.3 Hz, 6H, CH$_2$-CH_3), 0.70 ppm (t, $^{3}J(^{1}H,^{1}H)$ = 7.3 Hz, 6H, CH$_2$-CH_3).

Synthesis of [3]I_2. **2Cl**·2/3 C_6H_6 (429 mg, 0.478 mmol) is dissolved in toluene (25 mL), and the resulting orange solution is cooled to −80 °C. A solution of TMS−I (206 mg, 1.47 mmol) in toluene (0.5 mL) is prepared directly in a syringe and added dropwise over a period of 7 min under stirring. To ensure complete addition of the TMS−I, the syringe is washed with toluene (2 × 0.5 mL) and the washing solution is added to the reaction mixture. The solution is slowly warmed to ambient temperature over 150 min and subsequently stirred at ambient temperature for further 40 min undergoing a color change from orange over red to a brown suspension. All volatiles are removed *in vacuo* (1×10^{-3} mbar) at max. 30 °C to prevent decomposition. Afterward, the brownish solids are dried *in vacuo* (1×10^{-3} mbar) at ambient temperature for 150 min. The resulting raw product is dissolved in dichloromethane (10 mL), and the clear, dark red solution is left to stand overnight in the dark at ambient temperature, resulting in the precipitation of small dark crystals and fine red powder of [**3**]I_2. The supernatant is filtered off (pore 4), and the bright red residue is washed with dichloromethane (1 mL, ambient temperature) and subsequently dried *in vacuo* (1×10^{-3} mbar) at ambient temperature for 120 min. An amount of 0.6 to 0.8 equiv of dichloromethane remains in the product after drying. Yield (incl. 0.6 equiv CH_2Cl_2): 378 mg (0.350 mmol, 73%).

Mp. 115 °C (dec.). CHN (incl. 0.75 equiv CH_2Cl_2) calcd (found) in %: C 51.40 (51.36), H 4.57 (4.92), N 10.26 (10.24). $^{31}P\{^{1}H\}$-NMR (D_3CCN, 121.5 MHz): δ = −81.5 ppm (s). ^{1}H NMR (D_3CCN, 300.1 MHz): δ = 9.13 (d, $J(^{1}H,^{31}P)$ = 11.1 Hz, 2H, C*H* imine), 7.79 (dd, $^{3}J(^{1}H,^{1}H)$ = 4.1 Hz, $J(^{1}H,^{31}P)$ = 3.3 Hz, 2H, C*H* pyrrole), 7.02 (s, 2H, C*H* phenylene), 6.95 (dd, $J(^{1}H,^{31}P)$ = 6.3 Hz, $^{3}J(^{1}H,^{1}H)$ = 4.1 Hz, C*H* pyrrole), 6.78 (s, 2H, C*H* phenylene), 6.40 (dd, $^{2}J(^{1}H,^{31}P)$ = 21.8 Hz, $J(^{1}H,^{31}P)$ = 10.2 Hz, 2H, P-C*H*), 6.04−6.13 (m, 2H, C*H* pyrrole), 5.85−5.90 (m, 2H, C*H* pyrrole), 5.45 (s, 3.0H, CH_2Cl_2), 2.22 (s, 6H, C-CH_3), 2.14−2.21 (m, 4H, CH_2-CH_3), 2.13 (s, 6H, C-CH_3), 1.84−1.90 (m, 4H, CH_2-CH_3), 1.09 (d, $^{3}J(^{1}H,^{1}H)$ = 6.2 Hz, 2H, NMR solvent impurity), 0.91 (t, $^{3}J(^{1}H,^{1}H)$ = 7.5 Hz, 6H, CH$_2$-CH_3), 0.75 ppm (t, *J* = 7.3 Hz, $^{3}J(^{1}H,^{1}H)$ = 7.3 Hz, 6H, CH$_2$-CH_3).

Theoretical Calculations. Computations were carried out using Gaussian09[42] or ORCA 4.2.1[32,33] and the standalone version of NBO 6.0.[27,28] Structure optimizations employed the DFT functional PBE[43,44] in conjunction with Grimme's dispersion correction D3(BJ)[45,46] and the def2-TZVP[47,48] basis set for all elements except halogens; for fluorine, chlorine, and bromine, the more diffuse 6-311 + G(d,p)[49−51] basis set was used, and for iodine, the def2-TZVPD[47,52] basis set (notation PBE-D3/*m*TZVP) was used. The resolution of identity (RI) approximation was employed using the appropriate Coulomb fitting basis of the Weigend group[48] for all elements except fluorine, chlorine, and bromine, and for these elements, the fitting basis was generated automatically using Gaussian09.[42] All structures were fully optimized and confirmed as minima by frequency analyses. Chemical shifts and coupling constants were derived by the GIAO method.[53−57] The Gibbs free energies of solvation ΔG°_{solv} were computed as the differences between the SCF energies of the respective species in the gas phase and in solution. The SCF energies in solution discussed here were obtained by single point calculations on the optimized gas-phase structures using the SMD continuum solvation model[37] (PBE-D3/*m*TZVP). Be aware, that for the SMD model, we used adapted Coulomb radii for bromine (2.60 Å) and iodine (2.74 Å) published by the groups of Huber, Truhlar, and Cramer to receive reasonable results.[38] More accurate electronic energies for optimized structures were computed by single-point DLPNO-CCSD(T)[34−36] calculations employing triple zeta basis sets. For more detailed information, see SI, p. S76f.

■ ASSOCIATED CONTENT

Supporting Information

The Supporting Information is available free of charge at https://pubs.acs.org/doi/10.1021/acs.inorgchem.3c00481.

Experimental section, preparation of starting materials and compounds, structure elucidation, additional NMR spectra, and computational details (PDF)

Xyz-files of optimized structures (ZIP)

Accession Codes

CCDC 2204014−2204017 contain the supplementary crystallographic data for this paper. These data can be obtained free of charge via www.ccdc.cam.ac.uk/data_request/cif, or by emailing data_request@ccdc.cam.ac.uk, or by contacting The Cambridge Crystallographic Data Centre, 12 Union Road, Cambridge CB2 1EZ, UK; fax: +44 1223 336033.

CCDC 2204014−2204017 contains the supplementary crystallographic data for this paper. These data can be obtained free of charge at www.ccdc.cam.ac.uk/data_request/cif, by emailing data_request@ccdc.cam.ac.uk, or by contacting the Cambridge Crystallographic Data Centre, 12 Union Road, Cambridge CB2 1EZ, U.K.; fax: +44 1223 336033.

■ AUTHOR INFORMATION

Corresponding Author

Axel Schulz − *Institut für Chemie, Universität Rostock, D-18059 Rostock, Germany; Leibniz-Institut für Katalyse e.V., D-18059 Rostock, Germany;* orcid.org/0000-0001-9060-7065; Email: axel.schulz@uni-rostock.de

Authors

Liesa Eickhoff − *Institut für Chemie, Universität Rostock, D-18059 Rostock, Germany;* orcid.org/0000-0003-1368-5507

Pascal Kramer − *Institut für Chemie, Universität Rostock, D-18059 Rostock, Germany;* orcid.org/0000-0002-1130-3440

Jonas Bresien − *Institut für Chemie, Universität Rostock, D-18059 Rostock, Germany;* orcid.org/0000-0001-9450-3407

Dirk Michalik − *Institut für Chemie, Universität Rostock, D-18059 Rostock, Germany; Leibniz-Institut für Katalyse e.V., D-18059 Rostock, Germany*

Alexander Villinger − *Institut für Chemie, Universität Rostock, D-18059 Rostock, Germany;* orcid.org/0000-0002-0868-9987

Complete contact information is available at: https://pubs.acs.org/10.1021/acs.inorgchem.3c00481

https://doi.org/10.1021/acs.inorgchem.3c00481
Inorg. Chem. XXXX, XXX, XXX−XXX

Notes

The authors declare no competing financial interest.

■ ACKNOWLEDGMENTS

We gratefully acknowledge financial support by the Deutsche Forschungsgemeinschaft (DFG; SCHU 1170/12-2). L.E. gratefully acknowledges funding by the University of Rostock via the Ph.D. Scholarship Program. Moreover, we wish to thank the ITMZ at the University of Rostock for access to the cluster computer and especially Malte Willert for his assistance with the queuing system and software installations.

■ REFERENCES

(1) Maity, R.; Birenheide, B. S.; Breher, F.; Sarkar, B. Cooperative Effects in Multimetallic Complexes Applied in Catalysis. *ChemCatChem* **2021**, *13*, 2337−2370.
(2) Wang, Q.; Brooks, S. H.; Liu, T.; Tomson, N. C. Tuning Metal−Metal Interactions for Cooperative Small Molecule Activation. *Chem. Commun.* **2021**, *57*, 2839−2853.
(3) Navarro, M.; Moreno, J. J.; Pérez-Jiménez, M.; Campos, J. Small Molecule Activation with Bimetallic Systems: A Landscape of Cooperative Reactivity. *Chem. Commun.* **2022**, *58*, 11220−11235.
(4) Campos, J. Bimetallic Cooperation across the Periodic Table. *Nat. Rev. Chem.* **2020**, *4*, 696−702.
(5) Wodrich, M. D.; Hu, X. Natural Inspirations for Metal−Ligand Cooperative Catalysis. *Nat. Rev. Chem.* **2018**, *2*, No. 0099.
(6) Gil-Negrete, J. M.; Hevia, E. Main Group Bimetallic Partnerships for Cooperative Catalysis. *Chem. Sci.* **2021**, *12*, 1982−1992.
(7) Greb, L.; Ebner, F.; Ginzburg, Y.; Sigmund, L. M. Element-Ligand Cooperativity with p-Block Elements. *Eur. J. Inorg. Chem.* **2020**, *2020*, 3030−3047.
(8) Hasenbeck, M.; Gellrich, U. Boron−Ligand Cooperation: The Concept and Applications. *Chem. − Eur. J.* **2021**, *27*, 5615−5626.
(9) Collman, J. P.; Elliott, C. M.; Halbert, T. R.; Tovrog, B. S. Synthesis and Characterization of "Face-to-Face" Porphyrins. *Proc. Natl. Acad. Sci. U. S. A.* **1977**, *74*, 18−22.
(10) Chang, C. K.; Abdalmuhdi, I. Anthracene Pillared Cofacial Diporphyrin. *J. Org. Chem.* **1983**, *48*, 5388−5390.
(11) Collman, J. P.; Wagenknecht, P. S.; Hutchison, J. E. Molecular Catalysts for Multielectron Redox Reactions of Small Molecules: The "Cofacial Metallodiporphyrin" Approach. *Angew. Chem., Int. Ed. Engl.* **1994**, *33*, 1537−1554.
(12) Uppenbrink, J. Induced Fit in a Molecular Pac-Man. *Science* **2000**, *287*, 769.
(13) Iwatani, T. *Pac-Man*; Midway Games: Chicago, 1980.
(14) Lang, P.; Schwalbe, M. Pacman Compounds: From Energy Transfer to Cooperative Catalysis. *Chem. − Eur. J.* **2017**, *23*, 17398−17412.
(15) Love, J. B. A Macrocyclic Approach to Transition Metal and Uranyl Pacman Complexes. *Chem. Commun.* **2009**, 3154−3165.
(16) Eickhoff, L.; Ohms, L.; Bresien, J.; Villinger, A.; Michalik, D.; Schulz, A. A Phosphorus-Based Pacman Dication Generated by Cooperative Self-Activation of a Pacman Phosphane. *Chem. − Eur. J.* **2022**, *28*, No. e202103983.
(17) Givaja, G.; Blake, A. J.; Wilson, C.; Schröder, M.; Love, J. B. Macrocyclic Diiminodipyrromethane Complexes: Structural Analogues of Pac-Man Porphyrins. *Chem. Commun.* **2003**, 2508−2509.
(18) Holleman, A. F.; Wiberg, E.; Wiberg, N. *Anorganische Chemie. Band 1: Grundlagen Und Hauptgruppenelemente*; Walter de Gruyter: Berlin, 2017.
(19) Plinta, H.; Neda, I.; Fischer, A.; Jones, P. G.; Schmutzler, R. A New Synthesis of P-Substituted 2,3-Dihydro-1,3-Dimethyl-1,2λ^3-Benzodiazaphosphorin-4(1H)-Ones and Alkylaminodifluorophosphanes with Chlorodifluorophosphane. — Synthesis and Structure of {cis-Bis[Bis(2-Chloroethyl)Aminodifluorophosphane]Dichloro}-platinum(II). *Chem. Ber.* **1995**, *128*, 695−701.
(20) Nieger, M.; Hupfer, H.; Niecke, E.; Detsch, R. CCDC 114926. *CSD Communication*, 1999.
(21) Fei, Z.; Thönnessen, H.; Jones, P. G.; Schmutzler, R. Synthesis of Symmetrical Bis-(2-Chloro-1,3,2-Benzodiazaphosphorinones) Hydrolysis and Fluorination of Selected Compounds. *Z. Anorg. Allg. Chem.* **1999**, *625*, 1732−1739.
(22) Gudat, D.; Haghverdi, A.; Hupfer, H.; Nieger, M. Stability and Electrophilicity of Phosphorus Analogues of Arduengo Carbenes—An Experimental and Computational Study. *Chem. − Eur. J.* **2000**, *6*, 3414−3425.
(23) Reiß, F.; Schulz, A.; Villinger, A. The N,N-Bis(Terphenyl)-Aminophosphenium Cation − A Sensitive Probe for Interactions with Different Anions. *Eur. J. Inorg. Chem.* **2012**, *2012*, 261−271.
(24) Brückner, A.; Hinz, A.; Priebe, J. B.; Schulz, A.; Villinger, A. Cyclic Group 15 Radical Cations. *Angew. Chem., Int. Ed.* **2015**, *54*, 7426−7430.
(25) Hinz, A.; Schulz, A.; Villinger, A. Stable Heterocyclopentane-1,3-Diyls. *Angew. Chem., Int. Ed.* **2015**, *54*, 2776−2779.
(26) Mantina, M.; Chamberlin, A. C.; Valero, R.; Cramer, C. J.; Truhlar, D. G. Consistent van Der Waals Radii for the Whole Main Group. *J. Phys. Chem. A* **2009**, *113*, 5806−5812.
(27) Glendening, E. D.; Badenhoop, J. K.; Reed, A. E.; Carpenter, J. E.; Bohmann, J. A.; Morales, C. M.; Landis, C. R.; Weinhold, F. *NBO 6.0*; Theoretical Chemistry Institute, University of Wisconsin: Madison, 2013.
(28) Weinhold, F.; Landis, C. R.; Glendening, E. D. What Is NBO Analysis and How Is It Useful? *Int. Rev. Phys. Chem.* **2016**, *35*, 399−440.
(29) Tezgerevska, T.; Alley, K. G.; Boskovic, C. Valence Tautomerism in Metal Complexes: Stimulated and Reversible Intramolecular Electron Transfer between Metal Centers and Organic Ligands. *Coord. Chem. Rev.* **2014**, *268*, 23−40.
(30) Greb, L. Valence Tautomerism of p-Block Element Compounds − An Eligible Phenomenon for Main Group Catalysis? *Eur. J. Inorg. Chem.* **2022**, *2022*, No. e202100871.
(31) Schorpp, M.; Yadav, R.; Roth, D.; Greb, L. Calix[4]Pyrrolato Stibenium: Lewis Superacidity by Antimony(III)-Antimony(V) Electromerism. *Angew. Chem., Int. Ed.* **2022**, *61*, No. e202207963.
(32) Neese, F.; Wiley, J. The ORCA Program System. *WIREs Comput. Mol. Sci.* **2012**, *2*, 73−78.
(33) Neese, F. Software Update: The ORCA Program System, Version 4.0. *WIREs Comput. Mol. Sci.* **2018**, *8*, No. e1327.
(34) Riplinger, C.; Neese, F. An Efficient and near Linear Scaling Pair Natural Orbital Based Local Coupled Cluster Method. *J. Chem. Phys.* **2013**, *138*, No. 034106.
(35) Liakos, D. G.; Sparta, M.; Kesharwani, M. K.; Martin, J. M. L.; Neese, F. Exploring the Accuracy Limits of Local Pair Natural Orbital Coupled-Cluster Theory. *J. Chem. Theory Comput.* **2015**, *11*, 1525−1539.
(36) Riplinger, C.; Pinski, P.; Becker, U.; Valeev, E. F.; Neese, F. Sparse Maps—A Systematic Infrastructure for Reduced-Scaling Electronic Structure Methods. II. Linear Scaling Domain Based Pair Natural Orbital Coupled Cluster Theory. *J. Chem. Phys.* **2016**, *144*, No. 024109.
(37) Marenich, A. V.; Cramer, C. J.; Truhlar, D. G. Universal Solvation Model Based on Solute Electron Density and on a Continuum Model of the Solvent Defined by the Bulk Dielectric Constant and Atomic Surface Tensions. *J. Phys. Chem. B* **2009**, *113*, 6378−6396.
(38) Engelage, E.; Schulz, N.; Heinen, F.; Huber, S. M.; Truhlar, D. G.; Cramer, C. J. Refined SMD Parameters for Bromine and Iodine Accurately Model Halogen-Bonding Interactions in Solution. *Chem. − Eur. J.* **2018**, *24*, 15983−15987.
(39) Evans, D. F. The Determination of the Paramagnetic Susceptibility of Substances in Solution by Nuclear Magnetic Resonance. *J. Chem. Soc.* **1959**, 2003−2005.
(40) Budzelaar, P. H. M. *GNMR for Windows*; IvorySoft, 2006.
(41) Renard, S. L.; Fisher, J.; Kilner, C. A.; Thornton-Pett, M.; Kee, T. P. On the Mechanisms of Degenerate Halogen Exchange in Phosphorus(III) Halides. *Dalton Trans.* **2002**, *14*, 2921−2932.

https://doi.org/10.1021/acs.inorgchem.3c00481
Inorg. Chem. XXXX, XXX, XXX−XXX

(42) Frisch, M.J.; Trucks, G. W.; Schlegel, H. B.; Scuseria, G. E.; Robb, M. A.; Cheeseman, J. R.; Scalmani, G.; Barone, V.; Mennucci, B.; Petersson, G. A.; Nakatsuji, H.; Caricato, M.; Li, X.; Hratchian, H. P.; Izmaylov, A. F.; Bloino, J.; Zheng, G.; Sonnenberg, J. L.; Hada, M.; Ehara, M.; Toyota, K.; Fukuda, R.; Hasegawa, J.; Ishida, M.; Nakajima, T.; Honda, Y.; Kitao, O.; Nakai, H.; Vreven, T.; Montgomery, J. A., Jr.; Peralta, J. E.; Ogliaro, F.; Bearpark, M.; Heyd, J. J.; Brothers, E.; Kudin, K. N.; Staroverov, V. N.; Keith, T.; Kobayashi, R.; Normand, J.; Raghavachari, K.; Rendell, A.; Burant, J. C.; Iyengar, S. S.; Tomasi, J.; Cossi, M.; Rega, N.; Millam, J. M.; Klene, M.; Knox, J. E.; Cross, J. B.; Bakken, V.; Adamo, C.; Jaramillo, J.; Gomperts, R.; Stratmann, R. E.; Yazyev, O.; Austin, A. J.; Cammi, R.; Pomelli, C.; Ochterski, J. W.; Martin, R. L.; Morokuma, K.; Zakrzewski, V. G.; Voth, G. A.; Salvador, P.; Dannenberg, J. J.; Dapprich, S.; Daniels, A. D.; Farkas, Ö.; Foresman, J. B.; Ortiz, J. V.; Cioslowski, J.; Fox, D. J. *Gaussian 09, Revision E.01*; Gaussian, Inc.: Wallingford CT, 2013.

(43) Perdew, J. P.; Burke, K.; Ernzerhof, M. Generalized Gradient Approximation Made Simple. *Phys. Rev. Lett.* **1996**, *77*, 3865−3868.

(44) Perdew, J. P.; Burke, K.; Ernzerhof, M. Generalized Gradient Approximation Made Simple [Phys. Rev. Lett. 77, 3865 (1996)]. *Phys. Rev. Lett.* **1997**, *78*, 1396−1396.

(45) Grimme, S.; Antony, J.; Ehrlich, S.; Krieg, H. A Consistent and Accurate Ab Initio Parametrization of Density Functional Dispersion Correction (DFT-D) for the 94 Elements H-Pu. *J. Chem. Phys.* **2010**, *132*, 154104.

(46) Grimme, S.; Ehrlich, S.; Goerigk, L. Effect of the Damping Function in Dispersion Corrected Density Functional Theory. *J. Comput. Chem.* **2011**, *32*, 1456−1465.

(47) Weigend, F.; Ahlrichs, R. Balanced Basis Sets of Split Valence, Triple Zeta Valence and Quadruple Zeta Valence Quality for H to Rn: Design and Assessment of Accuracy. *Phys. Chem. Chem. Phys.* **2005**, *7*, 3297−3297.

(48) Weigend, F. Accurate Coulomb-Fitting Basis Sets for H to Rn. *Phys. Chem. Chem. Phys.* **2006**, *8*, 1057−1065.

(49) McLean, A. D.; Chandler, G. S. Contracted Gaussian Basis Sets for Molecular Calculations. I. Second Row Atoms, Z=11−18. *J. Chem. Phys.* **1980**, *72*, 5639−5648.

(50) Frisch, M. J.; Pople, J. A.; Binkley, J. S. Self-consistent Molecular Orbital Methods 25. Supplementary Functions for Gaussian Basis Sets. *J. Chem. Phys.* **1984**, *80*, 3265−3269.

(51) Clark, T.; Chandrasekhar, J.; Spitznagel, G. W.; Schleyer, P. V. R. Efficient Diffuse Function-Augmented Basis Sets for Anion Calculations. III. The 3-21+G Basis Set for First-Row Elements, Li-F. *J. Comput. Chem.* **1983**, *4*, 294−301.

(52) Rappoport, D.; Furche, F. Property-Optimized Gaussian Basis Sets for Molecular Response Calculations. *J. Chem. Phys.* **2010**, *133*, 134105.

(53) London, F. Théorie Quantique Des Courants Interatomiques Dans Les Combinaisons Aromatiques. *J. Phys. Radium* **1937**, *8*, 397−409.

(54) McWeeny, R. Perturbation Theory for the Fock-Dirac Density Matrix. *Phys. Rev.* **1962**, *126*, 1028−1034.

(55) Ditchfield, R. Self-Consistent Perturbation Theory of Diamagnetism. *Mol. Phys.* **1974**, *27*, 789−807.

(56) Wolinski, K.; Hinton, J. F.; Pulay, P. Efficient Implementation of the Gauge-Independent Atomic Orbital Method for NMR Chemical Shift Calculations. *J. Am. Chem. Soc.* **1990**, *112*, 8251−8260.

(57) Cheeseman, J. R.; Trucks, G. W.; Keith, T. A.; Frisch, M. J. A Comparison of Models for Calculating Nuclear Magnetic Resonance Shielding Tensors. *J. Chem. Phys.* **1996**, *104*, 5497−5509.

https://doi.org/10.1021/acs.inorgchem.3c00481
Inorg. Chem. XXXX, XXX, XXX−XXX

6.3 Coinage metal complexes of multidentate Pacman phosphane ligands

L. Ohms, L. Eickhoff, P. Kramer, A. Villinger, J. Bresien, A. Schulz*

Chem. Commun. **2023**, accepted.

DOI: 10.1039/D3CC01174G

ChemComm

COMMUNICATION

View Article Online
View Journal

Cite this: DOI: 10.1039/d3cc01174g

Received 9th March 2023,
Accepted 30th March 2023

DOI: 10.1039/d3cc01174g

rsc.li/chemcomm

Coinage metal complexes of multidentate Pacman phosphane ligands†

Leon Ohms, [a] Liesa Eickhoff, [a] Pascal Kramer, [a] Alexander Villinger, [a] Jonas Bresien [a] and Axel Schulz *[ab]

We present the extension of Pacman ligands to bidentate phosphane ligands enabling them to bind metals in their sterically protected cavity. The coordination of coinage metals shows the ability of the ligand to adopt different coordination modes by distortion, of which some additionally include the imine nitrogen atoms. Besides the coordinated metal, the substitution on the phosphorus atoms influences the type of coordination.

Pacman ligands were introduced in the late 70s and early 80s to mimic enzymes and investigate metal–metal interactions.[1,2] To serve these purposes, they consist of two chelating units forced into a parallel arrangement by a rigid connection on only one side of the molecule (*cf.* Chart 1, left). This leads to a more flexible structure with a variable distance between the chelating units and their coordinated metal centres. The name "Pacman ligands" was introduced by Collman in 1992 in reference to the videogame "Pac-Man™".[3,4] While previous Pacman ligands are mostly based on porphyrins, the groups of Sessler and Love independently introduced calix[4]pyrrole Schiff base ligands in 2003. These also act as Pacman ligands and are much easier to synthesize than porphyrin based Pacman ligands.[5,6] Since then, a variety of complexes have been published.[7,8] In most of them, each molecule half binds its own metal centre (Chart 1, left).

Recently, our group was able to introduce phosphorus(III) into a Pacman ligand, which may be regarded as the first non-metal Pacman complex (Chart 1, middle).[9] In this case, a phosphorus–chlorine unit is located in each half of the molecule. One chlorine substituent is directed into the cavity of the molecule and the other points outwards, forming the *endo-exo* isomer exclusively. In this paper, we show that increasing the steric demand of the substituents on the phosphorus forces the ligand to form an *exo–exo* isomer with both substituents pointing outwards. Accordingly, in this isomer the free electron pairs on the phosphorus are directed into the cavity of the molecule, qualifying them as bidentate phosphane ligands for the coordination of metals inside the cavity (Chart 1, right). We refer to such compounds as Pacman phosphane ligands, not to be confused with the Pacman ligands bearing no phosphorus atoms (*cf.* Scheme 1). We synthesized two different ligands and tested their coordination behaviour towards coinage metals, to investigate the influence of the substitution on the phosphorus atoms on the steric as well as electronic properties of the Pacman phosphane ligands.

The phosphane fragments bearing a flat phenyl or bulkier diisopropylamino substituent are introduced by reacting the Pacman ligand with the corresponding dichlorophosphanes and triethylamine as base (Scheme 1). The phenyl-substituted ligand **1** can be prepared in 40% yield and the diisopropylamino-substituted compound **2** in 55% yield. The comparably low yields occur because in addition to the desired *exo–exo* isomers (66% of **1** or **2** in the respective reaction solution), the reactions also form the *endo–exo* isomers, which are not feasible as bidentate ligands. In the single crystal, **1** forms a symmetric cavity with *d*(P–P) = 4.2368(6) Å, as shown in Fig. 1 (left). While the phosphorus–phosphorus distance in **2** is only slightly elongated by the substitution at the phosphorus (*d*(P–P) = 4.281(2) Å, Fig. 1, right), the overall structure of the ligand forms a strongly distorted cavity

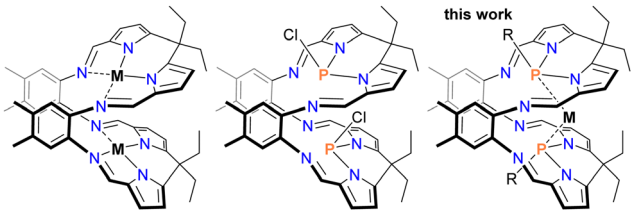

Chart 1 Pacman complex[17] (left), Pacman chlorophosphane[9] (middle) and a Pacman phosphane complex (right, M = metal).

[a] *Institut für Chemie, Universität Rostock, Albert-Einstein-Straße 3a, Rostock D-18059, Germany. E-mail: axel.schulz@uni-rostock.de*
[b] *Leibniz-Institut für Katalyse e.V., Albert-Einstein-Straße 29a, Rostock D-18059, Germany*

† Electronic supplementary information (ESI) available: Preparation of starting materials and compounds, structure elucidation, additional structural and NBO data. CCDC 2226460–2226467. For ESI and crystallographic data in CIF or other electronic format see DOI: https://doi.org/10.1039/d3cc01174g

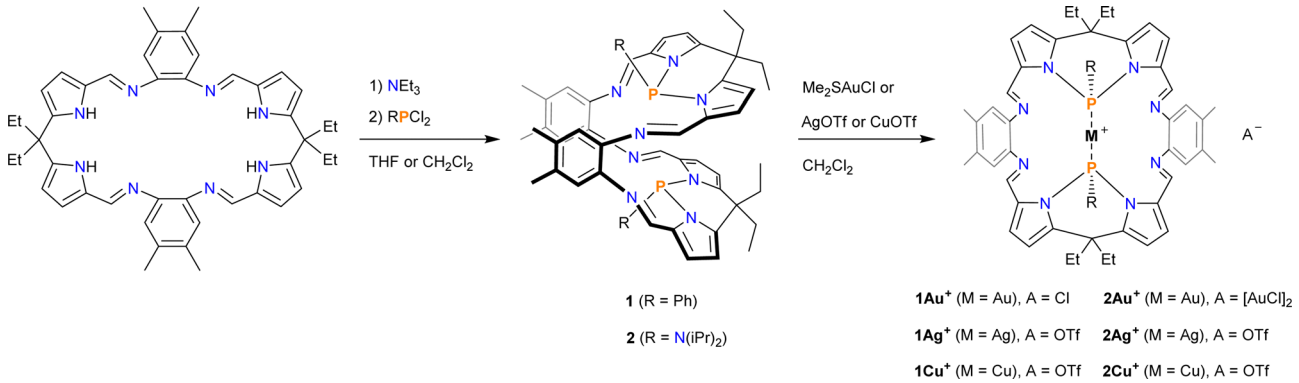

Scheme 1 Syntheses of the Pacman phosphane ligands **1** and **2** and their coinage metal complexes **1M** and **2M** (M = Au^+, Ag^+, Cu^+).

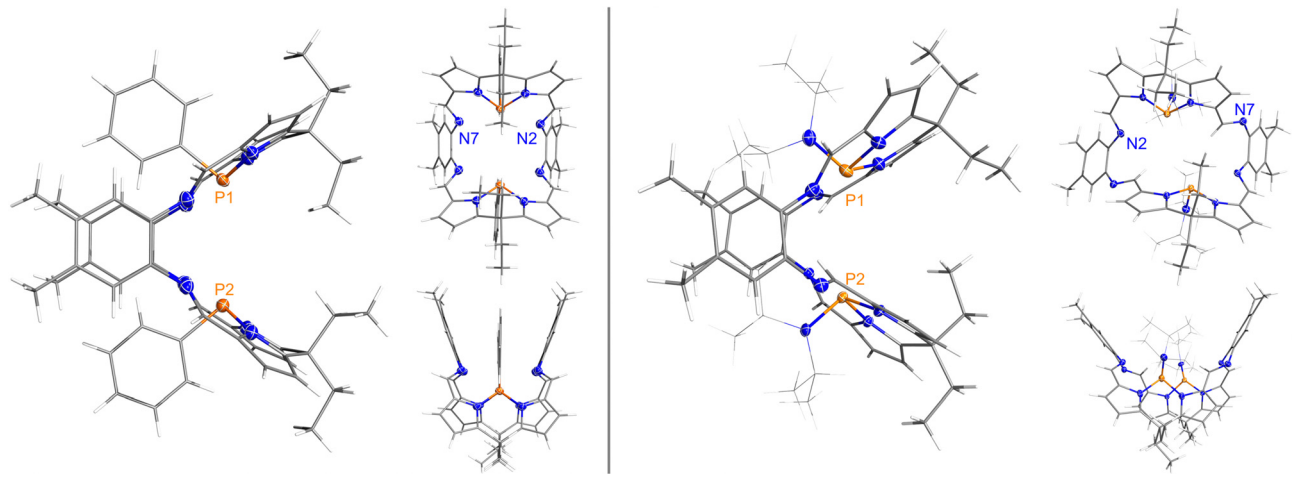

Fig. 1 Side, front and top view of the molecular structures of **1** (left) and **2** (right) in crystal. Ellipsoids are drawn at 50% probability at 203(2) K (**1**) or 123(2) K (**2**). iPr$_2$-groups displayed thinly for clarity. Solvent and disorder of one NiPr$_2$-group are omitted for clarity. Selected distances (Å) of **1**: P1–P2 4.2368(6), P1–N2 2.7553(13), P1–N7 2.7224(9). Selected distances (Å) of **2**: P1–P2 4.281(2), P1–N2 3.0140(27), P1–N7 4.312(4).

(Fig. 1, right), in which the isopropyl groups significantly increase the distance between the two phenylene units in the backbone of the ligand. Additionally, two imine nitrogen atoms in **2** are twisted out of the molecule cavity (*cf.* N2 *vs.* N7, Fig. 1) and interact with pyrrolic hydrogen atoms of neighbouring molecules (ESI,† Fig. S1). NBO (Natural bond orbital)[10,11] analyses (see ESI,† p. S42) reveal a

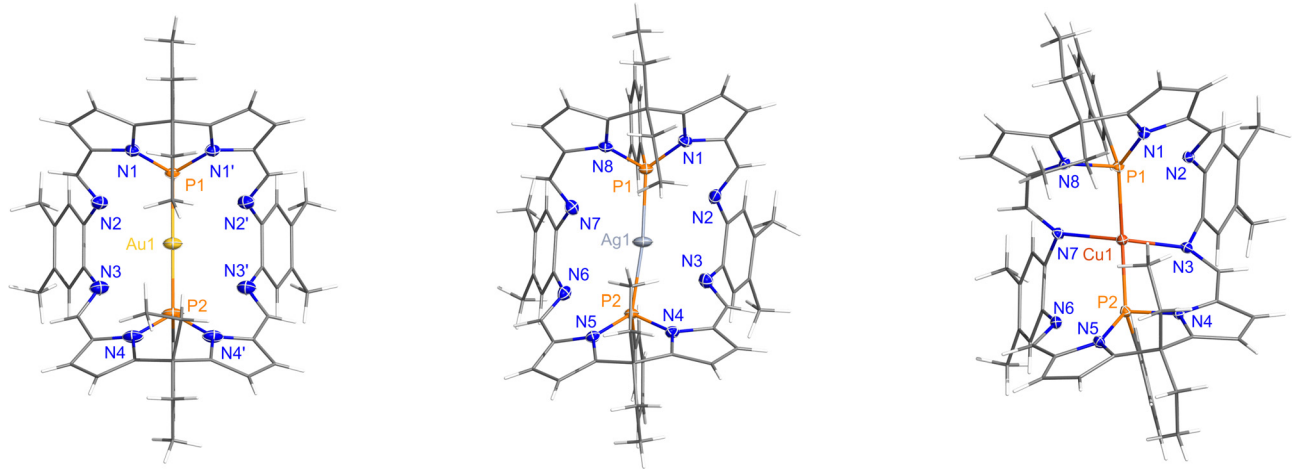

Fig. 2 Molecular structures of **1Au**$^+$, **1Ag**$^+$ and **1Cu**$^+$ in the solid state. Ellipsoids are drawn at 50% probability at 123(2) K. Counterions and solvent omitted for clarity. Selected structural parameters can be found in Table 1.

Table 1 Selected distances d in Å, angles α in ° and donor acceptor energies E_{DA} in kJ mol^{-1} (from NBO analysis) in the compounds **1Au$^+$**, **1Ag$^+$** and **1Cu$^+$**

		1Au$^+$	**1Ag$^+$**	**1Cu$^+$**
P1–M	$d_{exp.}$	2.286(1)	2.382(1)	2.273(1)
	E_{DA}	782	296	239
N2–M	$d_{exp.}$	3.043(3)	3.060(3)	3.192(2)
	E_{DA}	20	8	5
N3–M	$d_{exp.}$	3.071(3)	2.580(1)	2.120(2)
	E_{DA}	22	38	119
P1–M–P2	α	179.54(5)	168.95(6)	145.44(2)

positive charge on P1 of 1.22 e in **1** and an increased positive charge of 1.36 e in **2** (ESI,† Table S10).

Reactions of **1** and **2** with MeS_2AuCl, AgOTf or CuOTf in CH_2Cl_2 lead to the formation of cationic gold, silver and copper complexes (Scheme 1), in which the metal is located inside the cavity of the Pacman phosphane ligand, as anticipated. The phenyl substituted gold complex **1Au$^+$** shows a highly symmetric structure in single crystals, very similar to the pure ligand, with the gold coordinated almost linearly by the two phosphorus atoms (Fig. 2 and Table 1). Upon coordination, the P–P distance is elongated by approx. 0.33 Å to d(P–P) = 4.566(2) Å, which is in line with the typical flexibility of Pacman ligands. However, the Au–P distances fall within the normal range[12] (2.286(1) Å, Table 1). Additionally, the distances between the gold and the imine nitrogen atoms are slightly shorter than the sum of the van der Waals radii of 3.21 Å[13] (3.043(3)–3.071(3) Å, Table 1). Nevertheless, this is rather due to limited space in the Pacman cavity than a significant interaction (*vide infra*). For the silver complex **1Ag$^+$**, a slight distortion of the molecule is observed (Fig. 2). Compared to **1Au$^+$**, the silver is located deeper inside the cavity and its distances to the imine nitrogen atoms N3 and N7 are significantly shortened, while the distances to N2 and N6 remain nearly the same (2.382(1) Å, Table 1). This indicates an increasing interaction of the imine nitrogen atoms N3 and N7 with the silver atom. At the same time, the Ag–P distance is slightly longer compared to d(Au–P) (2.382(1) Å, Table 1), but still within the typical range for such complexes (2.4 Å).[12] The distortion is further increased in the copper complex **1Cu$^+$** (Fig. 2). The distances between the imine nitrogen atoms N3 and N7 and the copper are further shortened compared to **1Ag$^+$** (2.120(2) Å, Table 1) and therefore fall within the range of a nitrogen–copper bond (2.1 Å).[12] Together with the two phosphorus atoms, the coordination environment around the copper can be described as a distorted tetrahedron.

NBO analyses were used to investigate the bonding situations of the metal centres (Table 1), revealing a significant donor–acceptor energy between the phosphorus and the gold in **1Au$^+$**, while no significant interaction was observed between the imine nitrogen atoms and the gold (Table 1). This is in good agreement with the structural data. However, the donor–acceptor energies between the phosphorus and the metal atoms decrease significantly going to **1Ag$^+$** and **1Cu$^+$** (Table 1). At the same time, the donor acceptor energies between the imine nitrogen atoms N3 and N7 and the metal increase slightly in **1Ag$^+$** while they increase significantly in **1Cu$^+$** (Table 1), in accordance with the discussed CuN_2P_2 coordination mode.

Looking at the diisopropylamino-substituted Pacman phosphane ligand **2**, all of its complexes show stronger distortion compared to complexes of **1**, just like the ligand itself. In addition, the reaction of **2** with Me_2SAuCl in a 1 : 1 ratio shows full conversion and a single product according to NMR spectra of the reaction solution, but a product mixture consisting of **[2Au][Cl]** and **[2Au][AuCl$_2$]** is received upon crystallization. When a 1 : 2 ratio is used in the synthesis, pure **[2Au][AuCl$_2$]** is obtained. In **2Au$^+$**, the gold is not linearly coordinated by the two phosphorus atoms, but shifted towards the imine nitrogen atoms N6 and N7 (Fig. 3). Compared to **1Au$^+$**, the Au–P distance is slightly elongated, but still within the expected range (2.120(2) Å, Table 2). This is consistent with the decreased donor acceptor energy between the phosphorus and the gold of 508 kJ mol^{-1} (ESI,† Table S9). Despite the shortened distances, no significant donor acceptor energies between the imine nitrogen atoms N6 and N7 and the gold are observed.

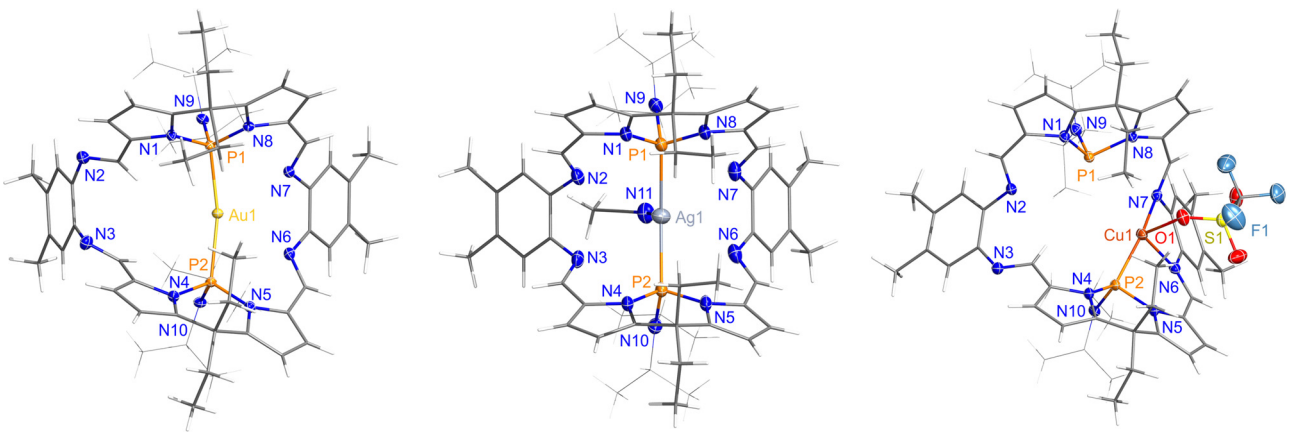

Fig. 3 Molecular structure of **2Au$^+$**, **2Ag$^+$·MeCN** and **[2Cu·OTf]** in the solid state. Ellipsoids are drawn at 50% probability at 123(2) K. N*i*Pr$_2$-groups displayed thinly for clarity. Counterions and solvent omitted for clarity. Selected structural parameters can be found in Table 2.

Table 2 Selected distances d in Å and angles α in ° in the compounds **2Au$^+$**, **2Ag$^+$·MeCN** and **[2Cu·OTf]**

	2Au$^+$	**2Ag$^+$·MeCN**	**[2Cu·OTf]**
d(P1,M)	2.120(2)	2.499(2)	3.391(1)
d(P2,M)	2.292(1)	2.494(2)	2.191(1)
d(N6,M)	3.005(4)	2.835(4)	2.104(2)
d(N7,M)	2.910(3)	2.904(4)	2.069(2)
d(N11,Ag)	—	2.439(4)	—
d(O1,Cu)	—	—	2.141(2)
α(P1,M,P2)	165.06(3)	143.03(3)	—

While all other complexes were crystallized from dichloromethane or THF, single crystals of the silver complex **[2Ag][OTf]** could only be obtained from acetonitrile leading to the cation **2Ag$^+$·MeCN** (Fig. 3). In addition to the two phosphorus atoms of the Pacman phosphane ligand, the silver is coordinated by an acetonitrile molecule in a distorted trigonal planar environment with the acetonitrile tilted out of plane by 10.82(8)°. The Ag–P distance is longer than in **1Ag$^+$** but still lies within the range of the sum of the covalent radii of 2.39 Å[14] (2.494(2) Å, Table 2). Due to the coordinated acetonitrile, the coordination role of the imine nitrogen atoms is decreased and therefore the overall structure of the complex less distorted (Fig. 3).

In all Pacman phosphane complexes discussed so far, no significant short anion–cation distances were found in the solid state, indicating only weak interactions between the ions. In contrast, coordination of the anion with the copper is found on complex formation of CuOTf with **2**, resulting in the formation of the neutral complex **[2Cu·OTf]**. Therefore, unlike all other complexes, the copper in **[2Cu·OTf]** is coordinated by only one of the phosphorus atoms of the Pacman phosphane ligand (Fig. 3). The Cu–P2 bond length of 2.191(1) is in the expected range, however, the Cu–P1 distance of 3.391(1) Å is even larger than the sum of the van der Waals radii of 3.20 Å,[13] despite the limited space in the cavity of the ligand (Table 2). The two imine nitrogen atoms N6 and N7 and an oxygen of the triflate complete the coordination environment in **[2Cu·OTf]**, which is best described as ''see-saw'' coordination with the P2–Cu1–N7 angle of 154.74(6)° and N6–Cu1–O1 of 99.11(7)°. This type of coordination mode is very rare for copper(I).[15,16] It should be noted that for a solution of **[2Cu·OTf]** only a single signal appears in the ^{31}P NMR spectrum, indicating a symmetric or very dynamic structure of the copper complex in solution. Dissociation of the triflate from the complex in solution can therefore not be excluded.

In summary, Pacman phosphane ligands show multidentate character upon coordination of coinage metals. Besides linear bidentate phosphane coordination, ligand distortion additionally allows for the participation of the imine nitrogen atoms in the coordination. Apart from that, bulkier substituents such as NiPr$_2$ on the phosphorus atoms lead to widening of the ligand backbone. Consequentially, stronger distortion and coordination of additional donors is possible using this ligand. The electronic impact of the substitution of the phosphorus atoms is difficult to assess due to the dominance of steric influences. Due to the position of the metal ion in the cavity centre of the Pacman phosphane ligand, we expect size exclusion effects in catalysis. The size of tolerated substrates is expected to depend on the nature of the substituents on the phosphorus atoms.

L. E. gratefully acknowledges funding by the University of Rostock *via* the PhD Scholarship Program.

Conflicts of interest

There are no conflicts to declare.

Notes and references

1 J. P. Collman, C. M. Elliott, T. R. Halbert and B. S. Tovrog, *Proc. Natl. Acad. Sci. U. S. A.*, 1977, **74**, 18–22.
2 J. P. Collman, P. S. Wagenknecht and J. E. Hutchison, *Angew. Chem., Int. Ed. Engl.*, 1994, **33**, 1537–1554.
3 R. Guilard, M. A. Lopez, A. Tabard, P. Richard, C. Lecomte, S. Brandes, J. E. Hutchison and J. P. Collman, *J. Am. Chem. Soc.*, 1992, **114**, 9877–9889.
4 T. Iwatani, *Pac-Man*, Midway Games, Chicago, 1980.
5 J. L. Sessler, W. S. Cho, S. P. Dudek, L. Hicks, V. M. Lynch and M. T. Huggins, *J. Porphyrins phthalocyanines*, 2003, **7**, 97–104.
6 G. Givaja, A. J. Blake, C. Wilson, M. Schröder and J. B. Love, *Chem. Commun.*, 2003, 2508–2509.
7 J. B. Love, *Chem. Commun.*, 2009, 3154–3165.
8 B. E. Cowie, J. M. Purkis, J. Austin, J. B. Love and P. L. Arnold, *Chem. Rev.*, 2019, **119**, 10595–10637.
9 L. Eickhoff, L. Ohms, J. Bresien, A. Villinger, D. Michalik and A. Schulz, *Chem. – Eur. J.*, 2022, **28**, e202103983.
10 E. D. Glendening, C. R. Landis and F. Weinhold, *J. Comput. Chem.*, 2013, **34**, 1429–1437.
11 F. Weinhold, C. R. Landis and E. D. Glendening, *Int. Rev. Phys. Chem.*, 2016, **35**, 399–440.
12 C. Kirst, J. Tietze, P. Mayer, H. C. Böttcher and K. Karaghiosoff, *ChemistryOpen*, 2022, **11**, 4–11.
13 A. Bondi, *J. Phys. Chem.*, 1964, **68**, 441–451.
14 P. Pyykkö and M. Atsumi, *Chem. – Eur. J.*, 2009, **15**, 186–197.
15 S. Ekici, M. Nieger, R. Glaum and E. Niecke, *Angew. Chem., Int. Ed.*, 2003, **42**, 435–438.
16 M. Albrecht, K. Hu, S. Zalis and W. Kaim, *Inorg. Chem.*, 2000, **38**, 4233–4242.
17 J. W. Leeland, F. J. White and J. B. Love, *J. Am. Chem. Soc.*, 2011, **133**, 7320–7323.

7 Appendix

In the appendix, only data for unpublished compounds is presented. For information about published compounds, please refer to the Supporting Information files of the publications presented in chapter 6.

7.1 Syntheses of Unpublished Compounds

7.1.1 General Experimental Information

All experiments were performed under inert conditions. For details about the standard working procedures, origin and purification of solvents as well as the methods used for the collection of analytical data, please refer to the Supporting Information files of the publications presented in chapter 6. The origin and purification of reagents used for the syntheses outlined in this chapter are listed in Table 3.

Table 3: Origin and purification of starting materials.

Substance	Origin	Purification
1	synthesized[41]	as described in the literature[41]
2Cl	synthesized[41]	as described in the literature[41] or crystallized from benzene (without further purification steps)
[3][OTf]$_2$	synthesized[41]	as described in the literature[41]
DMAP	Aldrich	used as received, stored in the glovebox
AgOTf	J&K Scientific, 98%	used as received, stored in the glovebox
NEt_3	Sigma Aldrich, 99%	dried over Na and freshly distilled prior to use
^{t}BuPCl$_2$	old stock	sublimed and stored in the glovebox
Mg	abcr (for Grignards 99.8%)	activated by stirring with a glass coated stirring bar in the glovebox for several days
Zn	Acros Organics (dust, 98+%)	activated by stirring with a glass coated stirring bar in the glovebox for several days
KC_8	synthesized[61]	stored in the glovebox
1,4-bis(TMS)-1,4-dihydropyrazine	synthesized[62]	as described in the literature[62]

7.1.2 Synthesis of **[2DMAP][OTf]$_2$**

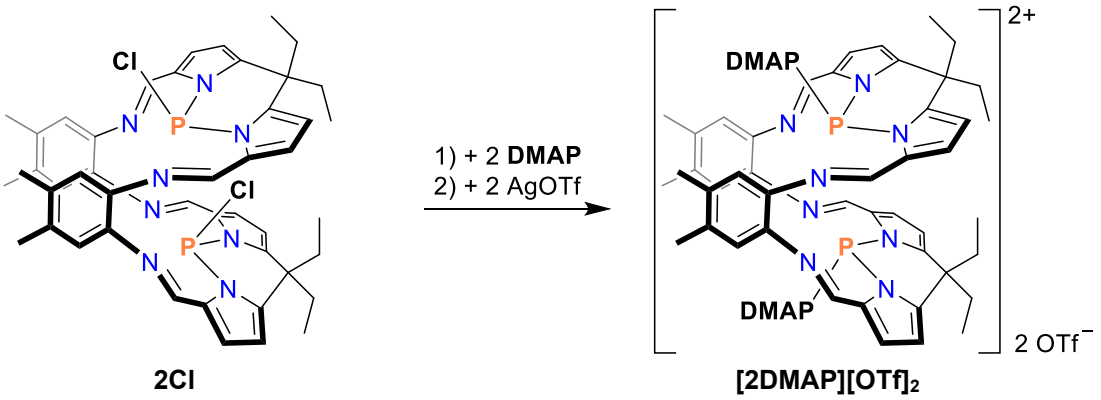

2Cl **[2DMAP][OTf]$_2$**

The reaction was performed in the dark until complete separation of AgCl. **2Cl** (408.5 mg, 0.4836 mmol) was mixed with DMAP (127.7 mg, 1.045 mmol) and AgOTf (283.3 mg, 1.042 mmol). Under stirring, dichloromethane (10 mL) was added at ambient temperatures and the mixture was stirred for 3 h. To extract the product from AgCl, the orange-brown suspension was left to settle overnight and on the next day filtered through a plug of silica on a pore 4 frit, giving a clear, brown filtrate. The fine residue was washed with dichloromethane (3 mL), left to settle for approx. 1.5 h and filtered through the same frit. The filtrate was dried *in vacuo* (1×10^{-3} mbar) for 15 min and the orange to brown powder was dissolved in MeCN (15 mL) resulting in a brown suspension with fine yellow precipitate. Another filtration through a plug of silica (pore 4 frit) gave a clear brown filtrate again. This was concentrated *in vacuo* (1×10^{-3} mbar) until incipient crystallization and stored in a fridge (5 °C) overnight. The flask with the yellow, square crystals was placed in a −40 °C cold isopropanol/nitrogen bath and the supernatant was removed *via* syringe. Afterwards the crystals were washed with cold MeCN (2× 0.5 mL, −40 °C). The cooling bath was removed and the crystals were dried *in vacuo* (1×10^{-3} mbar) at 50 °C (water bath) for 1.5 h.

In the NMR spectra of the product synthesized in the described way, 15-20% of another phosphorus-containing species can be detected. Additionally, problems with a proton source (possibly HOTf as impurity in the AgOTf) occur, leading to the formation of DMAP·HOTf which can be crystallized from the raw product in dichloromethane or THF. Due to these impurities, preliminarily no yield and only NMR data is given for **[2DMAP][OTf]$_2$** as received from the synthesis described above. We are working on the isolation of pure **[2DMAP][OTf]$_2$**.

^{31}P{^{1}H} NMR (121.5 MHz, CD_2Cl_2) δ = 85.1 (s, 0.4 P, impurity), 67.9 ppm (s, 2 P, *P*-DMAP).
^{1}H NMR (500.1 MHz, CD_2Cl_2) δ = 12.81 (br s, 0.5 H, impurity), 8.16 (s, 0.7 H, impurity), 7.82

(s, 4 H, imine C*H*), 7.42 (br s, 4 H, C*H* DMAP), 6.94 (d, $^{3}J(^{1}H,^{1}H)$ = 3.8 Hz, 4 H, C*H* pyrrole), 6.83 (s, 0.7 H, impurity), 6.73 (d, J = 3.6 Hz, 0.7 H, impurity), 6.55 (br s, 4 H, C*H* DMAP), 6.45 (d, $^{3}J(^{1}H,^{1}H)$ = 3.8 Hz, 4 H, C*H* pyrrole), 6.20 (s, 4 H, C*H* phenylene), 6.17 (d, J = 3.6 Hz, 0.7 H, impurity), 3.23 (s, 15 H, CH_3 DMAP, high integral probably due to superposition with impurity signal(s)), 2.34 (q, $^{3}J(^{1}H,^{1}H)$ = 7.2 Hz, 4 H, CH_2), 2.20 (s, 12 H, CH_3 phenylene), 2.04 (q, J = 7.2 Hz, 0.7 H, impurity), 1.75 (q, $^{3}J(^{1}H,^{1}H)$ = 7.3 Hz, 4 H, CH_2), 1.04 (t, $^{3}J(^{1}H,^{1}H)$ = 7.2 Hz, 6 H, CH_3 ethyl), 0.67 (t, J = 7.4 Hz, 1.0 H, impurity), 0.66 (t, J = 7.2 Hz, 1.0 H, impurity), 0.43 ppm (t, $^{3}J(^{1}H,^{1}H)$ = 7.3 Hz, 6 H, CH_3 ethyl).

Figure 25. NMR spectra of slightly impure **[2DMAP][OTf]$_2$** (solvent signal indicated by asterisk).

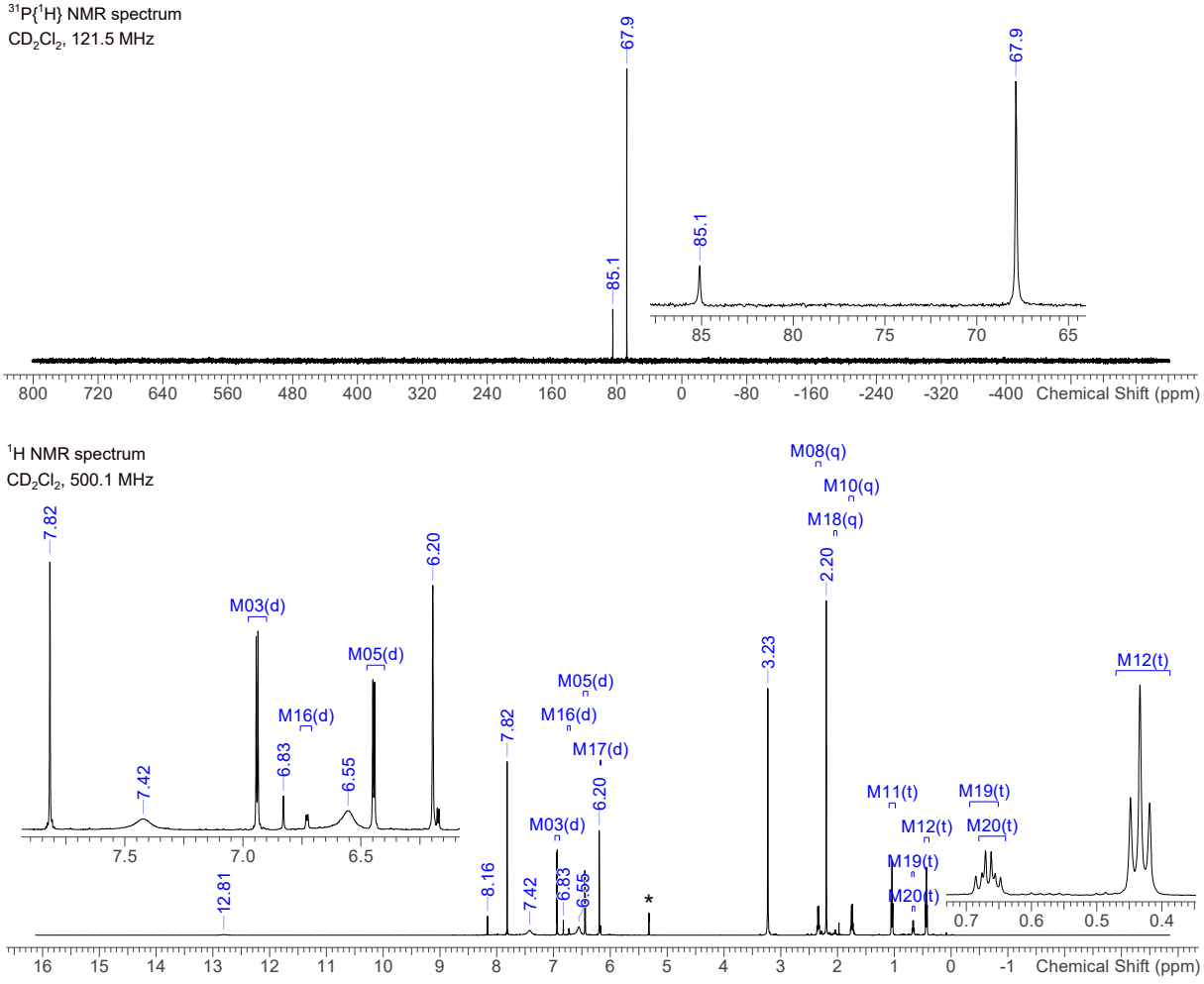

7.1.3 Synthesis of **[4][OTf]$_2$**

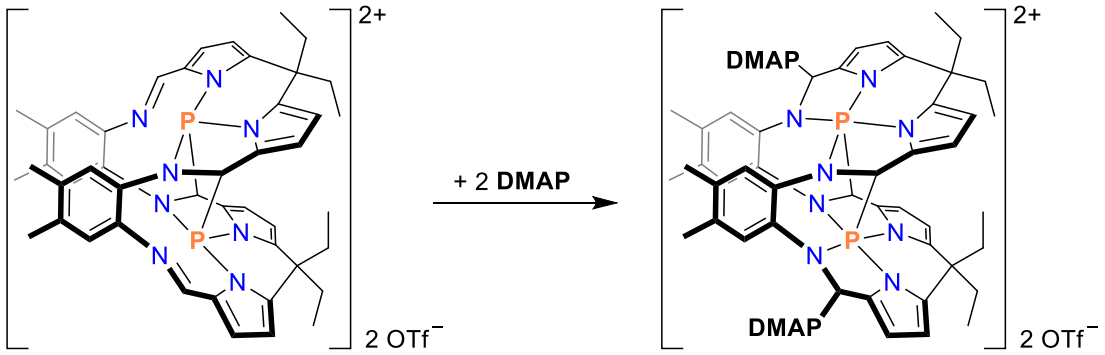

[3][OTf]$_2$ **[4][OTf]$_2$**

[3][OTf]$_2$ (210 mg, 0.196 mmol) and DMAP (48.8 mg, 0.399 mmol) were dissolved in MeCN (15 mL). During addition of the solvent, the solution turned partly dark red and partly yellow. After complete dissolution, the orange solution was concentrated *in vacuo* (1×10^{-3} mbar) to incipient crystallization and slowly cooled to 5 °C overnight. On the next day, the supernatant was removed *via* syringe, the yellow to orange crystals were washed with cold MeCN (−40 °C, 1 mL) and dried *in vacuo* (1×10^{-3} mbar) for 2 h at 30 °C (water bath). Upon drying, the crystals underwent a colour change to dark red-brown (dissolving these crystals, e.g. for NMR measurements, resulted in a light orange solution again).

The product isolated this way still contained a small amount of impurity, which could be decreased by washing the dried crystals with dichloromethane at ambient temperature (2× 2 mL) but this did not result in completely pure **[4][OTf]$_2$** (approx. 10% impurity according to the $^{31}P\{^1H\}$ NMR spectrum). Therefore, preliminarily no yield and only NMR data is given. We assume hydrolysis to be the main problem regarding the purity of **[4][OTf]$_2$** and further work on its isolation in pure form is in progress.

$^{31}P\{^1H\}$ NMR (202.5 MHz, MeCN-d_3) $\delta = -11.7$ (s, < 0.1 P, impurity), −54.4 (s, 0.1 P, impurity), −84.2 (s, 0.1 P, impurity), −85.4 ppm (s, 2 P, *P* of **4**$^{2+}$). **^{1}H NMR** (500.1 MHz, MeCN-d_3) $\delta = 7.98$ (br s, 4 H, C*H* DMAP), 6.75 (br d, $J = 2.9$ Hz, 4 H, C*H* DMAP), 6.68 (br s, 2 H, C(*H*)DMAP), 6.53 (br s, 2 H, C*H* phenylene), 6.36 - 6.46 (m, 4 H, superimposed signals of two different C*H* pyrrole), 5.84 (br s, 2 H, C*H* pyrrole), 5.66-5.70 (m, 2 H, C*H* pyrrole), 5.49 (br s, 2 H, C*H* phenylene), 5.45 (s, 1.2 H, CH_2Cl_2), 4.93 (br dd, $J(^1H,^{31}P) = 19.1$ Hz, $J(^1H,^{31}P) =$ 12.7 Hz, 2 H, C(*H*)P), 3.12 (s, 14 H, CH_3 DMAP, high integral probably due to superposition with impurity signal(s)), 2.16 (br s, 6 H, CH_3 phenylene), 2.00 - 2.15 (m, 4 H, CH_2), 1.96 (br s, 6 H, CH_3 phenylene), 1.80 - 1.96 (m, integration not possible due to superposition with solvent

signal, CH_2), 0.92 (t, $^3J(^1H,^1H)$ = 7.3 Hz, 6 H, CH_3 ethyl), 0.78 ppm (t, $^3J(^1H,^1H)$ = 7.2 Hz, 6 H, CH_3 ethyl). Due to their high number and low intensity, the impurity signals in the ^{1}H NMR spectrum are not given.

Figure 26. NMR spectra of slightly impure **[4][OTf]$_2$** (solvent signals indicated by asterisks).

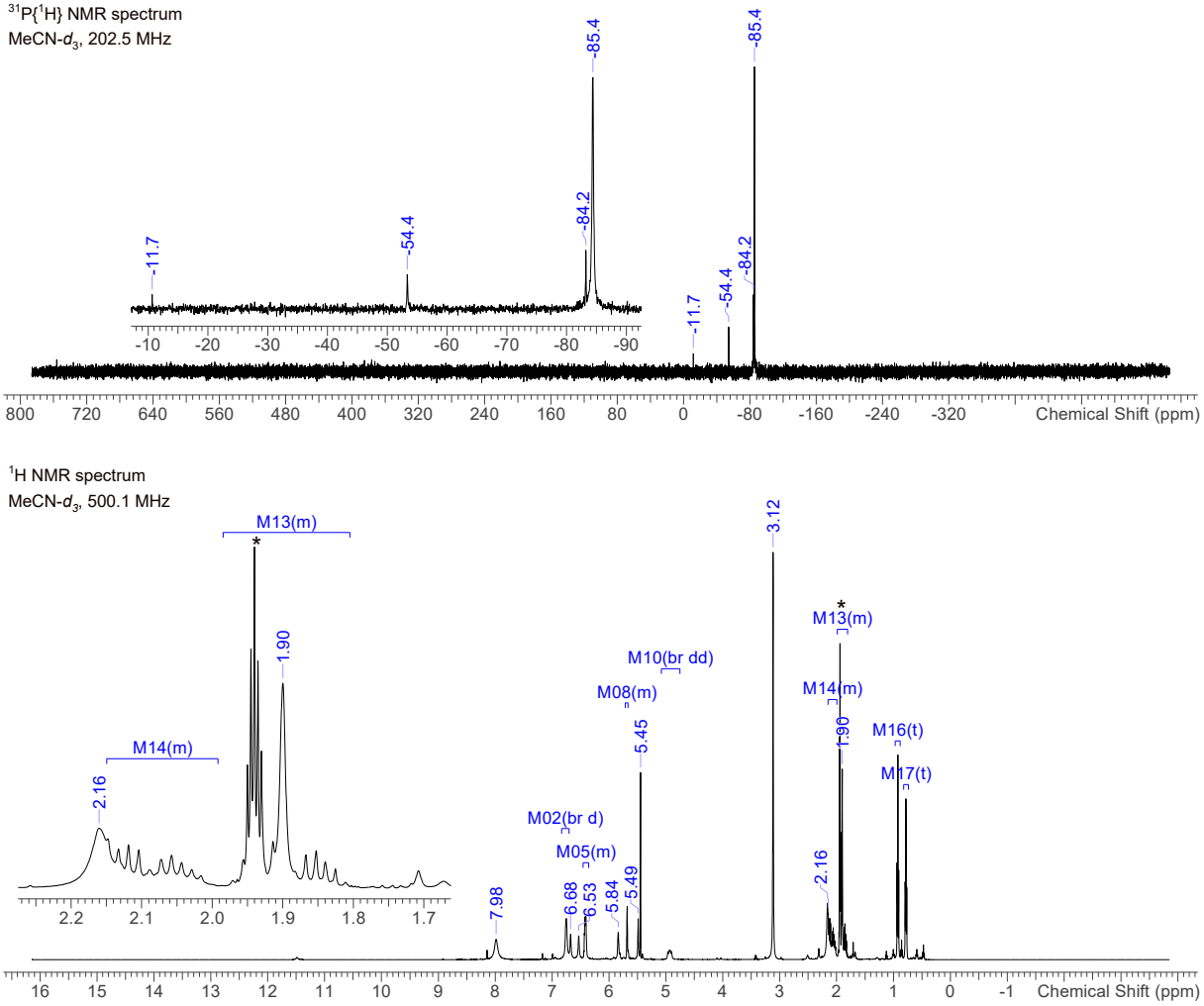

7.1.4 Unsuccessful Reactions

Table 4: Unsuccessful syntheses of **2^{t}Bu** and **[3][GaCl$_4$]$_2$**, failed low-temperature isolation of **2^{2+}** as well as reduction attempts of **2Cl**.

starting compound	reactant(s)	conditions	outcome
1 (1.21 g, 1.68 mmol)	NEt_3 (1.9 mL, 14 mmol), $^{t}BuPCl_2$ (540 mg, 3.39 mmol)	THF (25 mL), slow addition at −80 °C, warmed to ambient temperature overnight, extraction with Et_2O	unselective product formation, no crystallization of any product possible
2Cl·0.75 THF (7 mg, 0.008 mmol)	AgOTf (7 mg, 0.03 mmol)	MeCN-d_3 (0.5 mL) condensed on mixed reagents in an NMR tube (cooled by liquid N_2), warmed to −40 °C, orange solution, colourless precipitate, transferred to cooled NMR device, NMR spectra measured at −30 °C	different species in $^{31}P\{^{1}H\}$ NMR spectrum between 45 ppm and 120 ppm, no signal for **3^{2+}** until warming from −30 °C to 25 °C; repeated in larger scale in clean 1:2 stoichiometry for crystallization of an intermediate (see below)
2Cl·0.75 THF (417 mg, 0.463 mmol)	AgOTf (238 mg, 0.923 mmol)	MeCN (30 mL) condensed on mixed reagents (cooled by liquid N_2), warmed to −40 °C, orange solution filtered in the fridge at −40 °C, filtrate concentrated to crystallize an intermediate of the formation of **3^{2+}** several times	no formation of SCXRD-quality crystals
2Cl·C_6H_6 (503 mg, 0.581 mmol)	Mg (147 mg, 6.05 mmol)	stirred in THF (12 mL) for 4 days (until starting material was completely converted), dried *in vacuo*, extracted with benzene (20 mL) and residue additionally extracted with THF (15 mL)	dark brown solution, only solvent NMR signals, extracted benzene fraction very small, crystallization of both fractions not possible
2Cl·0.25 C_6H_6 (513 mg, 0.593 mmol)	Zn (390 mg, 5.97 mmol)	stirred in THF (15 mL) for 33 h (until staring material was completely converted), dried *in vacuo*, extracted with benzene (3×10 mL)	decrease of overall NMR intensity, two main signals in 1:1 ratio at 87.1 and 98.4 ppm, extraction of only negligible amount of product (< 1.5 mg)
2Cl·0.6 C_6H_6 (56 mg, 0.063 mmol)	KC_8 (18 mg, 0.13 mmol)	stirred in THF (2.5 ml) for 4 days	still starting material left, no product signals in the NMR spectra
2Cl·0.75 THF (21 mg, 0.023 mmol)	1,4-bis(TMS)-1,4-dihydropyrazine (5.2 mg, 0.023 mmol)	dissolved in THF-d_8 (0.5 mL), reaction control via NMR spectroscopy for several days	no intense colour change, complete conversion of **2Cl** after 7 d, products detectable in NMR spectra but unselective product formation

7.2 Crystallographic Details of **[2DMAP][OTf]$_2$** and **[4][OTf]$_2$**

For general information regarding collection and refinement of SCXRD data, please refer to the Supporting Information files of the publications presented in chapter 6.

Single crystals of **[4][OTf]$_2$** were received from a concentrated solution in acetonitrile, as described in the synthesis protocol (chapter 0) and yielded a publishable data set upon SCXRD.

Beautiful square crystals of **[2DMAP][OTf]$_2$** are formed during its synthesis (chapter 0). Unfortunately, they only give a poor data set in SCXRD due to mosaicity and merohedral twinning. Nevertheless, the SCXRD measurement together with the preliminary NMR spectra are trustworthy indicators for the highly symmetric structure of **2DMAP^{2+}**.

7.3 Unpublished Computational Results

All structures were optimized on triple zeta DFT level including dispersion correction (PBE-D3/*m*TZVP). Subsequent single-point coupled cluster calculations with triple zeta basis sets were performed for more accurate electronic energies (DLPNO-CCSD(T)/*m*TZVP). For details about the used programs, methods and basis sets, solvent correction, calculation of NMR properties, etc., please refer to the Supporting Information files of the publications presented in chapter 6. The unpublished calculated data of **[2DMAP]$^{2+}$** and **4^{2+}** is given in Table 5.

Table 5: Calculated data of **[2DMAP][OTf]$_2$** and **[4][OTf]$_2$**.

Compd.	Opt. method	PG	N_{imag}	E_{tot}[a]	ΔE^0 [b]	ΔU^{298} [c]	ΔH^{298} [d]	ΔG^{298} [e]	$E_{CCSD(T)}$[f]	T_1
[2DMAP]$^{2+}$	PBE-D3/def2TZVP	C_{2v}	0	−3663.9074	1.1478	1.2215	1.2225	1.0348	−3660.2753	0.0121
4^{2+}		C_1	0	−3663.9039	1.1566	1.2259	1.2269	1.0528	−3660.3032	0.0112

[a] Total SCF energy in a.u.; **[b]** zero-point correction in a.u.; **[c]** thermal correction to internal energy in a.u.; **[d]** thermal correction to enthalpy in a.u.; **[e]** thermal correction to Gibbs energy in a.u.; **[f]** single-point DLPNO-CCSD(T)/def2-*m*TVP energy in a.u.